UNIVERSITAT POLITÈCNICA DE VALÈNCIA

CHARACTERIZATION OF URI1 FROM *ARABIDOPSIS THALIANA* AND ITS ROLE IN STRESS RESPONSES

PhD in Biotechnology

Yaiza Gómez Mínguez

Advisor: Dr David Alabadí

Valencia, February 2024

UNIVERSITAT POLITÈCNICA DE VALÈNCIA

PhD in Biotechnology

Characterization of URI1 from *Arabidopsis thaliana* and its role in stress responses

Yaiza Gómez Mínguez

Advisor: Dr David Alabadí

Valencia, February 2024

A mis padres

A mi hermana Sandra

SUMMARY

It is of fundamental importance for the plant to trigger the corresponding signaling cascades in response to environmental stress and to keep proteins and protein complexes active despite the cellular stress. The chaperone Hsp90 plays an important role in coordinating these two processes, although the mechanisms that regulate its activity in response to the environment are not fully understood. Recent studies in animals show that the Hsp90 co-chaperones prefoldin-like (PFDLs) play a role in environmental signaling. Therefore, they have the potential to carry information about the environment to modulate both the assembly of protein complexes as part of the Hsp90-R2TP/PFDL and the signaling pathways in which they are involved. Currently, there is little information on PFDLs in plant species. We have now accumulated evidence that PFDLs, particularly URI1, may exert a similar, general role in *Arabidopsis*, coordinating protein homeostasis with growth pathways in response to stress, e.g. low energy stress. Here we show that the R2TP/PFDL complex is formed in *Arabidopsis* and that URI1 is one of its subunits. The activity of URI1 is essential for certain processes, such as embryonic development, as evidenced by the early arrest caused by the knock-out mutation of URI1. With a hypomorphic *uri1* allele, URI1 was shown to have a strong influence on the transcriptome. Consistent with this, the URI1 interactome shows that URI1 interacts with a relatively large number of partners, many of which are involved in fundamental processes related to mRNA metabolism. Thus, *Arabidopsis* URI1, like its orthologs in yeast and humans, appears to be involved in diverse cellular functions, including protein homeostasis, mRNA metabolism and signal transduction. URI is a highly versatile protein, although the molecular basis of this versatility is still unknown. Here we show that *Arabidopsis* URI1 possesses a large intrinsically disordered region spanning most of the C-terminal portion of the protein, a feature that is conserved in yeast and human orthologs. Our results reveal two main features of disordered proteins in URI1: promiscuity in interactions with partners and protein instability. We hypothesize that these two features contribute to endowing URI1 with functional versatility. Interestingly, the instability of URI1 is counteracted by sugar, and our genetic analysis places URI1 in the signaling pathway that controls growth in response to sugar deprivation-induced energy stress by acting as a negative upstream regulator of the master kinase TOR. We hypothesize that URI1 plays a role in preventing excessive seedling growth when energy conditions are favorable.

RESUM

És de vital importància per a una planta activar les corresponents cascades de senyalització en resposta a l'estrés ambiental i mantenir actives les proteïnes i els complexos proteics malgrat l'estrés cel·lular. La xaperona Hsp90, entre d'altres, s'encarrega de coordinar aquests dos processos, encara que els mecanismes que regulen la seua activitat en resposta a l'entorn no s'han arribat a comprendre del tot. Estudis recents en animals mostren que les co-xaperones de Hsp90*, prefoldin-like* (PFDLs), tenen un rol destacat en la senyalització ambiental. Per tant, tenen el potencial de portar informació sobre l'entorn per modular tant l'assemblatge de complexos proteics, com a part de l'Hsp90-R2TP/PFDL, i les vies de senyalització en les quals estan involucrats. Actualment, hi ha poca informació sobre PFDLs en espècies vegetals. Ara tenim l'evidència que els PFDLs, particularment URI1, poden exercir un paper similar en *Arabidopsis*, coordinant l'homeòstasi proteica amb les vies de creixement en resposta a l'estrés, per exemple, estrés energètic. En aquest treball mostrem que el complex R2TP/PFDL es forma a *Arabidopsis* i que URI1 és una de les seues subunitats. L'activitat d'URI1 és essencial per a alguns processos, com el desenvolupament embrionari, com es demostra per l'arrest precoç causat per la mutació *knock-out* d'URI1. Amb un al·lel hipomòrfic d'*uri1*, es va mostrar que URI1 té una forta influència en el transcriptoma. En consonancia amb l'observat amb el transcriptoma, l'interactoma d'URI1 mostra que URI1 interactua amb un nombre relativament gran de proteïnes, moltes de les quals estan involucrades en processos fonamentals relacionats amb el metabolisme de l'ARN missatger. Així, URI1 en *Arabidopsis*, com els seus ortòlegs en rent i humans, sembla estar involucrat en diverses funcions cel·lulars, incloent-hi l'homeòstasi proteica, el metabolisme del ARNm i la transducció de senyals. URI1 és una proteïna altament versàtil, encara que la base molecular d'aquesta versatilitat encara és desconeguda. Ací mostrem que *Arabidopsis* URI1 posseeix una gran regió intrínsecament desordenada que abasta la major part de la porció C-terminal de la proteïna, una característica que es conserva en els ortòlegs de rent i humans. Els nostres resultats revelen dues característiques principals de les proteïnes desordenades en URI1. La primera la promiscuïtat en les interaccions amb altres proteïnes, i la segona la inestabilitat proteica. Aleshores, hipotetitzem que aquestes dues característiques contribueixen a dotar URI1 de versatilitat funcional. Curiosament, la inestabilitat d'URI1 es contraresta amb el sucre, i la nostra anàlisi genètica situa URI1 en la via de senyalització que controla el creixement en resposta a l'estrés energètic induït per la privació de sucre, actuant com a regulador negatiu aigües amunt de la quinasa TOR. Hipotetitzem que URI1 exerceix un rol en prevenir el creixement excessiu de les plàntules quan les condicions energètiques són favorables.

RESUMEN

La activación de las diferentes cascadas de señalización en respuesta al estrés ambiental, así como mantener activas las proteínas y complejos proteicos en respuesta al estrés celular es fundamental para las plantas. La chaperona Hsp90 juega un papel importante en la coordinación de estos dos procesos, aunque los mecanismos que regulan su actividad en respuesta al ambiente no están completamente descritos. Estudios recientes en animales muestran que las proteínas *prefoldin-like* (PFDLs), co-chaperonas de Hsp90, desempeñan un papel importante en la señalización ambiental. Por lo tanto, son capaces de transmitir información sobre el medio ambiente para modular tanto el ensamblaje de complejos proteicos como parte del Hsp90-R2TP/PFDL como las vías de señalización en las que se encuentran involucradas. Hoy en día, se conoce muy poco sobre las proteínas PFDLs en especies vegetales. En este trabajo, hemos obtenido evidencia de que las PFDLs, particularmente URI1, pueden ejercer un papel similar en *Arabidopsis*, coordinando la homeostasis de las proteínas con las vías de crecimiento en respuesta a diferentes tipos de estrés, como por ejemplo el estrés por falta de energía. Así, mostramos que el complejo R2TP/PFDL se forma en *Arabidopsis* y que URI1 es una de sus subunidades. La actividad de URI1 es esencial para ciertos procesos, como el desarrollo embrionario, evidenciado por el arresto embrionario temprano causado por la mutación *knock-out* de URI1. Se ha observado que URI1 tiene una influencia notoria en el transcriptoma mediante el uso de un alelo hipomórfico de *uri1*. Coherentemente con lo observado en el transcriptoma, el interactoma de URI1 muestra que URI1 interactúa con un número relativamente grande de proteínas, muchas de las cuales están involucradas en procesos fundamentales relacionados con el metabolismo del ARN mensajero y la transducción de señales. URI1 es una proteína altamente versátil, aunque la base molecular de esta versatilidad aún es desconocida. Aquí mostramos que URI1 en *Arabidopsis* posee una región intrínsicamente desordenada que abarca la mayoría de la parte C-terminal de la proteína, característica que se conserva en los ortólodos de levadura y humanos. Nuestros resultados revelan en URI1 dos características principales de las proteínas desordenadas. La primera de ellas es la promiscuidad en las interacciones con otras proteínas y la segunda la inestabilidad de la proteína. Hipotetizamos que estas dos contribuyen a dotar a URI1 de versatilidad funcional. Es importante destacar que la inestabilidad de URI1 se contrarresta con el azúcar. El análisis genético realizado sitúa a URI1 en la vía de señalización que controla el crecimiento en respuesta al estrés energético inducido por la privación de azúcar, al desempeñar un papel como un regulador negativo aguas arriba de una de las quinasas principales, TOR. Hipotetizamos que URI1 desempeña un papel en la prevención del crecimiento excesivo de las plántulas cuando las condiciones energéticas son favorables.

ACKNOWLEDGEMENTS / AGRAÏMENTS /AGRADECIMIENTOS

En primer lloc, tot i que sé que no li agraden aquestes coses (encara estàs a temps de deixar de llegir), vull agrair al meu director de tesi l'oportunitat que em va brindar fa quasi set anys, sense saber ben bé qui era, per portar a terme el meu somni de ser doctora: moltes gràcies, David! Ara ja per sempre escoltaré en el meu cap el característic: "Xe Yaiza, els controls!". Et promet que ara és el primer que pense per a muntar un assaig. Tampoc oblidaré el "Tu fes-ho i ho mirem" perquè saps que sempre necessite saber-ho tot. He fet tresor de tots els coneixements que m'has donat i ensenyat i els guarde en la motxilla per a aplicar-los i transformar-los. Gràcies.

En segundo lugar, no podía faltar una mención especial a Blázquez, aunque no hayas sido mi director sí que me has enseñado mucho y has aportado a mi formación científica incontables lecciones, muchas horas en el despacho, y muchas horas preparando los seminarios pensando... ¿y que me preguntará Miguel? Muchas gracias por todo.

¿Qué, empezamos? Espero no dejarme a nadie, seis años dan para conocer a mucha, muchísima gente y de todos he aprendido algo, os voy a guardar con cariño para siempre. Muchas gracias a todas las personas con las que he compartido seminarios, congresos, laboratorio, cafés, fiestas, cervezas, cenas, viajes... Habéis demostrado que en el IBMCP sabemos divertirnos y que no siempre todo se trata de ciencia. Me habéis hecho muy feliz, y también estoy segura de que me habéis hecho enfadar alguna otra, pero os voy a echar muchísimo de menos. Tengo que agradecer a Noel la acogida en el laboratorio, todos sabemos que eras parte del pegamento del labo. Gracias por todo lo que me enseñaste, por dejarme ser tu sombra y dejarme aprender la mayoría de las cosas que sé. Gracias por cada café y por cada tarde hasta las mil, aguantando la frustración porque el clonning no funcionaba. El laboratorio nos unió, y aquí seguimos, años después de la misma manera, riéndonos con Alberto. Te echo de menos cada día. Annita... que ya estoy aquí, que he llegado, ¡por fin! Haber entrado juntas y ser co-FPI's nos hizo unirnos desde el principio, con nuestros más y menos, ¡pero aquí estamos! De la misma manera, gracias por todo lo que me has enseñado, por los viajes, por todas las imitaciones... Ya no soy capaz de ver algo roto y no pensar, ¿qué voz pondría annita? ("zoy un finofaurio"). Más tarde se unieron Alberto y Laura… ya sabéis que para mí habéis supuesto el sostén, la fuerza y el ánimo cuando las cosas se han puesto más crudas. Me habéis hecho reír hasta llorar y me habéis hecho reír después de llorar. No sólo ha sido la tesis, hemos pasado la vida, que se nos ha puesto tremendamente difícil en varias ocasiones. Gracias por no dejarme caer ni un solo momento. Os echo de menos. Os quiero. Ceci… ¿cómo puede ser que en tan poco tiempo hayas hecho tanto? Te uniste más tarde a este grupo y te trajeron para ponernos a los tres cuerdos. Con tu llegada trajiste luz para darnos palabras de ánimo, ideas y… ¡MANOS! Gracias por ser el hombro en el que nos hemos podido apoyar durante la etapa más dura, a nivel personal y laboral, te estaré eternamente agradecida, no sé si algún día podré devolveos todo lo que habéis hecho por mí.

A Maca, la artista detrás de las ilustraciones de esta tesis, y de muchas más. Gracias por haber sabido entenderme desde el principio, haberme hecho reír mucho mucho, y haber sabido plasmar todo lo que te decía con sólo dos palabras. A Paula, no saps el que et trobe a faltar! No hi ha ningú com tu al món! Borja, ¡te echaré de menos! Jaime, ¡gracias por estar ahí siempre! Asier, ¡eres Jesús abriendo las aguas! Antuan, ¡gracias por haberme enseñado tanto! Cynthia, I miss you so much! Anselm, Carlos, Eva, Santi, Mariana, Carlos, Juanma, Joan, Anselmo, Fede, Julián, Pepi, Eugene… ¡Qué bien nos lo hemos pasado! ¡Os voy a echar de menos!

Bruno, I do not have the words to thank you for everything you have helped me. Thank you for giving me your energy and your love for science, which inspired me even on the greyest of days.

A Cris Úrbez por ser la madre de todos, por estar ahí a cualquier hora y bajo cualquier concepto, por remar en la misma dirección, por hacer siempre todo más fácil, por ser incondicional. Siempre te lo he dicho, eres una profesional excepcional, y una persona absolutamente maravillosa, te voy a llevar conmigo siempre. MD, gracias… gracias, y mil gracias, te voy a echar de menos. Maite, Sonia, nos debemos unas cervezas. Ana Espinosa, gracias por todo lo que nos has ayudado, sin ti no hubiese sido posible. A Clau y Edu, gracias por haberme hecho más fácil la estancia y haberme enseñado los lugares más escondidos de Perpignan, nos vemos pronto.

A Isabel i Laura, ací ho teniu, ja està. Açò és el resultat de tot el sacrifici invertit, gràcies per haver estat de manera incondicional al meu costat, per haver-me dit tots els dies que soc un orgull per a vosaltres. No podria tindre millors amigues, i gràcies, sobretot, per saber traure'm sempre un somriure. On dieu que ens n'anem? Jo ja estic *ready*.

A Vicente, gràcies per haver-me donat suport en els moments més difícils. Gràcies per haver-me repetit que soc capaç quan fins i tot jo no ho creia. Gràcies per haver-me portat xocolate en quantitats industrials al despatx i, sobretot, gràcies per haver-me dit: Ja ho tens bé, anem a donar una volta! Ara, sí que sí, va de bo. T'estime molt. Gràcies també a Reme i a Paula, per haver-me acollit com una més en la vostra família i en la vostra casa. I a Vicente, que estic completament segura que estaria molt orgullós de veure fins on hem aplegat.

Finalmente, a mi familia: papá, mamá, teta…esto es para vosotros. Gracias por haberme enseñado a pelear por lo que uno quiere. Todo esfuerzo tiene recompensa, y esta os la quiero dedicar a vosotros. Gracias por haberme enseñado todo lo que sé. Sois mi lugar seguro y mi prioridad. Gracias por ser el mejor equipo de animación: "ya casi lo tienes, sólo un poquito más". Al resto de mi familia, por haberme apoyado siempre, a pesar de no saber muy bien que estaba haciendo, jaja. Por los que están, por los que se fueron y por todos los que vendrán. Os quiero.

La realización de esta Tesis Doctoral ha sido posible gracias a una Ayuda para Contratos Predoctorales para la Formación de Doctores FPI (BES-2017-081041) y una ayuda europea EMBO Scientific Exchange (9583). Así mismo, el trabajo experimental ha sido financiado por el proyecto [ILOVEPFD] del Ministerio de Ciencia e Innovación AEI-MICINN (PID2019-109925GB-I00).

TABLE OF CONTENTS

LIST OF FIGURES

Introduction

Chapter I

General Discussion

ABBREVIATIONS

2-DG	2-deoxyglucose
AP	affinity purification
AP-MS	affinity-purification and mass spectrometry
ASDURF	ASNSD1 UPSTREAM READING FRAME
ATP	Adenosine triphosphate
CCT	cytosolic chaperonin
CHX	cycloheximide
DCMU	3-(3,4-dichlorophenyl)-1,1-dimethylurea
DEGs	Differentially expressed genes
GFP	Green fluorescent protein
GO	Gene ontology
H_2O_2	Hydrogen peroxide
HSP90	Heat Shock Protein 90
IDRs	Intrinsically Disordered Regions
KEGG	Kyoto Encyclopedia of Genes and Genomes
MBP	maltose binding protein
MoRFs	molecular recognition features
mRNA	messenger RNA
MS medium	Murashige and Skoog medium
mTOR	mechanistic TOR
NAD+	Nicotinamide adenine dinucleotide
NADPH	Nicotinamide adenine dinucleotide phosphate
NES	nuclear export signal
NLS	nuclear localisation signal
OGT	O-GlcNAc transferase

PAQsome	Particle for Arrangement of Quaternary structure
P-bodies	Processing bodies
PDRG1	P53 DNA DAMAGE-REGULATED GENE 1
PFDD	PFD Domain
PFDL	prefoldin-like
PFDN2	PREFOLDIN 2
PFDN6	PREFOLDIN 6
PI	propidium iodide
PIKKs	phosphatidylinositol-3-kinase-related proteins
RNAPII	RNA polymerase II
RPAP3	RNAPII ASSOCIATED PROTEIN 3
RPB5D	RPB5-binding motif
RPS6	ribosomal protein S6
rRNA	Ribosomal RNA
RT-qPCR	Reverse transcription-quantitative polymerase chain reaction
S6K	ribosomal S6 kinase
SGs	Stress granules
TBLASTN	Translated Nucleotide Basic Local Alignment Search
TOR	Target of rapamycin
uORF	upstream open reading frame
URI	UNCONVENTIONAL PREFOLDIN RPB5 INTERACTOR
UV	Ultraviolet
UXT	UBIQUITOUSLY EXPRESSED TRANSCRIPT
WT	Wild type

INTRODUCTION

Eukaryotes have intricate signal transduction networks that regulate the interplay between external and internal cues to regulate cellular homeostasis. Maintenance of cellular homeostasis is of paramount importance. In the case of plants, maintaining homeostasis is more challenging because they cannot escape environmental fluctuations. Plants employ several mechanisms to maintain and control cellular function while eliciting appropriate responses to the changing environment (Baena-Gonzalez, 2010). This involves, for instance, different signalling cascades that regulate gene expression to re-allocate plant resources that usually cause growth arrest (Huot B *et al*., 2014). An essential aspect of cellular homeostasis is characterized by the maintenance of active forms of proteins and protein complexes (proteostasis), even under stressful cellular conditions (Zhu JK., 2016), which can lead to misfolding and subsequent aggregation of the resulting polypeptide chains (Hartl and Hayer-Hartl, 2002). Therefore, protein homeostasis and cell signalling must be harmoniously coordinated to achieve an appropriate adaptation to environmental changes. A protein or protein complex involved in the coordination of both processes must have the ability to recognise environmental stimuli and participate in the relevant signalling cascade(s) while contributing to protein homeostasis. Molecular chaperones serve as exemplary instances as they recognise stimuli, shield non-native proteins from unwanted aggregation and facilitate their folding into correct conformations. A major molecular chaperone is the Heat Shock Protein 90 (HSP90), which takes up partially folded proteins from HSP70 and promotes their complete folding by ATP consumption. HSP90 works with co-chaperones that can (i) induce conformational changes related to chaperone activity, (ii) act as adaptors to recruit client proteins, or (iii) perform both functions (Balchin *et al*. 2016; Prodromou, 2016; Schopf *et al*. 2017).

Lessons from animal models show that the prefoldin-like (PFDL) proteins are emerging as novel regulators of cell survival and proliferation in response to environmental stress (Chaves-Perez *et al*., 2018), and indicate that they have the potential to coordinate environmental signalling and protein homeostasis. This ability relies in two key features. First, PFDLs are co-chaperones of Hsp90, as part of the R2TP/PFDL complex, for the assembly of protein complexes with a role in basic processes such as transcription, splicing or nutrient signalling (Houry *et al.,* 2018). Thus, they participate in protein complex homeostasis. And second, they act as signalling elements in response to the cellular environment, e.g. nutrient availability, genotoxics or UV radiation (Chaves-Perez *et al*., 2018; Thomas *et al.,* 2018). Therefore, PFDLs have the potential ability to carry information about the cellular environment and modulate both, protein homeostasis, and downstream signalling pathways in which they participate. Whether PFDLs perform this role in plants is still elusive.

Prefoldin-like proteins.

The PFDL proteins were identified in several independent studies carried out in animals and yeast. They are UBIQUITOUSLY EXPRESSED TRANSCRIPT (UXT) (Schroer *et al*. 1999), UNCONVENTIONAL PREFOLDIN RPB5 INTERACTOR (URI; Bud27 in yeast) (Gstaiger *et al*. 2003; Miron-Garcia *et al*. 2013), P53 DNA DAMAGE-REGULATED GENE 1 (PDRG1) (Luo *et al*. 2003), ASNSD1 UPSTREAM READING FRAME (ASDURF) (Cloutier *et al*. 2020). Sequence analysis showed that they are related to the canonical prefoldins (PFDs), which were identified in humans and yeast several years earlier (Vainberg *et al*., 1998). PFDs form a heterohexameric complex conserved in eukaryotes that participates as a co-chaperone of the cytosolic chaperonin CCT in the folding of tubulin and actins (Vainberg *et al.,* 1998 and Gestaut *et al*., 2019). Each PFD is formed by a coiled-coil type structure: two α-helix connected by one or two β-hairpins (Martín-Benito *et al.,* 2002). PFDs with one β-hairpin are β-type PFDs (PFD1, 2, 4 and 6) and the ones with two are α-type PFDs (PFD3 and 5). The complex has a jelly-fish type structure, with α-helix protruding as tentacles to establish contacts with client proiteins (Martín-Benito *et al*., 2002). Although the structure of the PFDLs has not yet been solved, sequence comparison suggests that

URI and UXT adopt an α-type structure, and PDRG1 and ASDURF a β-type one (Cloutier *et al.,* 2020). Importantly, proteomic approaches aimed at defining the interactome of RNA polymerase II (RNAPII) in human cells showed that URI, UXT and PDRG1, and ASDURF form a complex, the PFDL complex (PFDLc), together with the canonical PREFOLDIN 2 (PFDN2) and PREFOLDIN 6 (PFDN6) (Cloutier *et al*., 2009; Cloutier *et al.,* 2020). The subunit of nuclear RNAPs RPB5 is usually associated with mammalian PFDLc as it interacts with URI (Dorjsuren *et al*. 1998). Although yeast possesses homologues of URI, PFDN6, PFDN2 and RPB5, designated as Bud27, Gim4, Gim1 and Rpb5, respectively, no genes coding for the homologues of PDRG1, ASDURF and UXT are present in this organism (Herranz-Montoya *et al*., 2021). The PFDL complex is usually associated to the R2TP complex, suggesting that they are subcomplexes that interact forming the R2TP/PFDL complex (Cloutier *et al*. 2017). The R2TP/PFDLc was recently named Particle for Arrangement of Quaternary structure (PAQsome; Houry *et al*., 2018).

The mammalian R2TPc is composed by RuvBL1, RuvBL2, PIH1D1 and RNAPII ASSOCIATED PROTEIN 3 (RPAP3) and each protein has a homolog in yeast, namely Rvb1, Rvb2, Pih1 and Tah1, respectively. The Rvb1/RuvBL1 and Rvb2/RuvBL2 subunits are highly conserved and essential for cell viability (Bauer *et al*. 2000; Kanemaki *et al*. 1999; Qiu *et al*. 1998). Pih1/PIH1D1 and Tah1/RPAP3 show differences in their dimensions and domain constitution, suggesting that they have evolved to more specialised functions and associations with different interaction partners (Inoue *et al*. 2010; Ni *et al*. 2009). The R2TPc has been identified in several organisms, suggesting its evolutionary conservation (Zhao *et al*. 2005; Ahmad *et al*. 2013; Benbahouche *et al*. 2014; Boulon *et al*. 2008).

The *Arabidopsis* genome encodes single putative homologues of the R2TP/PFDLc subunits, except for RuvBL2 (which has two gene copies): RuvBL1, RuvBL2a, RuvBL2b, RPAP3, URI1, UXT, PDRG1, ASDURF, PFD2, PFD6 and RPB5. Vascular plants have no homologous genes of *PIH1D1*. The latter is only present in plant lineages with that require flagellated cells, for example for motile sperm cells (Zur Lage *et al*. 2018).

In the following sections, the terms Rvb1, Rvb2, Pih1, Tah1, Bud27, Gim4 and Gim1 will be used in reference to yeast proteins, while RuvBL1, RuvBL2, PIH1D1, RPAP3, URI, PFDN2 and PFDN6 will be used to refer to mammalian proteins (Figure 1).

Subunits forming the R2TP/PFDL complex.

RT2P complex

RuvBL1 and RuvBL2 are two paralogous members of the AAA+ superfamily of ATPases and function as catalytic components within the R2TP/PFDL complex. Although both have intrinsic ATPase activity, RuvBL1 and RuvBL2 often work together as hetero-hexameric or hetero-dodecameric complexes in both yeast and mammals (Niewiarowski *et al*. 2010; Gorynia *et al*. 2011; Martino *et al*. 2018). In addition, they function as important components of ATP-dependent chromatin remodelling complexes such as INO80 and SWR1 (Jonsson *et al*. 2001; Krogan *et al*. 2003, Zhou *et al*. 2017), the histone acetyltransferase TIP60 complex (Ikura *et al*. 2000) and β-catenin complexes involved in transcriptional regulation (Kim *et al*. 2005).

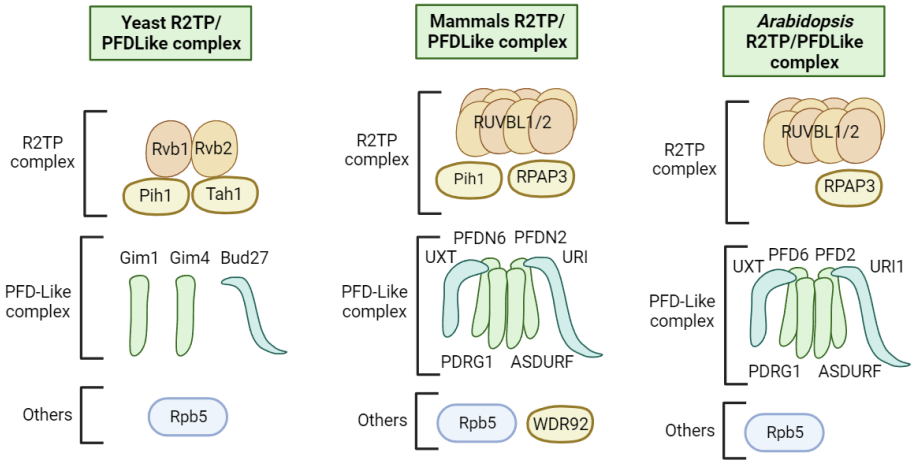

Figure 1. R2TP/PFDL along the eukaryotic kingdom. Schematic representation of the R2TP/PFDL complex in mammals, showing both the R2TP complex and the PFDL complex together with other associated proteins. This is then compared with their counterparts in yeast and *Arabidopsis thaliana*. In yeast, it remains unclear whether the PFDL complex exists independently or as encircling subunits. In *Arabidopsis*, the presence of the R2TP complex was observed, which is associated with numerous complexes due to its property as an AAA-ATPase. This study investigates the persistence of the PFDL complex in *Arabidopsis*, focussing on the activity of one of its subunits, URI1.

The PIH1D1/Pih1 subunit functions as a scaffold protein that mediates the recruitment of client protein complexes through serine-dependent phosphorylation of the PIH1 domain (Hořejší *et al*. 2014). Within the R2TP complex, the conformation of PIH1D1 is not well defined due to its flexibility, but it is similar to that of Pih1 in the yeast R2TP complex, where it binds to the Rvb1/2 heterohexamer (Martino *et al*. 2018; Tian *et al*. 2017). In addition, the C-terminus of PIH1D1/Pih1 contains a CS domain (CHORD domain-containing protein and Sgt1 domain), a domain also found in other co-chaperones that interact with Hsp90 (Zhao *et al*. 2005, 2008; Quinternet *et al*. 2015). The lack of PIH1D1/Pih1 in yeast only results in a defective temperature-sensitive phenotype, suggesting that it is not essential for cell viability (Gonzales *et al*. 2005) but for the integration of external cues. Several studies have also described PIH1D1/Pih1 as a regulator of rRNA synthesis and processing (Gonzales *et al*. 2005).

Following the identification of the R2TP complex in yeast, an examination of the human Hsp90 proteome revealed the presence of the human homologues of Rvb1, Rvb2 and Pih1, but not Tah1 (Te *et al*. 2007) (Figure 1). Later studies showed that Spag1, a *Drosophila* protein with TPR domains, could interact with human Hsp90 (Boulon *et al*. 2008). Previous yeast two-hybrid screens had also showed that Spag1 interacts with *Drosophila* Hsp90 and Pih1 (Giot *et al*. 2003; Te *et al*. 2007). In the human context, Spag1 is usually referred to as RPAP3 because it was also identified as a protein associated with RNAPII (Jeronimo *et al*. 2007). RPAP3 is the largest protein of the R2TPc in humans. It has two TPR domains that interact with Hsp90 and a C-terminal domain that serves as a contact site with RuvBL2 (Martino *et al*. 2018). RPAP3 exhibits high flexibility due to its long central segment that spans the RuvBL1/RuvBL2 heterohexamer and it serves as a flexible linker for Hsp90 binding. In contrast, yeast Tah1 is much smaller than RPAP3/Spag1 and consists of two TPR repeats followed by a C-t helix and an unstructured region (Jiménez *et al*. 2012). RPAP3/Spag1 functions in transcriptional regulation (Shimada *et al*. 2011), adult stem cell maintenance (Chen *et al*. 2018) and circadian rhythm regulation (Means *et al*. 2015).

PFDL complex

Apart from the canonical PFD2 and PFD6 (Chávez & Puerto-Camacho., 2016), the most studied PFD-like proteins in mammals are UXT and URI, as their overexpression triggers different types of cancer, making both proteins potential therapeutic targets. UXT, known as ART-27, is an α-type prefoldin that is ubiquitously expressed in mice and humans (Schroer *et al*. 1999). UXT is essential for mammalian cell growth and development and loss-of-function mutants are embryonic lethal in mice (Carter *et al*. 2014; Schafler *et al*. 2018; Zhao *et al*. 2005). In mammals, UXT is active in the nucleus and cytoplasm. In the nucleus, UXT functions as a cofactor for several transcription factors and complexes involved in the regulation of cell proliferation, inflammation, and differentiation (Chen *et al*. 2013; Kong *et al*. 2015; Li *et al*. 2014; Markus *et al*. 2002; Sánchez-Morgan *et al*. 2017; Taneja *et al*. 2004; Zhou *et al*. 2015). Nonetheless, in the cytoplasm, UXT reduces proteotoxicity in neurodegenerative diseases through selective autophagy (Yoon *et al*. 2021).

URI, named Bud27 in yeast, includes an α-like prefoldin domain and an elongated C-terminal domain that gives URI a larger size compared to the other prefoldins. URI was first described as a transcriptional regulator through its association with RPB5 (Dorjsuren *et al*. 1998). Human URI, and its homologue in yeast Bud27, coordinate interactions between RPB5/RNAPII and other protein complexes (Wei et al. 2003; Le et al. 2005; Yart et al. 2005; Mirón-Garcia et al. 2014). Bud27/URI is involved in several processes, such as regulation of transcription/elongation, translation, nutrient signalling and more processes (described in more detailed in the second point of general introduction).

PDRG1 is a β-type prefoldin-like protein and has been described as an oncogene that is downregulated by the tumour suppressor p53 (Luo *et al*. 2003). Conversely, it is upregulated in response to UV-induced DNA damage and genotoxic agents (Jiang *et al*. 2011). In addition, PDRG1 plays an important role in controlling epigenetic modifications. In the nucleus, PDRG1 interacts with MATα1, the catalytic subunit of methionine adenosyltransferase MAT I and MAT III, inhibits S-adenosylmethionine synthesis and reduces DNA methylation (Pérez *et al*. 2016).

Mapping of the human RNA polymerase II (RNAPII) interaction network has shown the presence of the R2TP/PFDL complex (R2TP/PFDLc) in association with the RNA polymerase subunit RPB5 (POLR2E) and the WD40 repeat protein WDR92 (Cloutier et al. 2009). The R2TP/PFDLc plays a role in the assembly and stabilisation of several macromolecular complexes that include: (i) L7Ae ribonucleoproteins (L7Ae RNPs), (ii) U5 small nuclear ribonucleoprotein (U5 snRNP), (iii) RNA polymerase II (RNAPII), (iv) phosphatidylinositol-3-kinase-related proteins (PIKKs) complexes and others (Boulon et al. 2008; Zhao et al. 2008; Machado-Pinilla et al. 2012; Cloutier et al. 2017; Malinova et al. 2017; Boulon et al. 2010).

While the R2TP/PFDL complex has been extensively studied in animals and yeast over the past 20 years, very little is known about its role in the green lineage. In plants, only two subunits of the R2TP/PFDL complex have been described: RPAP3 in *Arabidopsis* (also called TPR5; Sotta *et al*. 2016) and sorghum (Antonio *et al.* 2023) and URI1 in *Arabidopsis* (Yang *et al*. 2022). TPR5 is required for both the activity and direction of cell division in root meristems (Sotta *et al*. 2016), whereas URI1 regulates plant gravitational response through controlling PIN2 trafficking and, therefore, auxin transport (Figure 2) (Yang *et al*. 2022). In our laboratory, we have identified the *Arabidopsis* R2TP/PFDL complex through affinity-purification and mass spectrometry (AP-MS) using the PFD6 subunit as bait (unpublished results). This prompted us to ask study role of the R2TP/PFDL complex in plants and to what extent is similar to that in animals. This thesis dissertation is exclusively dedicated to the characterization of the URI1 protein in *Arabidopsis.*

2. Deciphering the role of URI protein.

URI is an important protein for the development of multicellular organisms, since its deletion leads to embryo lethality in several of them (Parusel *et al*. 2006; Kirchner *et al*. 2008). In a PFDLc context, its absence promotes the degradation of UXT and PDRG1 in mammals, while its overexpression increases the stability of UXT, PDRG1 and the associated protein RPB5, suggesting that it is pivotal for the stabilisation of the whole complex (Mita *et al*. 2013). Furthermore, inactivation of Bud27, but not of GIM1/PFD6, alters the assembly of RNA polymerases in yeast, suggesting that Bud27 may act independently of other prefoldins (Mirón-Garcia *et al*. 2013).

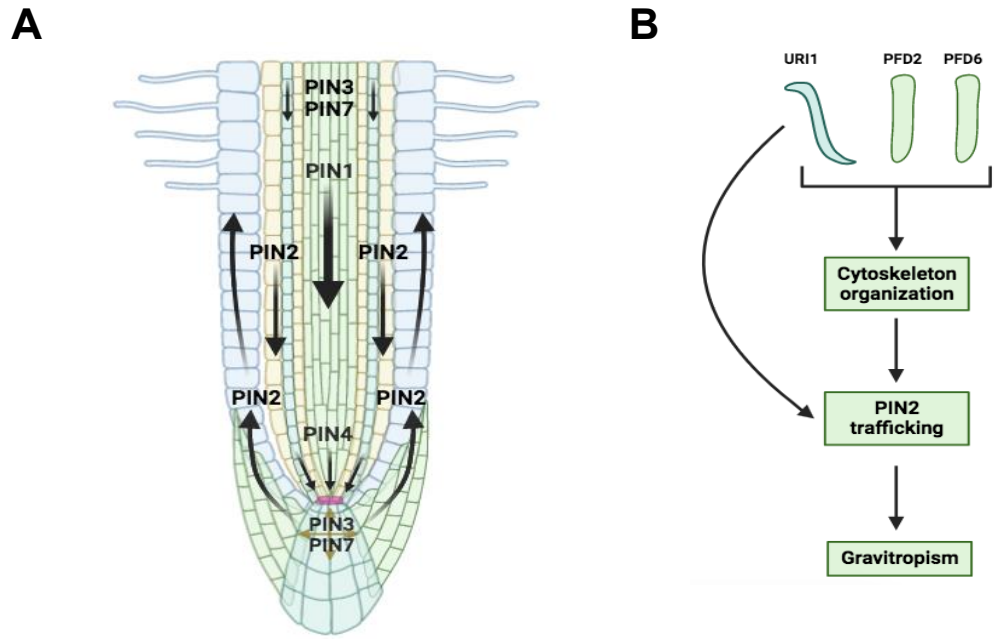

Figure 2. The function of URI1 in *Arabidopsis* as elucidated by Yang *et al.* (2022). **A**. Auxin entry into the plant is facilitated by auxin influx transporters, while export is mainly regulated by transporters such as PGP transporters and polar localised PIN transporters. In *Arabidopsis*, PIN export transporters exhibit polar localisation, which determines the direction of auxin flux. The orientation of PIN transporters is a dynamic process, constantly switching between the plasma membrane and the endosome. **B.** Model proposed by Yang *et al.* (2022) in which URI1 interacts with PFD2 and PFD6 to co-regulate the organisation of the cytoskeleton. This collaboration promotes the transport of PIN2 between the endosome and the plasma membrane, thereby influencing auxin distribution in the roots and controlling the gravitropic response. Yang *et al.* (2022) also showed that URI1 contributes to PIN2 recycling independently of the PFD complex. Figure modified from Yang *et al.,* 2022.

As for the structure of the URI1 protein, *in silico* analyses suggest that it contains an α-type prefoldin domain occupying the N-terminus (PFD Domain, PFDD), followed by the RPB5-binding motif (RPB5D), an asparagine-rich region and the URI box (Gstaiger *et al*. 2003; Delgermaa *et al*. 2004; Mirón-García *et al*. 2013). In mammals, the PFDD is considered indispensable for mediating interactions between prefoldin-like modular components such as PDRG1 and UXT (Mita *et al*., 2013). The RPB5D plays a crucial role in facilitating its interaction with RPB5, a common subunit of the three eukaryotic nuclear RNAPs (Gstaiger *et al*. 2003; Mirón-Garcia *et al*. 2013; Deplazes *et al*. 2009). Moreover, this domain is essential for orchestrating the assembly of RNAPs (Mirón-García *et al*. 2013). The third domain is an asparagine-rich region that can stabilise RPB5 by acting

as a DNA mimic (Gstaiger *et al*. 2003). This domain appears to be disorganised and has features of Intrinsically Disordered Regions (IDRs) (see Chapter 2). The fourth conserved part of the protein is URI box, whose functional properties remain unclear, has been shown to be important for translation in yeast (Deplazes *et al*. 2009). The URI box has also been shown to interact with the transcription factor TFIIF in human cells (Wei *et al*. 2003).

Several studies have shown that URI is present in both the nucleus and cytoplasm and may have different functions in each cellular compartment. Analysis of the Bud27 sequence revealed the existence of a plausible leucine-rich nuclear export signal (NES) and a nuclear localisation signal (NLS), both located in the asparagine-rich region. The NES sequence plays a central role in controlling the nuclear accumulation of Bud27 (Mirón-Garcia *et al*. 2013). In humans, URI1 has only the NLS domain, which allows it to shuttle between the cytoplasm and the nucleus via the Exportin 1. However, its main localisation remains predominantly in the cytoplasmic compartment (Delgermaa *et al*. 2004; Mita *et al*. 2013). Drosophila Uri, which is located mainly in the cytoplasm, also shows some perinuclear localisation (Kirchner *et al*. 2008).

While URI/Bud27 is primarily localised in the cytoplasm, its inactivation exerts a discernible influence on several nuclear mechanisms. First, Bud27 has been shown to be involved in the biogenesis of the three nuclear RNA polymerases (Mirón-García *et al*. 2013; Cieśla *et al*. 2015). Bud27 acts in a Rpb5-dependent manner, possibly influencing the final stage of assembly of RNAPs in the cytoplasm before they are translocated to the nucleus (reviewed at Martínez-Fernádez *et al.* 2018). Second, Bud27 interacts with the phosphorylated forms of active RNAPII (Ser5P-CTD and Ser2P-CTD), indicating its involvement in transcription elongation processes and, accordingly, there is reduced occupancy of RNAPII in many target genes in *bud27* mutant cells (Mirón-García *et al*. 2014). Third, it has been also proposed that Bud27 could be involved in DNA-repair processes in yeast because it represses the accumulation of Rad52, a protein involved in the repair of DNA double-strand breaks (Muñoz-Galván *et al*. 2013). Fourth, Bud27 interacts *in vivo* with Sth1, the catalytic subunit of chromatin remodeler RSC and is required for the recruitment of the complex to the chromatin (Mirón-García *et al.,* 2014 and Cuevas-Bermúdez *et al.,* 2023).

Similarly, human URI is also involved in the assembly of cytoplasmic RNAPII as part of R2TP/PFDLc (Figure 3) (Boulon *et al.* 2010; Cloutier and Coulombe, 2010). URI regulates transcription through several other binding partners, such as the PAF1 complex, which is involved in in promoting RNAPII CTD phosphorylation and histone modification during elongation (Figure 3) (Yart *et al*. 2005). The role of URI in the nucleus goes beyond transcription. For instance, it plays a role in maintaining DNA integrity in *C. elegans* and *Drosophila* (Parusel *et al*. 2006; Kirchner *et al*. 2008) and contributes to tumour formation by inhibiting de novo NAD+ synthesis in mice (Figure 3) (Tummala *et al*. 2014; Burén *et al*. 2016).

There is experimental evidence that Bud27 plays a role in translation at several levels, including translation regulation and protein folding. For instance, Bud27 coordinates the transcription and processing of rRNAs leading to ribosomal biosynthesis, which has a clear impact in translation mechanisms (Martínez-Fernández *et al*. 2020). Bud27 is also involved in translation initiation by promoting the efficient recruitment of the ternary complex to the 40S ribosome subunit (Deplazes *et al*. 2009). In addition, Bud27 interacts with Hsp70 and Hsp40 with a role in protein synthesis.

Chapter 1 presents a general characterisation of URI1 in *Arabidopsis*, including the identification of its interactome *in vivo* and the transcriptomic changes associated to the lack of functional URI1. **Chapter 2** examines features of URI1 protein that may determine the functionality of the protein in *Arabidopsis*.

3. Role of URI under stress conditions

URI mediates several cellular functions in response to environmental stressors such as genotoxic agents or nutrient availability in animals. In *C. elegans*, URI is involved in the prevention and repair of DNA damage induced by genotoxic agents to maintain the integrity of the genome (Parusel *et al*. 2006). In concert with this, the lack of URI results in sterile adults with a small germline due to a defect in cell proliferation resulting from cell cycle arrest due to DNA damage. In addition, overexpression of URI in mammals has been found to protect against gastrointestinal syndrome, a fatal intestinal disease that occurs after a high dose of radiation, demonstrating an active role of URI in maintaining cellular homeostasis after exposure to this stress (Figure 3) (Chaves-Perez *et al*. 2019).

Genetic and biochemical studies in yeast and human cells have shown that URI is modulated by energy stress and plays a role in regulating Target Of Rapamycin (TOR)-dependent transcriptional programmes (Figure 3) (Gstaiger *et al*. 2003; Djouder *et al*. 2007; Martínez-Fernández *et al.,* 2020; Gutiérrez-Santiago *et al.,* 2022). The evolutionarily conserved TOR pathway occupies a pivotal role in the integration and transmission of nutritional signals to coordinate cellular growth. Under favorable conditions, TOR remains active and thus promotes cell growth. Conversely, in the case of nutrient deficiency causing energy stress (or treatment with a rapamycin inhibitor), TOR is negatively regulated, leading to growth arrest. Bud27 is downregulated in response to amino acids starvation, and yeast mutants lacking Bud27 exhibit phenotypes such as cell elongation and agar penetration characteristic of nutrient deficiency-induced invasive growth (Gstaiger *et al*. 2003). In addition, this mutation leads to a decrease in several tRNA species and an increase in the expression of genes encoding proteins involved in amino acid metabolism. A significant proportion of genes activated in yeast by deficiency in Bud27 have an upstream open reading frame (uORF) in their 5' promoter region and a consensus binding site for the Gcn4p transcription factors. Remarkably, there is a significant overlap between these Gcn4p-dependent genes and genes upregulated by amino acid deficiency or inactivation of TOR. These findings indicate that Bud27 acts in the TOR pathway that represses the expression of genes whose transcription is dependent on Gcn4 (Gstaiger *et al*. 2003). In addition, lack of Bud27 leads to reduced activity of TOR in yeast cells, supporting the functional involvement of Bud27 in the TOR pathway (Martínez-Fernández *et al.* 2020).

The role of URI in energy stress pathways is conserved in mammals as evidenced by its involvement in mechanistic TOR (mTOR) signalling (Gstaiger *et al*. 2003; Djouder *et al*. 2007). In humans, URI is phosphorylated when exposed to growth factors such as insulin (Gstaiger *et al*. 2003) and is unphosphorylated in the presence of mTOR inhibitors such as rapamycin (Figure 3). This observation suggests that URI functions as a downstream component within the mTOR signalling cascade. It also suggests that mTOR exerts its role on nutrient-dependent transcription, at least in part, via phosphorylation of URI through the S6K1 kinase (Djouder *et al*. 2007). Indeed, URI in mammals is part of a feedback mechanism to control excessive cell growth in response to nutrients. Unphosphorylated URI inhibits the protein phosphatase PP1γ, whereas in response to nutrient availability, phosphorylation of URI by the mTOR/S6K1 pathway causes its dissociation of PP1γ, which in turn inactivates S6K1 (Figure 3) (Djouder *et al*. 2007).

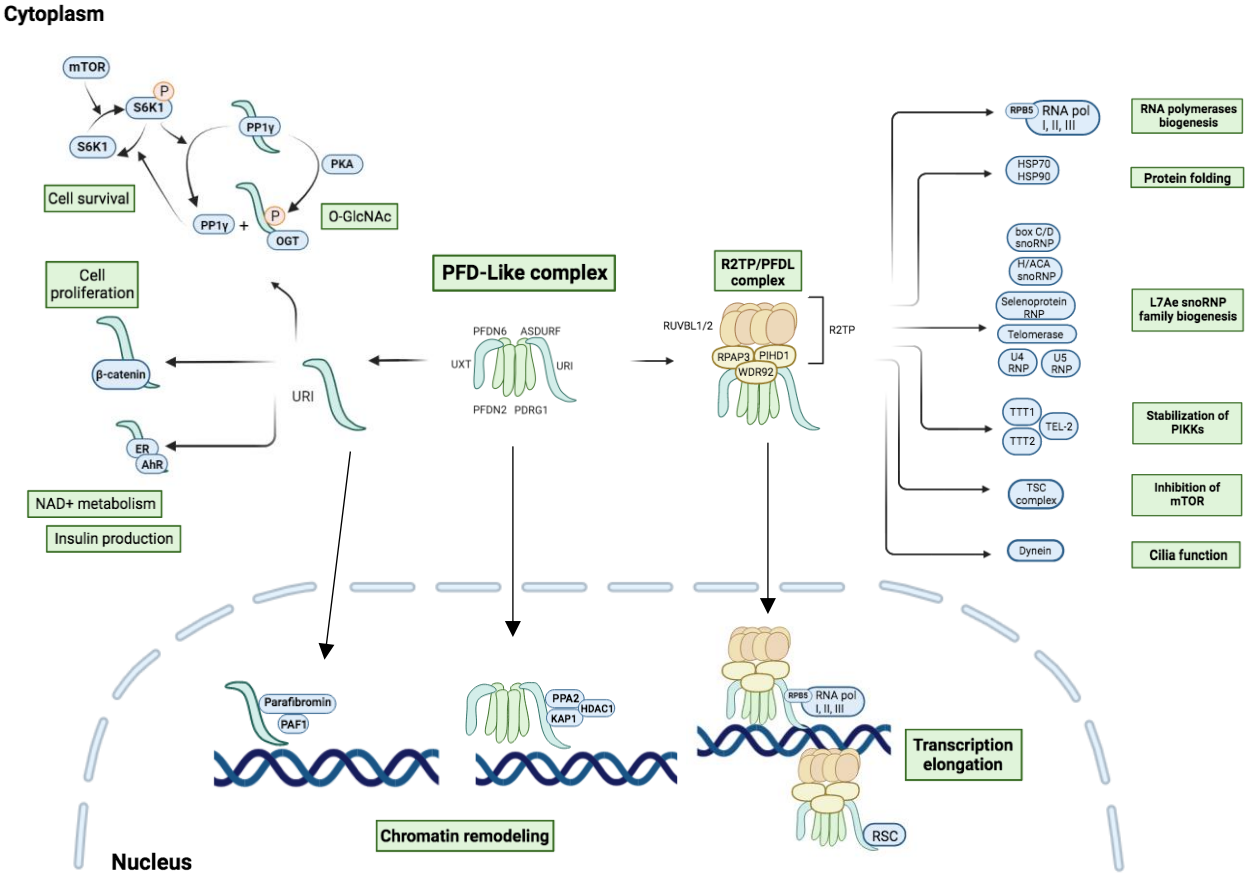
Cytoplasm
mTOR
S6K1
P
S6K1
Cell survival
PP1γ
PKA
PP1γ
+
P
OGT
O-GlcNAc
Cell proliferation
β-catenin
URI
ER
AhR
NAD+ metabolism
Insulin production
PFD-Like complex
PFDN6
ASDURF
UXT
URI
PFDN2
PDRG1
R2TP/PFDL complex
RUVBL1/2
R2TP
RPAP3
PIHD1
WDR92
RPB5
RNA pol I, II, III
RNA polymerases biogenesis
HSP70
HSP90
Protein folding
box C/D snoRNP
H/ACA snoRNP
Selenoprotein RNP
Telomerase
U4 RNP
U5 RNP
L7Ae snoRNP family biogenesis
TTT1
TTT2
TEL-2
Stabilization of PIKKs
TSC complex
Inhibition of mTOR
Dynein
Cilia function
Parafibromin
PAF1
PPA2
KAP1
HDAC1
RPB5
RNA pol I, II, III
Transcription elongation
RSC
Chromatin remodeling
Nucleus

Figure 3. PFDL complex in mammals. Together with the R2TP, the PFDLc forms the R2TP/PFDL complex, which is involved in various mechanisms as cochaperone of HSP90, mainly involving the assembly of a variety of protein complexes such as RNA polymerases, the L7Ae snoRNP family of ribonucleoproteins, PIKK, or dyneins in cilia. R2TP/PFDL also plays a role in the nuclei by promoting transcription elongation through its interaction with polymerases and chromatin remodelling complexes such as RSC. The PFDL complex is involved in chromatin remodelling by binding KAP1 and PPA2 together to enable regulation of the histone deacetylase HDAC1. URI itself has other functions outside the PFDL complex. URI influences cell proliferation by binding β-catenin, preventing its translocation to the nucleus, and cell survival thanks to its relationship with PP1γ. It also influences post-translational modifications such as O-glucosyl-N-acetylation of proteins such as c-Myc through its PKA-dependent interaction with OGT. Loss of URI is associated with an increase in DNA damage that impairs NAD+ metabolism by binding AhR and ER receptors, thus impairing insulin production in pancreatic beta cells. In the nucleus, URI is associated with interaction with the PAF1 complex and parafibromin for chromatin remodelling. Figure modified from Herranz-Montoya *et al,* 2021.

URI is also a target of another master kinase in response to nutrient availability, PKA. When glucose is scarce, PKA phosphorylates URI causing its dissociation of PP1γ, which allows URI to interact with and inhibit the O-GlcNAc transferase OGT (Burén *et al*. 2016). The reduced activity of OGT destabilizes c-Myc, conferring cell survival under limited resources. The regulation of PP1γ, and OGT by URI is important for cell adaptation to low glucose, to cope with low energy stress (Chaves-Perez *et al.* 2019). It is important to note that URI, in turn, can regulate mTOR signalling. The R2TP/PFDLc, in which URI is involved, is able to sense the energy state of the cell thanks to the RuvBL1/2 ATPases (Kim *et al*., 2013), thus controling cell growth and proliferation by promoting the assembly and stability of mTOR complexes (Hořejší *et al*. 2010) (Figure 3). In summary, URI is an evolutionarily conserved component of a signalling pathway that coordinates nutrient availability and gene expression and ultimately controls cell metabolism, growth, survival, and proliferation.

Considering this information, **Chapter 3** examines the response of the *Arabidopsis* URI1 under a variety of stresses to determine whether it is involved in the plant response to stress, particularly to low energy stress.

REFERENCES

Ahmad, M., Afrin, F., & Tuteja, R. (2013). Identification of R2TP complex of Leishmania donovani and Plasmodium falciparum using genome wide in-silico analysis. *Communicative & integrative biology*, *6*(6), e26005.

Antonio, L. M., Martins, G. H., Aragão, A. Z. B., Quel, N. G., Zazeri, G., Houry, W. A., & Ramos, C. H. I. (2023). Unveiling the Role of Sorghum RPAP3 in the Function of R2TP Complex: Insights into Protein Assembly in Plants. *Plants (Basel, Switzerland)*, *12*(16), 2925.

Baena-González, E. (2010). Energy signalling in the regulation of gene expression during stress. Molecular Plant, 3(2), 300–313.

Balchin, D., Hayer-Hartl, M., & Hartl, F. U. (2016). In vivo aspects of protein folding and quality control. Science (New York, N.Y.), 353(6294), aac4354.

Bauer, A., Chauvet, S., Huber, O., Usseglio, F., Rothbächer, U., Aragnol, D., Kemler, R., & Pradel, J. (2000). Pontin52 and reptin52 function as antagonistic regulators of beta-catenin signalling activity. *The EMBO journal*, *19*(22), 6121–6130.

Benbahouche, N.H., Iliopoulos, I., Török, I., Marhold, J., Henri, J., Kajava, A. V., Farkaš, R., Kempf, T., Schnölzer, M., Meyer, P., Kiss, I., Bertrand, E., Mechler, B. M., & Pradet-Balade, B. (2014). Drosophila Spag is the homolog of RNA polymerase II-associated protein 3 (RPAP3) and recruits the heat shock proteins 70 and 90 (Hsp70 and Hsp90) during the assembly of cellular machineries. *The Journal of biological chemistry*, *289*(9), 6236–6247.

Boulon, S., Marmier-Gourrier, N., Pradet-Balade, B., Wurth, L., Verheggen, C., Jády, B. E., Rothé, B., Pescia, C., Robert, M. C., Kiss, T., Bardoni, B., Krol, A., Branlant, C., Allmang, C., Bertrand, E., & Charpentier, B. (2008) The Hsp90 chaperone controls the biogenesis of L7Ae RNPs through conserved machinery. *The Journal of cell biology*, *180*(3), 579–595.

Boulon, S., Pradet-Balade, B., Verheggen, C., Molle, D., Boireau, S., Georgieva, M., Azzag, K., Robert, M. C., Ahmad, Y., Neel, H., Lamond, A. I., & Bertrand, E. (2010) HSP90 and its R2TP/Prefoldin-like cochaperone are involved in the cytoplasmic assembly of RNA polymerase II. *Molecular cell*, *39*(6), 912–924.

Burén, S., Gomes, A. L., Teijeiro, A., Fawal, M. A., Yilmaz, M., Tummala, K. S., Perez, M., Rodriguez-Justo, M., Campos-Olivas, R., Megías, D., & Djouder, N. (2016). Regulation of OGT by URI in Response to Glucose Confers c-MYC-Dependent Survival Mechanisms. *Cancer cell*, *30*(2), 290–307.

Carter, D. R., Buckle, A. D., Tanaka, K., Perdomo, J., & Chong, B. H. (2014). Art27 interacts with GATA4, FOG2 and NKX2.5 and is a novel co-repressor of cardiac genes. *PloS one*, *9*(4), e95253.

Chaves-Pérez, A., Thompson, S., & Djouder, N. (2018). Roles and Functions of the Unconventional Prefoldin URI. Advances in experimental medicine and biology, 1106, 95–108.

Chaves-Pérez, A., Yilmaz, M., Perna, C., de la Rosa, S., & Djouder, N. (2019). URI is required to maintain intestinal architecture during ionizing radiation. *Science (New York, N.Y.)*, *364*(6443), eaaq1165.

Chávez, S., & Puerto-Camacho, P. (2016). Prefoldins. In eLS. John Wiley & Sons, Ltd. (Ed.).

Chen, D., Tao, X., Zhou, L., Sun, F., Sun, M., & Fang, X. (2018). Spaghetti, a homolog of human RPAP3 (RNA polymerase II-associated protein 3), determines the fate of germline stem cells in Drosophila ovary. *Cell biology international*, *42*(7), 769–780.

Chen, S., Chen, K., Zhang, Q., Cheng, H., & Zhou, R. (2013). Regulation of the transcriptional activation of the androgen receptor by the UXT-binding protein VHL. *The Biochemical journal*, *456*(1), 55–66.

Cieśla, M., Makała, E., Płonka, M., Bazan, R., Gewartowski, K., Dziembowski, A., & Boguta, M. (2015). Rbs1, a new protein implicated in RNA polymerase III biogenesis in yeast Saccharomyces cerevisiae. *Molecular and cellular biology*, *35*(7), 1169–1181.

Cloutier, P., & Coulombe, B. (2010). New insights into the biogenesis of nuclear RNA polymerases?. *Biochemistry and cell biology, 88*(2), 211–221.

Cloutier, P., Al-Khoury, R., Lavallée-Adam, M., Faubert, D., Jiang, H., Poitras, C., Bouchard, A., Forget, D., Blanchette, M., & Coulombe, B. (2009) High-resolution mapping of the protein interaction network for the human transcription machinery and affinity purification of RNA polymerase II-associated complexes. Methods (San Diego, Calif.), 48(4), 381–386.

Cloutier, P., Poitras, C., Durand, M., Hekmat, O., Fiola-Masson, É., Bouchard, A., Faubert, D., Chabot, B., & Coulombe, B. (2017) R2TP/Prefoldin-like component RUVBL1/RUVBL2 directly interacts with ZNHIT2 to regulate assembly of U5 small nuclear ribonucleoprotein. *Nature communications*, *8*, 15615.

Cloutier, P., Poitras, C., Faubert, D., Bouchard, A., Blanchette, M., Gauthier, M. S., & Coulombe, B. (2020). Upstream ORF-Encoded ASDURF Is a Novel Prefoldin-like Subunit of the PAQosome. *Journal of proteome research*, *19*(1), 18–27.

Cuevas-Bermúdez, A., Martínez-Fernández, V., Garrido-Godino, A. I., Jordán-Pla, A., Peñate, X., Martín-Expósito, M., Gutiérrez, G., Govind, C. K., Chávez, S., Pelechano, V., & Navarro, F. (2023). The association of the RSC remodeler complex with chromatin is influenced by the prefoldin-like Bud27 and determines nucleosome positioning and polyadenylation sites usage in Saccharomyces cerevisiae. Biochimica et biophysica acta. Gene regulatory mechanisms, 1867(1), 194995. Advance online publication.

Delgermaa, L., Hayashi, N., Dorjsuren, D., Nomura, T., Thuy, leT. T., & Murakami, S. (2004). Subcellular localization of RPB5-mediating protein and its putative functional partner. *Molecular and cellular biology*, *24*(19), 8556–8566.

Deplazes, A., Möckli, N., Luke, B., Auerbach, D., & Peter, M. (2009). Yeast Uri1p promotes translation initiation and may provide a link to cotranslational quality control. *The EMBO journal*, *28*(10), 1429–1441.

Djouder, N., Metzler, S. C., Schmidt, A., Wirbelauer, C., Gstaiger, M., Aebersold, R., Hess, D., & Krek, W. (2007). S6K1-mediated disassembly of mitochondrial URI/PP1gamma complexes activates a negative feedback program that counters S6K1 survival signalling. Molecular cell, 28(1), 28–40.

Dorjsuren, D., Lin, Y., Wei, W., Yamashita, T., Nomura, T., Hayashi, N., & Murakami, S. (1998). RMP, a novel RNA polymerase II subunit 5-interacting protein, counteracts transactivation by hepatitis B virus X protein. *Molecular and cellular biology*, *18*(12), 7546–7555.

Gestaut D, Roh SH, Ma B, Pintilie G, Joachimiak LA, Leitner A, Walzthoeni T, Aebersold R, Chiu W, Frydman J (2019). The chaperonin TRiC/CCT associates with prefoldin through a conserved electrostatic interface essential for cellular proteostasis. Cell 177**:**751–765 e15

Giot, L., Bader, J. S., Brouwer, C., Chaudhuri, A., Kuang, B., Li, Y., Hao, Y. L., Ooi, C. E., Godwin, B., Vitols, E., Vijayadamodar, G., Pochart, P., Machineni, H., Welsh, M., Kong, Y.,

Zerhusen, B., Malcolm, R., Varrone, Z., Collis, A., Minto, M., Rothberg, J. M. (2003). A protein interaction map of Drosophila melanogaster. *Science (New York, N.Y.)*, *302*(5651), 1727–1736.

Gonzales, F. A., Zanchin, N. I., Luz, J. S., & Oliveira, C. C. (2005). Characterization of Saccharomyces cerevisiae Nop17p, a novel Nop58p-interacting protein that is involved in Pre-rRNA processing. Journal of molecular biology, 346(2), 437–455.

Gorynia, S., Bandeiras, T. M., Pinho, F. G., McVey, C. E., Vonrhein, C., Round, A., Svergun, D. I., Donner, P., Matias, P. M., & Carrondo, M. A. (2011). Structural and functional insights into a dodecameric molecular machine - the RuvBL1/RuvBL2 complex. *Journal of structural biology*, *176*(3), 279–291.

Gstaiger, M., Luke, B., Hess, D., Oakeley, E. J., Wirbelauer, C., Blondel, M., Vigneron, M., Peter, M., & Krek, W. (2003). Control of nutrient-sensitive transcription programs by the unconventional prefoldin URI. *Science (New York, N.Y.)*, *302*(5648), 1208–1212.

Gutiérrez-Santiago, F., Cintas-Galán, M., Martín-Expósito, M., Del Carmen Mota-Trujillo, M., Cobo-Huesa, C., Perez-Fernandez, J., & Navarro Gómez, F. (2022). A High-Copy Suppressor Screen Reveals a Broad Role of Prefoldin-like Bud27 in the TOR Signaling Pathway in *Saccharomyces cerevisiae*. *Genes*, *13*(5), 748.

Hartl, F. U., & Hayer-Hartl, M. (2002). Molecular chaperones in the cytosol: from nascent chain to folded protein. Science (New York, N.Y.), 295(5561), 1852–1858.

Herranz-Montoya, I., Park, S., & Djouder, N. (2021). A comprehensive analysis of prefoldins and their implication in cancer. iScience, 24(11), 103273.

Houry, W. A., Bertrand, E., & Coulombe, B. (2018). The PAQosome, an R2TP-Based Chaperone for Quaternary Structure Formation. *Trends in biochemical sciences*, *43*(1), 4–9.

Hořejší, Z., Takai, H., Adelman, C. A., Collis, S. J., Flynn, H., Maslen, S., Skehel, J. M., de Lange, T., & Boulton, S. J. (2010). CK2 phospho-dependent binding of R2TP complex to TEL2 is essential for mTOR and SMG1 stability. *Molecular cell*, *39*(6), 839–850.

Hořejší, Z., Stach, L., Flower, T. G., Joshi, D., Flynn, H., Skehel, J. M., O'Reilly, N. J., Ogrodowicz, R. W., Smerdon, S. J., & Boulton, S. J. (2014). Phosphorylation-dependent PIH1D1 interactions define substrate specificity of the R2TP cochaperone complex. *Cell reports*, *7*(1), 19–26.

Huot, B., Yao, J., Montgomery, B. L., & He, S. Y. (2014). Growth-defense tradeoffs in plants: a balancing act to optimize fitness. Molecular Plant, 7(8), 1267–1287.

Ikura, T., Ogryzko, V. V., Grigoriev, M., Groisman, R., Wang, J., Horikoshi, M., Scully, R., Qin, J., & Nakatani, Y. (2000). Involvement of the TIP60 histone acetylase complex in DNA repair and apoptosis. *Cell*, *102*(4), 463–473.

Inoue, M., Saeki, M., Egusa, H., Niwa, H., & Kamisaki, Y. (2010). PIH1D1, a subunit of R2TP complex, inhibits doxorubicin-induced apoptosis. *Biochemical and biophysical research communications*, *403*(3-4), 340–344.

Jeronimo, C., Forget, D., Bouchard, A., Li, Q., Chua, G., Poitras, C., Thérien, C., Bergeron, D., Bourassa, S., Greenblatt, J., Chabot, B., Poirier, G. G., Hughes, T. R., Blanchette, M., Price, D. H., & Coulombe, B. (2007). Systematic analysis of the protein interaction network for the human transcription machinery reveals the identity of the 7SK capping enzyme. *Molecular cell*, *27*(2), 262–274.

Jiang, L., Luo, X., Shi, J., Sun, H., Sun, Q., Sheikh, M. S., & Huang, Y. (2011). PDRG1, a novel tumor marker for multiple malignancies that is selectively regulated by genotoxic stress. *Cancer biology & therapy*, *11*(6), 567–573.

Jiménez, B., Ugwu, F., Zhao, R., Ortí, L., Makhnevych, T., Pineda-Lucena, A., & Houry, W. A. (2012). Structure of minimal tetratricopeptide repeat domain protein Tah1 reveals mechanism of its interaction with Pih1 and Hsp90. *The Journal of biological chemistry*, *287*(8), 5698–5709.

Jonsson, Z. O., Dhar, S. K., Narlikar, G. J., Auty, R., Wagle, N., Pellman, D., Pratt, R. E., Kingston, R., & Dutta, A. (2001). Rvb1p and Rvb2p are essential components of a chromatin remodeling complex that regulates transcription of over 5% of yeast genes. *The Journal of biological chemistry*, *276*(19), 16279–16288.

Kanemaki, M., Kurokawa, Y., Matsu-ura, T., Makino, Y., Masani, A., Okazaki, K., Morishita, T., & Tamura, T. A. (1999). TIP49b, a new RuvB-like DNA helicase, is included in a complex together with another RuvB-like DNA helicase, TIP49a. *The Journal of biological chemistry*, *274*(32), 22437–22444.

Kim, J. H., Kim, B., Cai, L., Choi, H. J., Ohgi, K. A., Tran, C., Chen, C., Chung, C. H., Huber, O., Rose, D. W., Sawyers, C. L., Rosenfeld, M. G., & Baek, S. H. (2005). Transcriptional regulation of a metastasis suppressor gene by Tip60 and beta-catenin complexes. *Nature*, *434*(7035), 921–926.

Kim, S. G., Hoffman, G. R., Poulogiannis, G., Buel, G. R., Jang, Y. J., Lee, K. W., Kim, B. Y., Erikson, R. L., Cantley, L. C., Choo, A. Y., & Blenis, J. (2013). Metabolic stress controls mTORC1 lysosomal localization and dimerization by regulating the TTT-RUVBL1/2 complex. Molecular cell, 49(1), 172–185.

Kirchner, J., Vissi, E., Gross, S., Szoor, B., Rudenko, A., Alphey, L., & White-Cooper, H. (2008). Drosophila Uri, a PP1alpha binding protein, is essential for viability, maintenance of DNA integrity and normal transcriptional activity. *BMC molecular biology*, *9*, 36.

Kong, X., Ma, S., Guo, J., Ma, Y., Hu, Y., Wang, J., & Zheng, Y. (2015). Ubiquitously expressed transcript is a novel interacting protein of protein inhibitor of activated signal transducer and activator of transcription 2. *Molecular medicine reports*, *11*(4), 2443–2448.

Krogan, N. J., Keogh, M. C., Datta, N., Sawa, C., Ryan, O. W., Ding, H., Haw, R. A., Pootoolal, J., Tong, A., Canadien, V., Richards, D. P., Wu, X., Emili, A., Hughes, T. R., Buratowski, S., & Greenblatt, J. F. (2003). A Snf2 family ATPase complex required for recruitment of the histone H2A variant Htz1. *Molecular cell*, *12*(6), 1565–1576.

Le, T. T., Zhang, S., Hayashi, N., Yasukawa, M., Delgermaa, L., & Murakami, S. (2005). Mutational analysis of human RNA polymerase II subunit 5 (RPB5): the residues critical for interactions with TFIIF subunit RAP30 and hepatitis B virus X protein. *Journal of biochemistry*, *138*(3), 215–224.

Li, W., Wang, L., Jiang, C., Li, H., Zhang, K., Xu, Y., Hao, Q., Li, M., Xue, X., Qin, X., Zhang, C., Wang, H., Zhang, W., & Zhang, Y. (2014). UXT is a novel regulatory factor of regulatory T cells associated with Foxp3. *European journal of immunology*, *44*(2), 533–544.

Luo, X., Huang, Y., & Sheikh, M. S. (2003). Cloning and characterization of a novel gene PDRG that is differentially regulated by p53 and ultraviolet radiation. *Oncogene*, *22*(46), 7247–7257.

Machado-Pinilla, R., Liger, D., Leulliot, N., & Meier, U. T. (2012) Mechanism of the AAA+ ATPases pontin and reptin in the biogenesis of H/ACA RNPs. *RNA (New York, N.Y.)*, *18*(10), 1833–1845.

Malinova, A., Cvačková, Z., Matějů, D., Hořejší, Z., Abéza, C., Vandermoere, F., Bertrand, E., Staněk, D., & Verheggen, C. (2017) Assembly of the U5 snRNP component PRPF8 is controlled by the HSP90/R2TP chaperones. *The Journal of cell biology*, *216*(6), 1579–1596.

Markus, S. M., Taneja, S. S., Logan, S. K., Li, W., Ha, S., Hittelman, A. B., Rogatsky, I., & Garabedian, M. J. (2002). Identification and characterization of ART-27, a novel coactivator for the androgen receptor N terminus. *Molecular biology of the cell*, *13*(2), 670–682.

Martin-Benito J, Boskovic J, Gomez-Puertas P, Carrascosa JL, Simons CT, Lewis SA, Bartolini F, Cowan NJ, Valpuesta JM (2002) Structure of eukaryotic prefoldin and of its complexes with unfolded actin and the cytosolic chaperonin CCT. EMBO J 21**:**6377–6386

Martínez-Fernández, V., & Navarro, F. (2018). Rpb5, a subunit shared by eukaryotic RNA polymerases, cooperates with prefoldin-like Bud27/URI. *AIMS genetics*, *5*(1), 63–74.

Martínez-Fernández, V., Cuevas-Bermúdez, A., Gutiérrez-Santiago, F., Garrido-Godino, A. I., Rodríguez-Galán, O., Jordán-Pla, A., Lois, S., Triviño, J. C., de la Cruz, J., & Navarro, F. (2020). Prefoldin-like Bud27 influences the transcription of ribosomal components and ribosome biogenesis in *Saccharomyces cerevisiae*. *RNA (New York, N.Y.)*, *26*(10), 1360–1379.

Martino, F., Pal, M., Muñoz-Hernández, H., Rodríguez, C. F., Núñez-Ramírez, R., Gil-Carton, D., Degliesposti, G., Skehel, J. M., Roe, S. M., Prodromou, C., Pearl, L. H., & Llorca, O. (2018). RPAP3 provides a flexible scaffold for coupling HSP90 to the human R2TP co-chaperone complex. *Nature communications*, *9*(1), 1501.

Means, J. C., Venkatesan, A., Gerdes, B., Fan, J. Y., Bjes, E. S., & Price, J. L. (2015). Drosophila spaghetti and doubletime link the circadian clock and light to caspases, apoptosis and tauopathy. *PLoS genetics*, *11*(5), e1005171.

Mirón-García, M. C., Garrido-Godino, A. I., García-Molinero, V., Hernández-Torres, F., Rodríguez-Navarro, S., & Navarro, F. (2013). The prefoldin bud27 mediates the assembly of the eukaryotic RNA polymerases in an rpb5-dependent manner. *PLoS genetics*, *9*(2), e1003297.

Mirón-García, M. C., Garrido-Godino, A. I., Martínez-Fernández, V., Fernández-Pevida, A., Cuevas-Bermúdez, A., Martín-Expósito, M., Chávez, S., de la Cruz, J., & Navarro, F. (2014). The yeast prefoldin-like URI-orthologue Bud27 associates with the RSC nucleosome remodeler and modulates transcription. *Nucleic acids research*, *42*(15), 9666–9676.

Mita, P., Savas, J. N., Ha, S., Djouder, N., Yates, J. R., 3rd, & Logan, S. K. (2013). Analysis of URI nuclear interaction with RPB5 and components of the R2TP/prefoldin-like complex. *PloS one*, *8*(5), e63879.

Muñoz-Galván, S., Jimeno, S., Rothstein, R., & Aguilera, A. (2013). Histone H3K56 acetylation, Rad52, and non-DNA repair factors control double-strand break repair choice with the sister chromatid. *PLoS genetics*, *9*(1), e1003237.

Ni, L., Saeki, M., Xu, L., Nakahara, H., Saijo, M., Tanaka, K., & Kamisaki, Y. (2009). RPAP3 interacts with Reptin to regulate UV-induced phosphorylation of H2AX and DNA damage. *Journal of cellular biochemistry*, *106*(5), 920–928.

Niewiarowski, A., Bradley, A. S., Gor, J., McKay, A. R., Perkins, S. J., & Tsaneva, I. R. (2010). Oligomeric assembly and interactions within the human RuvB-like RuvBL1 and RuvBL2 complexes. *The Biochemical journal*, *429*(1), 113–125.

Parusel, C. T., Kritikou, E. A., Hengartner, M. O., Krek, W., & Gotta, M. (2006). URI-1 is required for DNA stability in C. elegans. *Development (Cambridge, England)*, *133*(4), 621–629.

Pérez, C., Pérez-Zúñiga, F. J., Garrido, F., Reytor, E., Portillo, F., & Pajares, M. A. (2016). The Oncogene PDRG1 Is an Interaction Target of Methionine Adenosyltransferases. *PloS one*, *11*(8), e0161672.

Prodromou, C. (2016). Mechanisms of Hsp90 regulation. The Biochemical Journal, 473(16), 2439–2452

Qiu, X. B., Lin, Y. L., Thome, K. C., Pian, P., Schlegel, B. P., Weremowicz, S., Parvin, J. D., & Dutta, A. (1998). An eukaryotic RuvB-like protein (RUVBL1) essential for growth. *The Journal of biological chemistry*, *273*(43), 27786–27793.

Quinternet, M., Rothé, B., Barbier, M., Bobo, C., Saliou, J. M., Jacquemin, C., Back, R., Chagot, M. E., Cianférani, S., Meyer, P., Branlant, C., Charpentier, B., & Manival, X. (2015). Structure/Function Analysis of Protein-Protein Interactions Developed by the Yeast Pih1 Platform Protein and Its Partners in Box C/D snoRNP Assembly. *Journal of molecular biology*, *427*(17), 2816–2839.

Sánchez-Morgan, N., Kirsch, K. H., Trackman, P. C., & Sonenshein, G. E. (2017). UXT Is a LOX-PP Interacting Protein That Modulates Estrogen Receptor Alpha Activity in Breast Cancer Cells. *Journal of cellular biochemistry*, *118*(8), 2347–2356.

Schafler, E. D., Thomas, P. A., Ha, S., Wang, Y., Bermudez-Hernandez, K., Tang, Z., Fenyö, D., Vigodner, M., & Logan, S. K. (2018). UXT is required for spermatogenesis in mice. *PloS one*, *13*(4), e0195747.

Schopf, F. H., Biebl, M. M., & Buchner, J. (2017). The HSP90 chaperone machinery. Nature Reviews Molecular Cell Biology, 18(6), 345–360.

Schroer, A., Schneider, S., Ropers, H., & Nothwang, H. (1999). Cloning and characterization of UXT, a novel gene in human Xp11, which is widely and abundantly expressed in tumor tissue. *Genomics*, *56*(3), 340–343.

Shimada, K., Saeki, M., Egusa, H., Fukuyasu, S., Yura, Y., Iwai, K., & Kamisaki, Y. (2011). RPAP3 enhances cytotoxicity of doxorubicin by impairing NF-kappa B pathway. *Biochemical and biophysical research communications*, *404*(4), 910–914.

Siegers K, Waldmann T, Leroux MR, Grein K, Shevchenko A, Schiebel E, Hartl FU (1999) Compartmentation of protein folding in vivo: sequestration of non-native polypeptide by the chaperonin-GimC system. EMBO J 18**:**75–84

Sotta, N., Shantikumar, L., Sakamoto, T., Matsunaga, S., & Fujiwara, T. (2016). TPR5 is involved in directional cell division and is essential for the maintenance of meristem cell organization in *Arabidopsis thaliana*. *Journal of experimental botany*, *67*(8), 2401–2411.

Taneja, S. S., Ha, S., Swenson, N. K., Torra, I. P., Rome, S., Walden, P. D., Huang, H. Y., Shapiro, E., Garabedian, M. J., & Logan, S. K. (2004). ART-27, an androgen receptor coactivator regulated in prostate development and cancer. *The Journal of biological chemistry*, *279*(14), 13944–13952.

Te, J., Jia, L., Rogers, J., Miller, A., & Hartson, S. D. (2007) Novel subunits of the mammalian Hsp90 signal transduction chaperone. *Journal of proteome research*, *6*(5), 1963–1973.

Thomas, P. A., Mita, P., Ha, S., & Logan, S. K. (2018). Role of the Unconventional Prefoldin Proteins URI and UXT in Transcription Regulation. *Advances in experimental medicine and biology*, *1106*, 85–94.

Tian, S., Yu, G., He, H., Zhao, Y., Liu, P., Marshall, A. G., Demeler, B., Stagg, S. M., & Li, H. (2017). Pih1p-Tah1p Puts a Lid on Hexameric AAA+ ATPases Rvb1/2p. *Structure (London, England : 1993)*, *25*(10), 1519–1529.e4.

Tummala, K. S., Gomes, A. L., Yilmaz, M., Graña, O., Bakiri, L., Ruppen, I., Ximénez-Embún, P., Sheshappanavar, V., Rodriguez-Justo, M., Pisano, D. G., Wagner, E. F., & Djouder, N. (2014). Inhibition of de novo NAD(+) synthesis by oncogenic URI causes liver tumorigenesis through DNA damage. *Cancer cell*, *26*(6), 826–839.

Vainberg, I. E., Lewis, S. A., Rommelaere, H., Ampe, C., Vandekerckhove, J., Klein, H. L., & Cowan, N. J. (1998). Prefoldin, a chaperone that delivers unfolded proteins to cytosolic chaperonin. Cell, 93(5), 863–873.

Wei, W., Gu, J. X., Zhu, C. Q., Sun, F. Y., Dorjsuren, D., Lin, Y., & Murakami, S. (2003). Interaction with general transcription factor IIF (TFIIF) is required for the suppression of activated transcription by RPB5-mediating protein (RMP). *Cell research*, *13*(2), 111–120.

Yang, Y., Liu, F., Liu, L., Zhu, M., Yuan, J., Mai, Y. X., Zou, J. J., Le, J., Wang, Y., Palme, K., Li, X., Wang, Y., & Wang, L. (2022). The unconventional prefoldin RPB5 interactor mediates the gravitropic response by modulating cytoskeleton organization and auxin transport in *Arabidopsis*. *Journal of integrative plant biology*, *64*(10), 1916–1934.

Yart, A., Gstaiger, M., Wirbelauer, C., Pecnik, M., Anastasiou, D., Hess, D., & Krek, W. (2005). The HRPT2 tumor suppressor gene product parafibromin associates with human PAF1 and RNA polymerase II. *Molecular and cellular biology*, *25*(12), 5052–5060.

Yoon, M. J., Choi, B., Kim, E. J., Ohk, J., Yang, C., Choi, Y. G., Lee, J., Kang, C., Song, H. K., Kim, Y. K., Woo, J. S., Cho, Y., Choi, E. J., Jung, H., & Kim, C. (2021). UXT chaperone prevents proteotoxicity by acting as an autophagy adaptor for p62-dependent aggrephagy. *Nature communications*, *12*(1), 1955.

Zhao, R., Davey, M., Hsu, Y. C., Kaplanek, P., Tong, A., Parsons, A. B., Krogan, N., Cagney, G., Mai, D., Greenblatt, J., Boone, C., Emili, A., & Houry, W. A. (2005) Navigating the chaperone network: an integrative map of physical and genetic interactions mediated by the hsp90 chaperone. *Cell*, *120*(5), 715–727.

Zhao, R., Kakihara, Y., Gribun, A., Huen, J., Yang, G., Khanna, M., Costanzo, M., Brost, R. L., Boone, C., Hughes, T. R., Yip, C. M., & Houry, W. A. (2008) Molecular chaperone Hsp90 stabilizes Pih1/Nop17 to maintain R2TP complex activity that regulates snoRNA accumulation. *The Journal of cell biology*, *180*(3), 563–578.

Zhou, Y., Ge, R., Wang, R., Liu, F., Huang, Y., Liu, H., Hao, Y., Zhou, Q., & Wang, C. (2015). UXT potentiates angiogenesis by attenuating Notch signalling. *Development (Cambridge, England)*, *142*(4), 774–786.

Zhou, C. Y., Stoddard, C. I., Johnston, J. B., Trnka, M. J., Echeverria, I., Palovcak, E., Sali, A., Burlingame, A. L., Cheng, Y., & Narlikar, G. J. (2017). Regulation of Rvb1/Rvb2 by a Domain within the INO80 Chromatin Remodeling Complex Implicates the Yeast Rvbs as Protein Assembly Chaperones. *Cell reports*, *19*(10), 2033–2044.

Zhu, J. K. (2016). Abiotic Stress Signalling and Responses in Plants. Cell, 167(2), 313–324.

Zur Lage, P., Stefanopoulou, P., Styczynska-Soczka, K., Quinn, N., Mali, G., von Kriegsheim, A., Mill, P., & Jarman, A. P. (2018). Ciliary dynein motor preassembly is regulated by Wdr92 in association with HSP90 co-chaperone, R2TP. *The Journal of cell biology*, *217*(7), 2583–2598.

OBJECTIVES

Due to their dual role as signaling elements and co-chaperones of Hsp90, the PFDL complex, and in particular its subunit URI1 have emerged as central components for cellular homeostasis in response to environmental stress in animals. Focusing on URI1, we have tested the hypothesis that it participates in the signaling pathways connecting stress and growth responses, in particular low energy stress, in plants. To test our hypothesis, we have pursued the following objectives:

1. **To identify URI1-dependent cellular pathways**. To accomplish this goal, we performed a basic analysis of URI1 function in *Arabidopsis* using the *uri1-1* mutant, including transcriptomic analysis. We complemented the genetic analysis by identifying the URI1 *in vivo* interactome.

2. **To identify the molecular basis of URI1 functional versatility.** URI is a very versatile protein according to the roles defined in animals and yeast. However, the molecular basis of this versatility was unknown. We found that *Arabidopsis* URI has an intrinsically disordered region and hypothesized that it confers URI1 with functional versatility.

3. **To explore the possible role of URI1 in low energy stress signaling.** URI is involved in the pathway triggered by energy stress in animals and yeast, and we hypothesize that this role is also conserved in plants. Given the central role of TOR in energy status signaling in eukaryotes and the fact that URI1 acts in the TOR pathway in animals and yeast, we investigated the possible functional relationship between URI1 and the TOR pathway in *Arabidopsis*.

CHAPTER I.

GENETIC AND BIOCHEMICAL APPROACHES REVEAL THE CELLULAR PATHWAYS OF URI1

URI1 protein is evolutionary highly conserved.

In order to retrieve the putative URI1 sequences from yeast, animals and a range of different plant species, we used the Translated Nucleotide Basic Local Alignment Search tool (TBLASTN) to search in the NCBI, Phytozome and OneKP databases, using as a query the amino acid sequence of the URI1 protein encoded in the *H. sapiens* genome for yeast and mammals, and the URI1 protein encoded in the *A. thaliana* (*Arabidopsis*) genome for the plant species analysed. Only sequences resembling a full length URI1 protein were considered for subsequent analyses. After aligning all the URI1 protein sequences, amino acid sequences were manually curated to obtain an unambiguously aligned column. The resulting trimmed alignment contained 13 URI1 sequences and it was used to infer a Maximum-likelihood phylogenetic tree (Figure 1A). This phylogenetic analysis showed that URI1 is a protein conserved in eukaryotes. Moreover, the URI1 proteins appear to be encoded by a single-copy gene in all the species analysed.

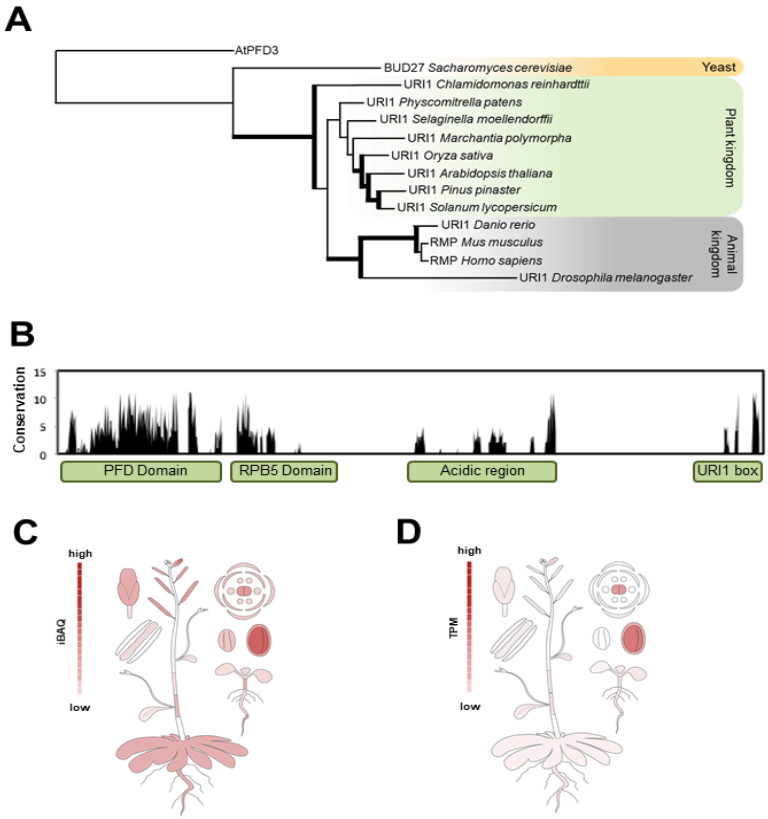

Figure 1. URI1 protein is evolutionary highly conserved and expressed along *Arabidopsis* plants. **A.** URI1 maximum-likelihood phylogenetic tree using representative species of yeast, plants and animals. Branch thickness represents branch support by bootstrap. **B.** Amino acid conservation though URI1 protein from sequences used for maximum-likelihood phylogenetic tree inference (A). **C and D**, Figures obtained from ProteomicsDB showing: **C**, Protein URI1 detection calculated using intensity-based absolute quantification (iBAQ) showing that URI1 is expressed in different *Arabidopsis* tissues. **D**, mRNA of *URI1* detection using Transcripts Per Milion (TPM) showing highest expression in the seeds.

The URI1 protein sequences presented conserved domains and regions (Figure 1B), such as the PFD domain, indicating that URI1 is a Prefoldin-like protein, the RPB5-interacting

domain, which is required for the interaction with the RPB5 subunit common of nuclear RNA polymerases (Dorjsuren *et al.,* 1998), and the URI1 box with unknown function.

Since at the time when I started this work the function of URI1 was unknown in plants, we started to analyse the *in silico* expression pattern of the protein and mRNA in *Arabidopsis* using the ProteomicsDB resources. The URI1 protein was present throughout the plant, but showed its maximum in the carpels, in the ovule of the embryo sac and in the seed (at the imbibition stage) (Figure 1C, Supp Table 1). Although URI1 protein was found in almost all tissues in *Arabidopsis*, *URI1* mRNA expression was mainly localised in the ovule of the embryo sac and in the seed (at the imbibition stage and at the dry stage), while *URI1* mRNA expression was relatively low in the carpels, shoot axis node and hypocotyl of the seedling (Figure 1D, Supp Table 2).

GUS reporter lines reveals *URI1* tissue-specific expression pattern.

To start exploring the role that URI1 performs in *Arabidopsis*, we decided to generate different reporter lines to detect the spatial expression of URI1. To determine the promoter activity of *URI1 (At1g03760)*, firstly a fragment of 1307 bp between gene *At1g03770* and *At103760* were cloned without taking the ATG of *At1g03770* (Figure 2). Then, GUS promoter fusion lines were prepared as described in Material and Methods. We analysed three independent promoter fusion lines for *pURI1::GUS*. The activity of the *URI1* promoter was consistent in all three lines analysed. In the aerial part of the seedling, the expression of *pURI1::GUS* was highest in the vascular tissue of the hypocotyl and cotyledons, in the guard cells, in the stipules and in the cotyledon tips (Figure 3A, 3B, 3C, 3D and 3E, respectively). In the root, the strongest *pURI1::GUS* signal was observed in the transition zone between the hypocotyl and the root (Figure 3A). In adult plants (30-day-old), the GUS signal was observed in the vascular tissue of rosette leaves, in trichomes and in the stigma, septum, and style of fruits (Figure 3F, 3G, 3H and 3I, respectively).

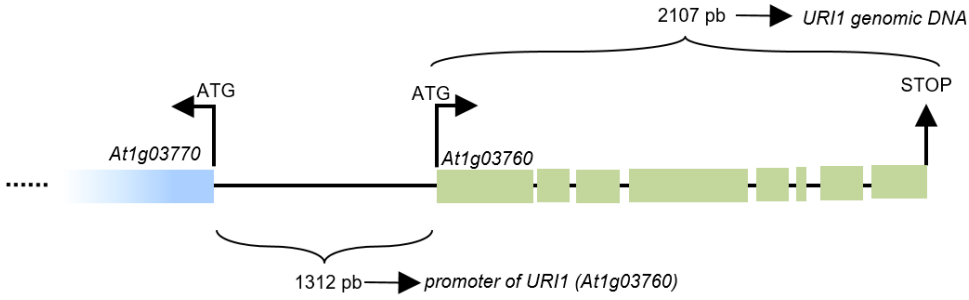

Figure 2. Schematic representation of the regions cloned and used as promoter and genomic DNA for URI1 (*At1g03760*). *At1g03760* is the gene encoding URI1, and it is very close to *At1g03770*. The promoter sequence for URI1 was considered to be the region between the two genes without retaining the ATG of *At1g03770*, totalling 1312 bp. The genomic DNA of URI1 contains 2107 bp from the ATG to the STOP codon. These two regions were used to generate all constructs used in this work.

In the context of the cotyledon tip and stipules, the detected signal is typically correlated with the accumulation of auxin (Bai *et al.,* 2008), suggesting a possible involvement of URI1 in auxin pathway. Auxin is a phytohormone that regulates cell division, cell elongation, cell differentiation, and patterning (Sachs, 1991). In fact, URI1 has been recently shown to regulate the trafficking and localisation of the PIN auxin transporters in *Arabidopsis* (Yang *et al.,* 2022). Altogether, these results indicate that *URI1* might be active in different tissue and cell types during *Arabidopsis* development.

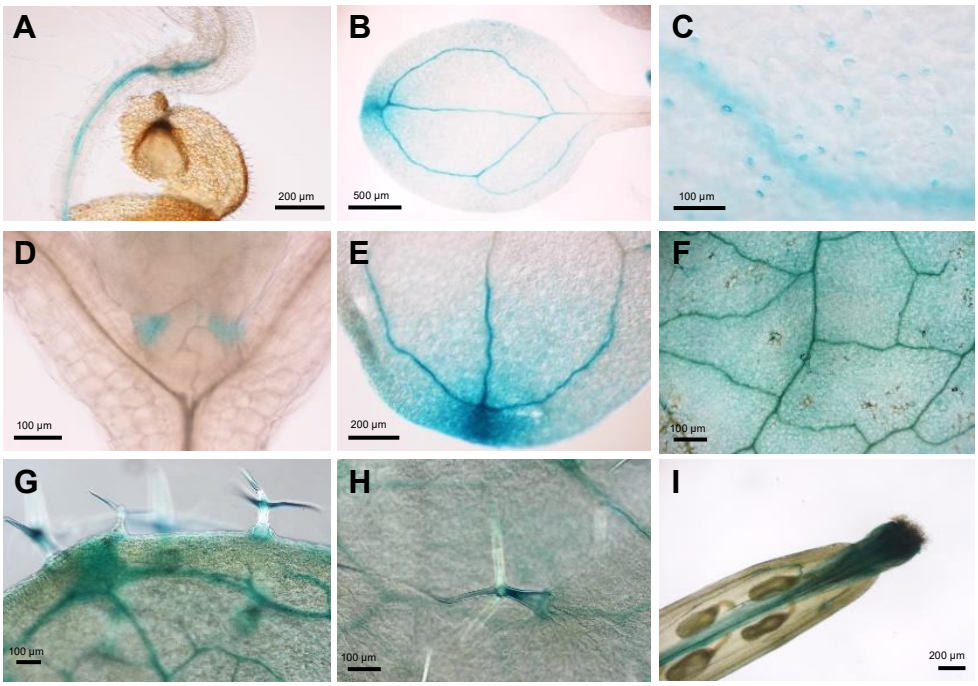

Figure 3. *pURI1* is active in different *Arabidopsis* tissues. **A.** Transition zone between hypocotyl and root. **B.** Cotyledons vascular tissue. **C.** Guard cells. **D.** Stipules. **E.** Cotyledon tips. **F.** Vascular tissue from rossette leaves. **G and H.** Trichomes. **I.** Stigma, style and septum. Scale bar is marked on each image.

URI1 protein localises both in the cytoplasm and nucleus.

To determine the cellular localisation of URI1, we fused URI1 to YFP under the control of a constitutive promoter (*p35S*) and expressed this construct transiently in *Nicotiana benthamiana (N. benthamiana)* leaves. In most cases, we found that the fluorescence corresponding to the full-length URI1 fusion (URI1-WT) was localised simultaneously in the nucleus and cytoplasm (Figure 4B). This subcellular localization is similar to that observed for URI1 orthologs in yeast and mammals (Mirón-Garcia *et al.,* 2013; Delgermaa *et al.*, 2004; Mita *et al*., 2011). The nuclear localization was striking to us because although the mammalian URI1 protein has Nuclear Localisation Signal (NLS) sequences, the NLS are absent in *Arabidopsis* URI1 (Yang *et al.,* 2022), suggesting that the nuclear localization of URI1 is supported by a partner protein or that it has non-canonical NLS.

The absence of NLS signals prompted us to identify the part of URI1 responsible for its nuclear localisation. As explained in the Introduction, URI1 has 4 regions identified: the PFD domain, the RPB5 domain, an aspartic acid-rich region, and the URI1 box (Figure 4A). To examine the contribution of the different parts of the protein to the subcellular pattern of URI1, especially to the nuclear localization, we fused three deleted versions of URI1 to YFP. The first contained only the PFD domain (URI1-PFD domain), the second contained the RPB5 domain, the acidic region

and the URI1 box (URI1-ΔPFD), and the third lacked the Uri1 box (URI1-ΔURI1 box). Each fusion was expressed under the constitutive *35S* promoter. We found that the fluorescence distribution corresponding to the URI1-PFD and URI1-ΔURI1 box fusions was similar to that of the full-length protein, i.e. it was located into the nucleus and cytoplasm (Figure 4B). In contrast, the fluorescence of the URI1-ΔPFD fusion was exclusively located in the cytoplasm, suggesting that the PFD domain is required for URI1 nuclear localisation (Figure 4B). As mentioned earlier, there are two possibilities: first, that there is a non-canonical NLS in the PFD domain. And second, that this domain is required for interaction with a partner present in *N. benthamiana* cells that carries URI1 into the nucleus.

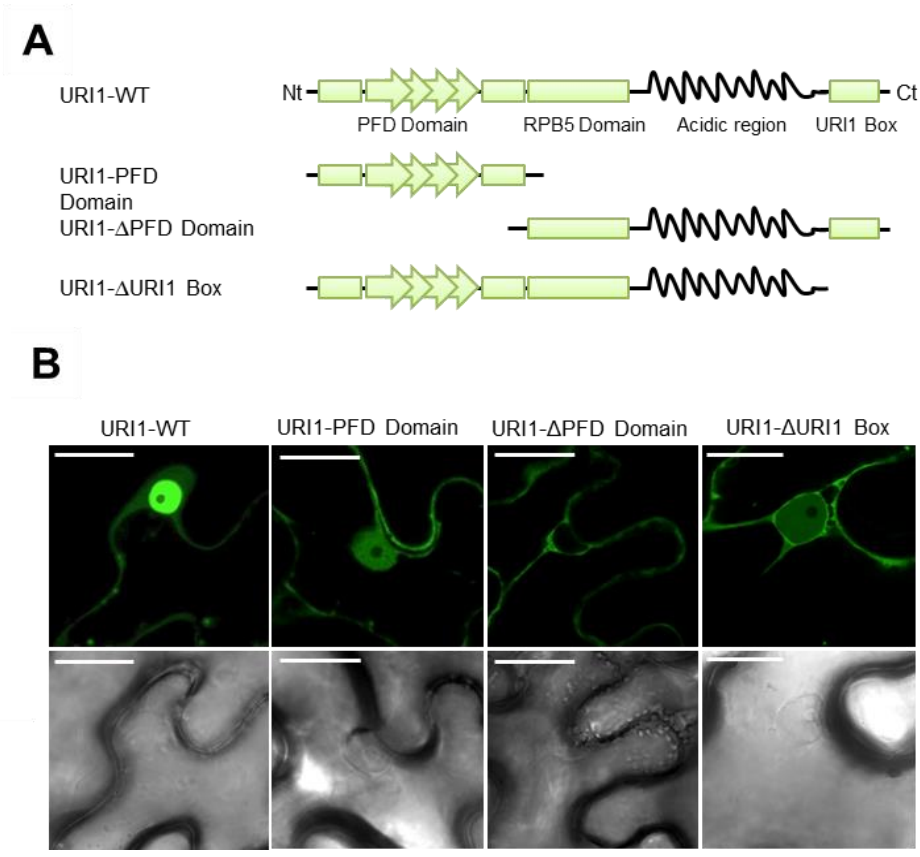

Figure 4. YFP-URI1 transition expression showed signal in nuclei and cytoplasm of *N. benthamiana* leaves. **A.** Representation of URI1 protein domains showing the different versions used in this work: WT, PFD domain, ΔPFD Domain and ΔURI1 Box. All this constructions were clonned, fused to YFP and expressed in *N. benthamiana* leaves. **B.** Confocal imaging from *N. benthamiana* leaves expressing *p35S::YFP-URI1 WT*, *p35S::YFP-URI1 PFD Domain*, *p35S::YFP-URI1 ΔPFD Domain* and *p35S::YFP-URI1 ΔURI1 Box* after 3 days of agroinfiltration. Scale bar 25 µm.

To determine the localization of URI1 in *Arabidopsis* under conditions more similar to the endogenous ones, we generated a construct expressing a GFP fused to the C-terminus of URI1 in the genomic context, *pURI1::URI1-GFP* (WT). We grew *pURI1::URI1-GFP* seedlings in vertical plates for five days and were stained with propidium iodide (PI) to easily visualize the root cells and locate the GFP fluorescence under the confocal microscope. We found URI1-GFP mainly in the cytoplasm with a faint signal in the nuclei (Figure 5A). This confirmed the results obtained in *N. benthamiana* and are similar to the localization of URI1 recently reported in *Arabidopsis* (Yang

et al., 2022). The presence of URI1 in nuclei was confirmed by an alternative approach, subcellular cell fractionation. To this end, we prepared a URI1-3xFLAG fusion in the genomic context that complemented the full KO *uri1-2* mutant. Seven-day-old seedlings were used to prepare different subcellular fractions (cytoplasm, nucleoplasm and chromatin) and to check where URI1-3xFLAG was located. We found that URI1-3xFLAG was not only present in the cytoplasm but also in the nucleoplasm and in the chromatin fraction (Figure 5B).

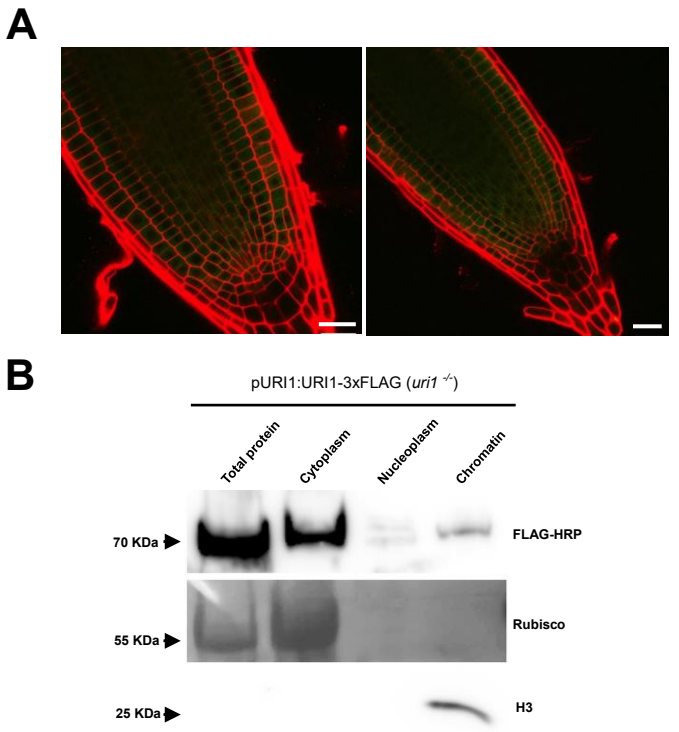

Figure 5. URI1 is expressed in nuclei and cytoplasm in *Arabidopsis* plants. A. Confocal imaging from *pURI1::URI1-GFP* roots of 5-day-old showing GFP signal in cytoplasm and faint signal in the nuclei. Scale bar 25 µm. **B.** Western blot image showing *pURI1::URI1-3xFLAG* subcellular fractionation. URI1-3xFLAG (70 KDa) is detected in total extracts, cytoplasm, nucleoplasm and attached to the chromatin. RuBisCo (55KDa) protein stained with Ponceau S is used as loading control for total extracts and cytoplasm extracts. H3 antibody is used as loading control of chromatin fraction.

URI1 is part of the Prefoldin-like complex in *Arabidopsis*

In animals, URI1 forms the PFDL complex with the prefoldin-like proteins UXT, PDRG1, and ASDURF and the canonical prefoldins PFD2 and PFD6 (Gstaiger *et al.*, 2003; Sardiu *et al*., 2008; Cloutier *et al*., 2020). In *Arabidopsis*, URI1 interacts with PFD2 and PFD6, as shown by yeast 2-hybrid (Y2H) and by co-immunoprecipitation assays (Yang *et al*., 2022). Nevertheless, it remained unknown whether the PFDL complex exists in *Arabidopsis* and URI1 is one of its subunits. To investigate this possibility, we identified the URI1 interactors *in vivo* in *Arabidopsis* PSB-D cell suspensions (Van Leene *et al*., 2015). To this end, we fused to the N-terminal end of URI1 the GS tag, which consists of a protein G tag and the streptavidin binding peptide (Van Leene *et al*., 2015).

Although the GS tag was designed for a two-step affinity purification, we performed a single immunoprecipitation to increase the chance of identifying weak or transient interactions (Figure 6A) (Antosz *et al*., 2017). Transgenic PSB-D cell suspensions expressing GS-URI1 (Figure 6B) or the unfused GS tag (Figure 6D) were prepared and extracts from three biological replicates were subjected to an affinity purification (AP) step using mouse IgG-coated paramagnetic beads (Figure 6C, 6E). Although enough beads were added to the mixture, we still observed GS-URI1 and GS protein in the flow-through (Figure 6C, 6E), indicating that the IgG magnetic beads were fully saturated. Nonetheless, the inmunoprecipitation worked correctly as we found the bait protein after eluting from the magnetic beads. Proteins in the eluates were identified by mass spectrometry (MS) analysis. We only considered proteins for which at least one unique peptide was identified in the three biological replicates, rather than two peptides, and that were not present in the GS control AP-MS list. Among the top interactors, we identified PFD2 and PFD6 in the eluates of GS-URI1 (Figure 7, Supp Table 3, Supp Table 4). We also identified the putative ortholog of the prefoldin-like protein PDRG1 (encoded by the *At3g15351* gene) and two proteins annotated as “Prefoldin

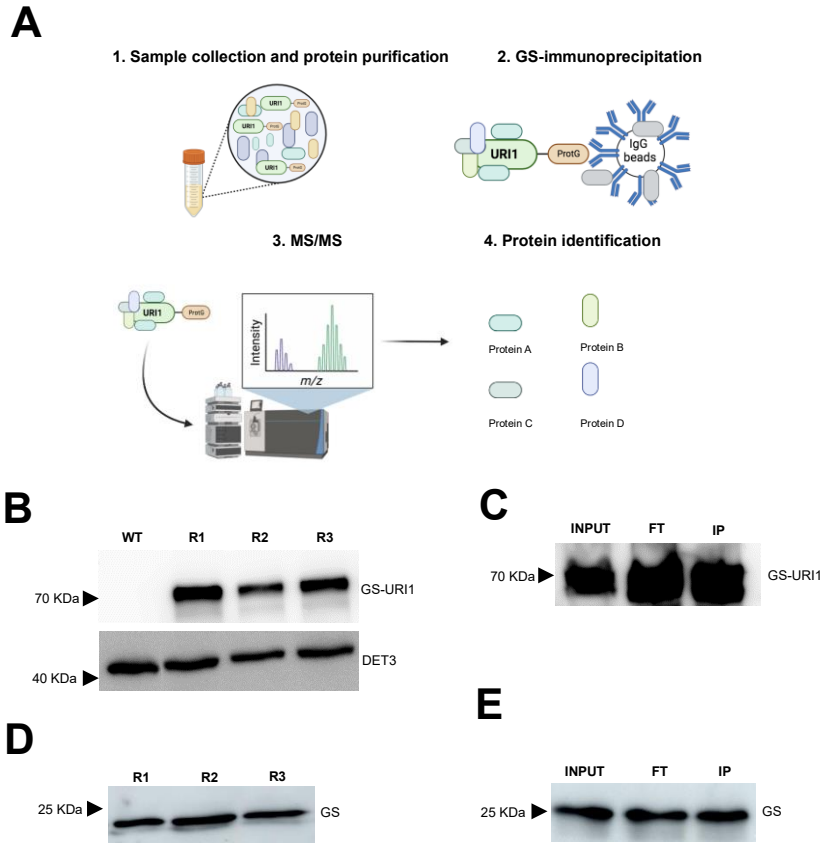

Figure 6. URI1 *in-vivo* interactome definition. A. Flowchart showing the pipeline followed to identify URI1 interactome in-vivo using *A. thaliana* suspension cells. **B.** Western blot showing the expression of GS-URI1 (70 KDa) on the three replicates (R1, R2 and R3) used to identify URI1 i*n-vivo* interactome. DET3 (40 KDa) were used as loading control. **C.** Western blot image showing the GS-URI1 (70 KDa) inmunoprecipitation assay performed, lines: input, flow-through (FT) and inmunoprecipitation (IP). **D.** Western blot showing the expression of GS (25 KDa) on the three replicates (R1, R2 and R3) used to define the control list. **E.** Western blot image showing the GS (25 KDa) inmunoprecipitation assay performed, lines: input, flow-through (FT) and inmunoprecipitation (IP).

chaperone subunit family protein", encoded by *At1g26660* and *At1g49245* genes. None of these proteins were identified in the eluates from the control GS cell suspensions (Supp Table 3, Supp Table 4). Phylogenetic analysis revealed that the proteins encoded by the *At1g26660* and *At1g49245* genes were the likely orthologs of the UXT and ASDURF prefoldin-like proteins from animals, respectively (Supp Figure 1A - 1B). This result suggested the existence of the PFDL complex in *Arabidopsis*. To confirm this, we performed a reciprocal AP-MS using extracts from PSB-D cell suspensions expressing the GS-UXT fusion (Figure 8A, 8B). URI1, PFD2, PFD6, PDRG1, and ASDURF were identified as top interactors of UXT (Figure 7, Supp Table 3; Supp Table 4). These results confirmed the presence of the PFDL complex in *Arabidopsis* and that URI1 is one of its subunits.

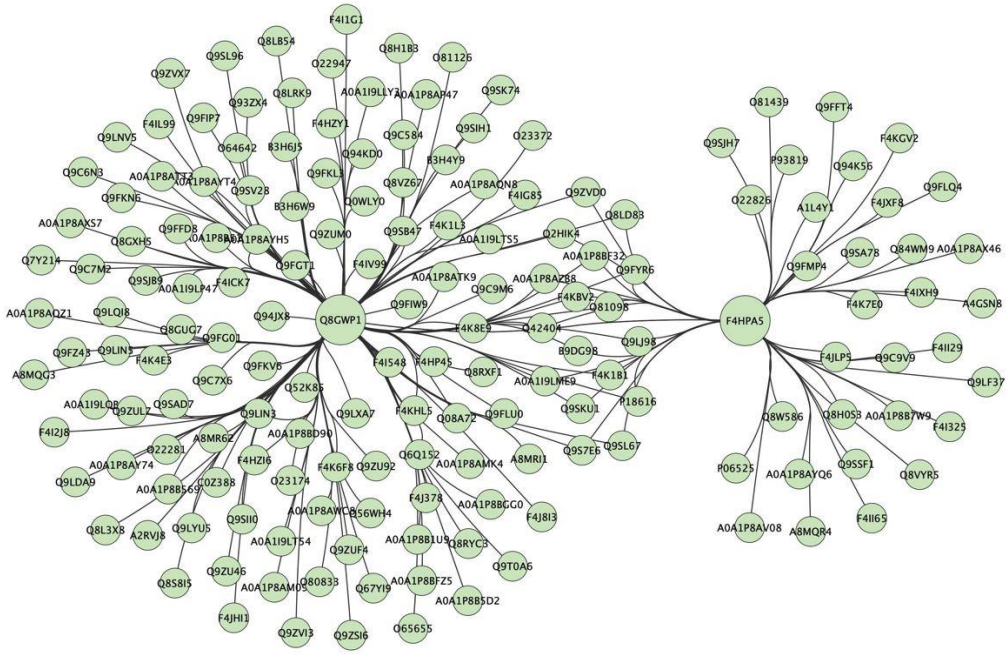

Figure 7. URI1 and UXT *in vivo* interactome of *Arabidopsis* cells suspensions. Protein interactors of URI1 and UXT that are common in the three replicates are shown. Each replicate is compared to the list of interactors obtained after immunoprecipitation of the GS tag to determine which interactors bound tightly to the proteins under study. The final list of interactors was categorised using Panther (www.pantherdb.org) according to a statistical overrepresentation test using the biological process GO annotation set.

Interestingly, in our AP-MS experiments, we did not pull down any canonical prefoldin other than PFD2 and PFD6. This result suggests that both URI1 and UXT are part of the PFDL complex and do not appear to form alternative complexes with other canonical prefoldins. This situation is very similar to that in animals, where URI1 and UXT co-immunoprecipitated only PFDN2 and PFDN6 among the canonical prefoldins (Cloutier and Coulombe, 2010). However, in animals, ASDURF and PDRG1 have been suggested to be part of alternative PFD complexes, with ASDURF and PDRG1 replacing PFDN1 and PFDN4, respectively (Cloutier and Coulombe, 2010; Cloutier *et al.*, 2020). Whether these alternative complexes exist in plants needs further investigation.

Predicted structure of the Prefoldin-like complex

Although the structure of the PFDLc is not known for any organism, the structure of the complex in humans has been predicted based on the jellyfish-like structure of the canonical PFD complex (Cloutier *et al.*, 2020). Therefore, we wanted to determine whether the subunits of the PFDLc from *Arabidopsis* could arrange themselves in a similar structure. The canonical PFDc consists of two types of subunits, α-type, in which two β-hairpins connect two α-helices, and β-type, in which one β-hairpin connects the two α-helices (Arranz *et al.*, 2018). Prediction based on modelling showed that the *Arabidopsis* PFD2 and PFD6 can adopt the structure of β-type prefoldins (Blanco-Touriñán *et al.*, 2021), and the URI1 prefoldin domain that of an α-type (Yang *et al.*, 2022). We modelled the structures of the *Arabidopsis* UXT, PDRG1, and ASDURF based on the structure of the human orthologues. *Arabidopsis* UXT adopted an α-type structure (Figure 9A), whereas PDRG1 and ASDURF adopted a β-type structure (Figure 9B, 9C), all with relatively high accuracy (higher than 0.3, which is the cut-off for good models), as determined by the Predicted Native Overlap (Eramian *et al.*, 2008). Using the predicted structures and the arrangement of the predicted PFDLc from humans (Cloutier e*t al.*, 2020), we could assemble the PFDLc from *Arabidopsis* (Figure 9D). The structural similarity between *Arabidopsis* and human prefoldins and prefoldin-like proteins strongly suggests that the *Arabidopsis* PFDLc adopts a jellyfish-like structure *in vivo* that resembles the canonical one.

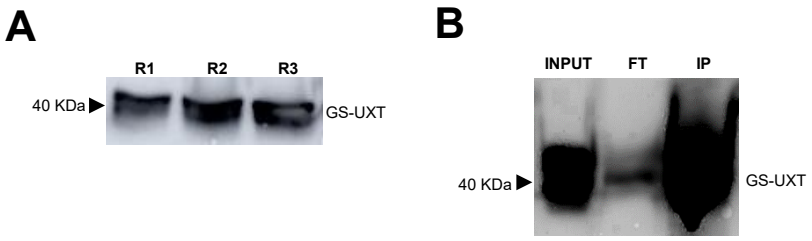

Figure 8. UXT interactome *in-vivo* definition. A. Western blot showing the expression of GS-UXT (40 KDa) on the three replicates (R1, R2 and R3) used. **B.** Western blot image showing the GS-UXT (40 KDa) inmunoprecipitation assay performed, lines: input, flow-through (FT) and inmunoprecipitation (IP).

Interactions of URI1 within the Prefoldin-like complex

In the predicted PFDL complex, URI1 occupies a central position together with UXT as α-type subunits, surrounded by the four β-type subunits. We next examined by Y2H the direct interactions established by URI1 with other subunits of the complex. In agreement with the arrangement in the predicted structure of the PFDLc, URI1 interacted with the other α-type subunit, UXT, and with the two closest β-type subunits, PFD2 and PDRG1 (Figure 10A) (Yang *et al.*, 2022). As reported, URI1 also interacted with PFD6 (Figure 10A) (Yang *et al.*, 2022), although the two subunits did not appear to occupy adjacent positions within the complex (Figure 9D). This result could indicate that the interactions between the β-hairpins of the subunits within the complex are more extensive than assumed in the predicted model. However, it may also suggest that URI1 and PFD6 have the ability to interact with each other outside the PFDLc. We next examined the direct interaction between the two α-type subunits, URI1 and UXT, *in vivo*. To this end, we transiently expressed YFP-URI1 and HA-UXT fusion proteins in leaves of *N. benthamiana* and assessed the interaction by co-immunoprecipitation (Figure 10B). We were able to efficiently immunoprecipitate HA-UXT with anti-GFP antibodies from leaf extracts co-expressing both proteins, indicating that they are

able to establish strong interaction *in vivo*. Interestingly, we found a higher level of HA-UXT when co-expressed with YFP-URI1, possibly reflecting parallelisms with the stabilizing effect that URI1 exerts on the UXT protein in the human cell line LNCaP (Mita *et al*., 2013).

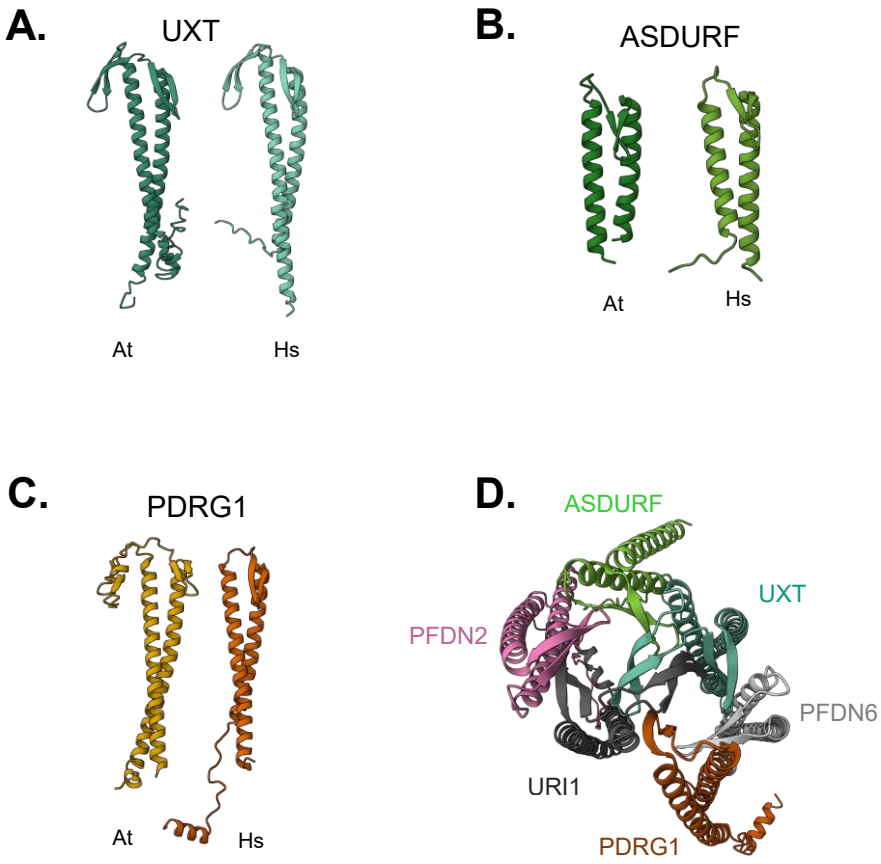

Figure 9. Predicted structure of Arabidopsis UXT, ASDURF, and PDRG1. **A.** The structure of *Arabidopsis* (At) UXT, **B.** ASDURF and **C.** PDRG1 is shown together with the structure of their human (Hs) orthologs. **D.** Predicted structure of the human PFDL complex. Only the URI1 PFD domain is included in the structure.

The URI1 in vivo interactome revealed that URI1 is involved in a variety of molecular pathways.

We used AP-MS with PSB-D cells expressing GS-URI1 to identify URI1 partners other than PFDL subunits. The list of interactors was manually curated using GO orthology to categorise the interactors in terms of their molecular function and biological process.

We found 189 proteins in addition to the PFDL subunits. URI1 was found in association with a number of proteins involved in multiple molecular pathways (Figure 7, Supp Table 4). The largest group was those related to the regulation of gene expression, including interactors involved in RNA metabolism, mRNA splicing, processing body formation, chromatin remodelling and interactors directly related to RNAPII, such as the NRPB1 subunit. We also found interactors related to the primary metabolism, embryonic development, defence response, response to various stimuli, protein posttranslational modification, and cytoskeletal motor activity.

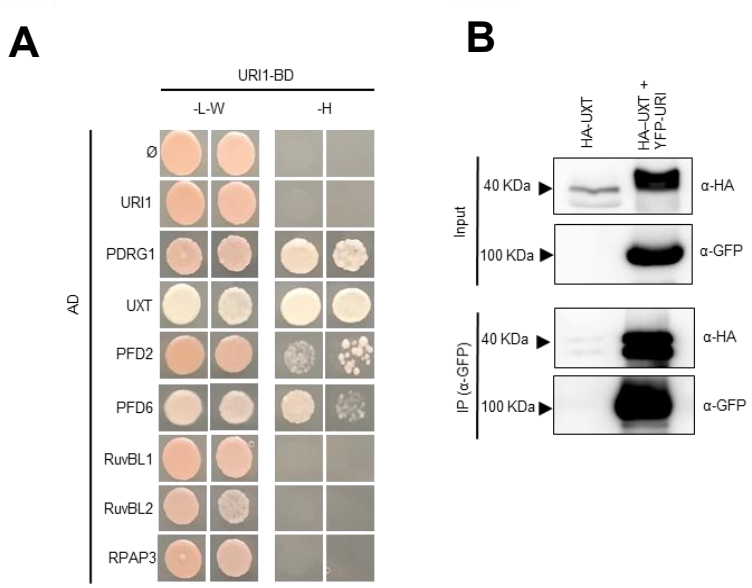

Figure 10. URI1 interacts with other partners involved in PFDLc. A. Yeast-two hybrid assay (Y2H) between BD-URI1 and R2TPc (RuvBL1-, RuvBL2- and RPAP3 – AD) and PFDLc (URI1-, PDRG1-, UXT-, PFD2- and PFD6-AD) in growth control (-L-W), and in histidine-free SD media (-L-W-H). Y2H empty vector containing Gal4 Activation Domain (AD) were used as negative control. **B.** co-immunoprecipitation (co-IP) assay showing the interaction between URI1 (expected size at 75KDa, but it was found around 100 KDa) and UXT (40 KDa) in agroinfiltrated *N. benthamiana l*eaves. After three days of agroinfiltration, the tissue was used for the IP with anti-GFP paramagnetic beads and were detected by western blot using anti-HA and anti-FLAG-HRP antibodies. The position of molecular weight marker is shown on the left.

We compared the curated list of URI1 interactors with those of UXT. Only 9.6% of both interactomes were shared by URI1 and UXT (Figure 11). In this list, in addition to the other subunits of the PFDL complex and NRPB5, a known accessory subunit (Dorjsuren *et al*., 1998), we found other proteins that are part of different protein complexes, such as (i) U1 snRNP, U2B (component of U2B), TSCC4 (component of U5 snRNP) and SmD3 (core component of U1, U2, U4 and U5 snRNPs) (Swaraz *et al.,* 2011); (ii) NRPB1 and NRPA1, the catalytic subunits of RNAPI and II, respectively, and RPAP2, involved in RNAPII assembly and traslocation to the nucleus (Boulon *et al.,* 2010); and (iii) PABN1 and RPT2B, two subunits of the proteasome (Lee *et al*., 2011). Interestingly, we also found NTF2 (Nuclear Transport Factor 2) (Zhao *et al.,* 2006), which could be involved in the translocation of URI1 to the nucleus, a possibility that we will investigate in the future. Unexpectedly, URI1 and UXT shared a small fraction of interactors, suggesting that most of the identified interactors bound to URI1 could be interactors of URI1 alone. However, it is important to note that we cannot completely exclude the possibility that URI1 interacts with its partners as part of the PFDL, and the fact that we could not identify a larger number of UXT

interactors may be due to technical limitations of the immunoprecipitation. The proteomic analysis of the other PFDL subunits would be helpful to determine the exclusive partners of URI1.

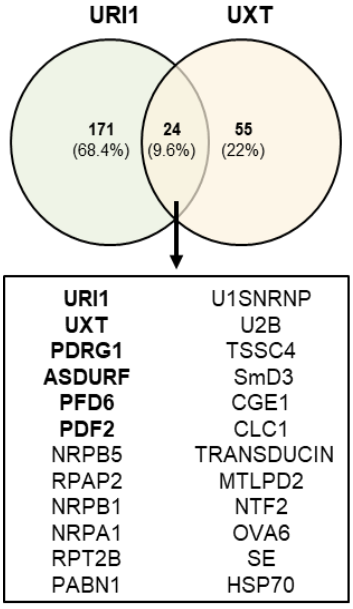

Figure 11. Interactors common to URI1 and UXT in *Arabidopsis* cell suspensions. Curated list of interactors from URI1 and UXT were compared to obtain the interactors that are common to both, this interactors would be considered as interactors from PFDLc. Most of the proteins found are part of protein complexes, suggesting that the co-chaperone role of the PFDL complex is conserved in *Arabidopsis*. Graph were done using VENNY 2.1 (https://bioinfogp.cnb.csic.es/tools/venny/).

URI1 is required for embryo development.

To determine the function of URI1, we analysed different mutant alleles. We first analysed an insertion mutant (SALK_038314) that contains the T-DNA in the second intron of *URI1* and a DS-transposon (Ds-t) insertion mutant from RIKEN (pst10814) (Figure 12A), recently named as *uri1-2* and *uri1-3* (Yang *et al*., 2022). Heterozygous but not the homozygous plants were identified for the insertions from a self-pollinated population of *uri1/+* for any of the two alleles, suggesting that the insertion may cause embryo lethality in homozygosis in both cases. Indeed, *uri1-2* and *uri1-3*, showed 25% approximately aborted seeds in the immature siliques of heterozygous plants (Figure 12B). We next checked at which stage the embryo arrested its development in the *uri1-2* mutant. We found that embryo arrested at a very early stage, just 2 days after fertilisation (Figure 12C). The URI1 proteome showed that URI1 interacts with proteins playing a role in embryo development, such as OVA6 and SED1 (Berg *et al*., 2005; Ju *et al*., 2016), suggesting that the lack of interaction in the mutant may be one of the causes leading to the lethal phenotype (Figure 7, Supp Table 4). Also, this defect could be due to failure in assembly of nuclear RNAPs or TORC kinase, which are clients of the R2TP/PFDL complex in animals and yeast (Houry *et al.,* 2018). Together, these data suggest that URI1 is required for early stages of embryo development in *Arabidopsis*. During the course of the investigations, a viable mutant allele of *URI1* was reported, *uri1-1*, presenting a point mutation in the third exon (Yang *et al*, 2022). Although the *uri1-1* mutant

is viable, the mutant plants showed some disturbance in embryonic development, as reflected by smaller siliques with some gaps (Figure 12B).

URI1 is required for post-embryonic development.

We used the *uri1-1* mutant allele to determine the role of URI1 in post-embryonic development. To this end, we analysed several growth and developmental phenotypes in the mutant and compared them with the wild type (WT). First, we measured the length of the roots compared with the WT (Figure 13A). Roots of *uri1-1* mutant were drastically reduced compared to the WT. Furthermore, when stained with PI, 5-day-old roots showed cellular damage in the root apical meristem (RAM), reflected in cells filled with the dye, and abnormal cellular divisions were observed in different cell layers (Figure 13B). The latter is likely due to the fact that *uri1-1* mutants also exhibit disrupted cytoskeletal organization (Yang *et al.,* 2022), which is directly related to cell divisions (Serra *et al.,* 2020). A defect in cell division in the RAM is also present in the *pfd6* mutant (Gu *et al.,* 2008), defective in another subunit of the PFDL, suggesting that this could be due to failure in the activity of the complex, rather than in the activity of individual subunits acting on their own. The smaller size of the RAM and thus the entire root could be due to these defects in cell division, resulting in a smaller number of cells available for differentiation.

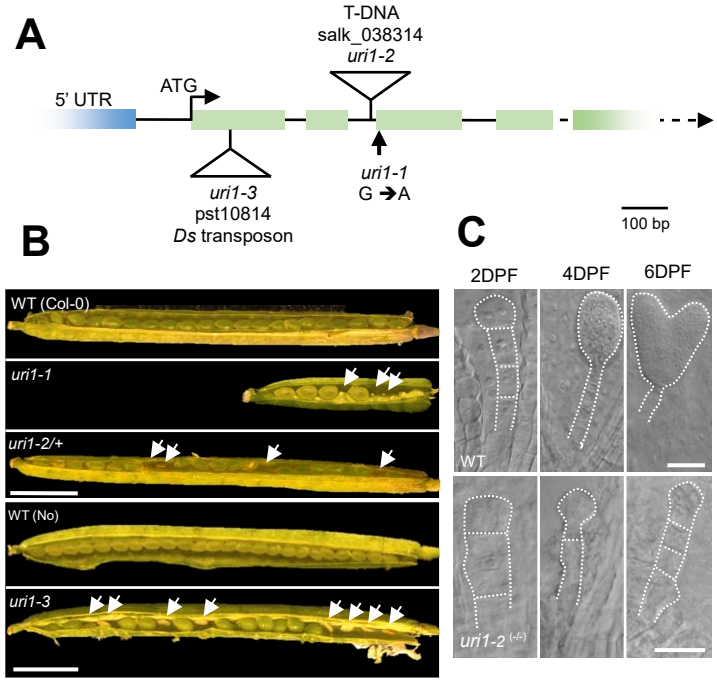

Figure 12. URI1 is required for embryo development. A. *AT1G03760* gene chart that encodes to URI1 in *Arabidopsis.* Location of mutant lines used in this project are showed on the chart: *uri1-1* is a line with a point mutation that changes G to A, *uri1-2* is a T-DNA insertion mutant from SALK (salk_038314), and *uri1-3* (*pst10814)* is an insertion of a Ds-transposon from RIKEN. Scale bar 100 bp. **B.** *uri1-1, uri1-2* and *uri1-3* valves dissection showing embryo abortions (marked with white arrows) compared to WT (Col-0 and No). Scale bar 2 mm. **C.** Nomarski microscopy used to determine at which stage of embryo development on *uri1-2* $^{(-/-)}$ mutant the embryo stopped. Scale bar 25 µm.

Then, we analysed the shoot apical meristem (SAM) to determine whether it was also affected. As observed in the RAM, SAM size was also dramatically reduced compared with the WT (Figure 14). Impaired SAM growth could also be the consequence of altered cell divisions planes, as previously described (Bencivenga *et al.,* 2016), a possibility that awaits further investigation. In any case, our results indicate that URI1 is necessary for the normal activity of both the SAM and the RAM.

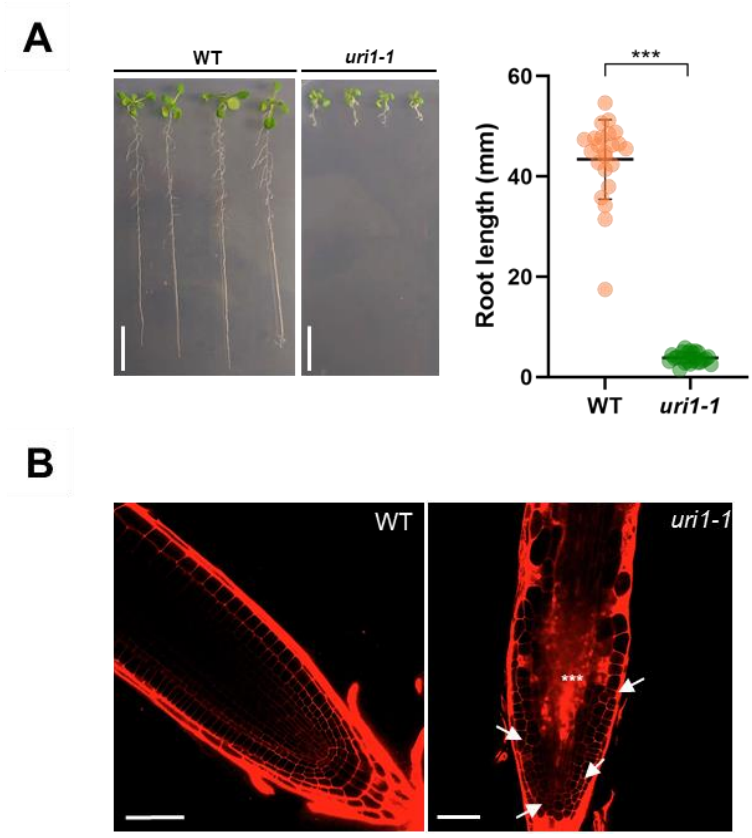

Figure 13. URI1 impairment causes root growth deficiency. **A**. *uri1-1* mutant were grown vertically on CL (continuous light) together with WT during 10 days to quantify root growth length. *uri1-1* mutant roots were quantified with FiJi, and then t-test were performed to determine that roots from *uri1-1* are significantly shorter than WT roots. (0.12 (ns), 0.033 (*), 0.002 (**) and 0.001 (***)). Scale bar 10 mm. **B.** Confocal imaging of WT and *uri1-1* roots grown during five days and stained with PI. White arrows show improper cell division observed. White asterisk showed cell death detected inside the root. Scale bar 50 µm.

While growing the plants in the greenhouse, we noticed that the mutant plants had a tendency to flower earlier than the WT. Thus, we checked the flowering time under long- and short-day conditions to determine whether the regulation of this developmental transition was affected in the mutant and if this was dependent on the photoperiod. Regarding long-day conditions and confirming our observation, *uri1-1* mutant presented an early-flowering phenotype, with tiny rosettes leaves and short stems compared to WT (Figure 15A). In contrast, in short-day conditions, *uri1-1* mutant presented a late-flowering phenotype (Figure 15B) compared to WT. The contrasting effect of the *uri1-1* mutation in the flowering time anticipates a complex relationship of URI1 with

the signalling pathways that regulate this developmental transition. It has been observed that canonical PFDs are involved in flowering and delay the flowering of *Arabidopsis* by attenuating the expression of certain integrator genes for flowering (Blanco-Touriñán *et al*., 2021). One possibility is that URI1 as PFDL could also be involved in this process. However, further studies are needed.

The *uri1-1* mutation has a strong influence on the transcriptome

To confirm and explore possible additional roles of URI1 in post-embryonic development, we performed RNA-seq analyses in WT and *uri1-1* mutant. To this end, we compared the transcriptomic differences in 7-day-old seedlings of WT and *uri1-1* mutant. As expected based on the morphological phenotypes, the *uri1-1* mutant showed a significant number of differentially expressed genes (DEG). We found 1751 DEG in the mutant compared to WT plants (1394 down-regulated and 357 up-regulated) (*q* value < 0.05, $|\log_2 FC| > 1$) (Figure 16A-B, Supp Table 5). To determine if there were physiological pathways preferentially affected in the mutant, we did a GO enrichment analysis using the BGI's online tool Dr. Tom for genomic analyses. We found that the

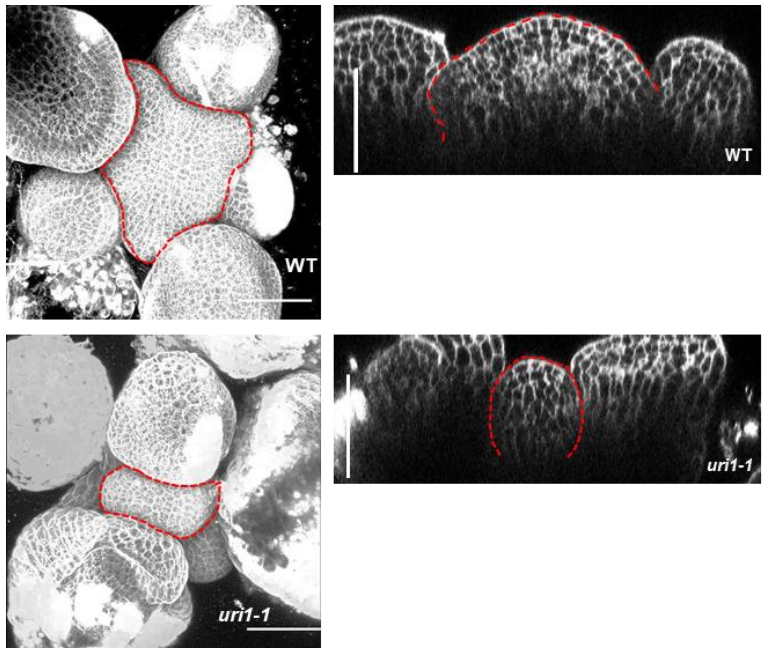

Figure 14. URI1 is required for proper Shoot Apical Meristem (SAM) development. WT and *uri1-1* plants were sowed on soil and before bolting, SAM was dissected and stainned with PI. 3D reconstruction of *uri1-1* shows an impaired and reduced SAM compared to the 3D reconstruction of WT SAM. Scale bar 50 µm.

most enriched categories in “Biological process” were related with metabolic processes and cell wall organization/modification (Figure 17, Supp Table 6).

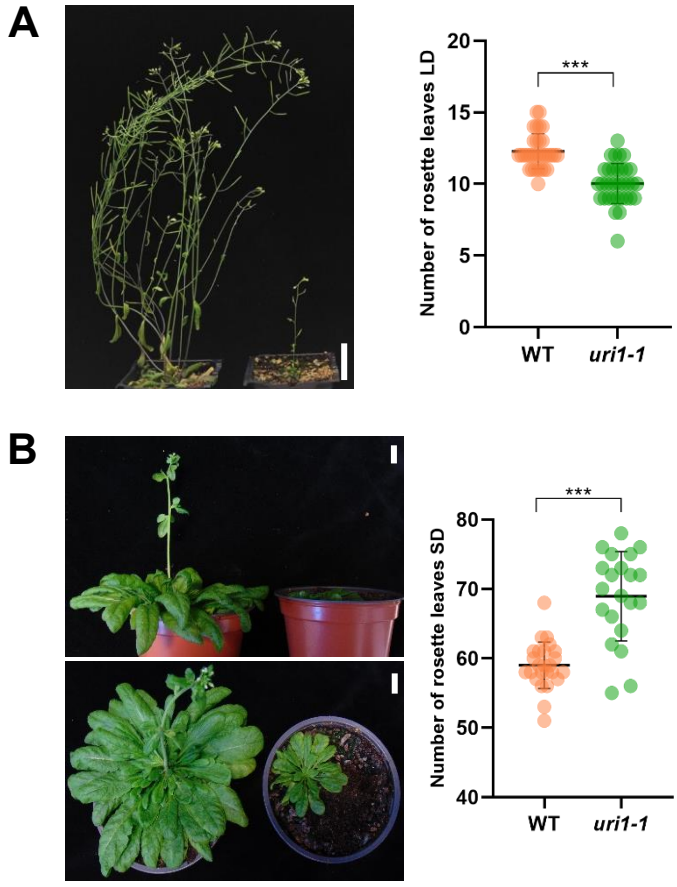

Figure 15. Flowering time of *uri1-1* is altered under different circadian cycles. *uri1-1* mutant and WT seeds were sown in soil, maintained at 4ºC during 7 days and then germinated under each light regime. **A.** Flowering time results representation using long day conditions (16 hrs light at 22ºC and 8 hrs dark at 19ºC). *uri1-1* mutant flowered before WT, forming less rosette leaves. **B.** Flowering time results representation using short day conditions (8 hrs light at 22ºC and 16 hrs dark at 19ºC). *uri1-1* mutant flowered later than WT, forming more rosette leaves. Quantifications were done manually once a week. Scale bar, 2 cm. t-test were done to determine that differences between groups in both light regimes are significant using APA style (0.12 (ns), 0.033 (*), 0.002 (**) and 0.001 (***)).

Most genes of categories related to cell wall processes were downregulated in the *uri1-1* mutant, consistently with the dwarf phenotype observed in *uri1-1* mutant plants (Figure 18A, Suppl Table 7). Interestingly, there were many affected categories related with primary and secondary metabolism, such as sterol, terpenoid/diterpenoid/triterpenoid, carbohydrates, polysaccharides and more (Figure 18B, Suppl Table 7). The possible involvement of URI1 in primary metabolism, particularly in the context of the response to energy stress, has been investigated in the Chapter 3. The fact that several genes related to primary metabolism are repressed is directly related to the dwarf phenotype of the *uri1-1* mutant. This is because both primary and secondary metabolism ultimately oversee the regulation of all plant processes (Erb *et al*., 2020). In addition, it is noteworthy that there were also enrichment in categories related to pathogen defense, plant immune system and stress (Figure 18C, Suppl Table 7).

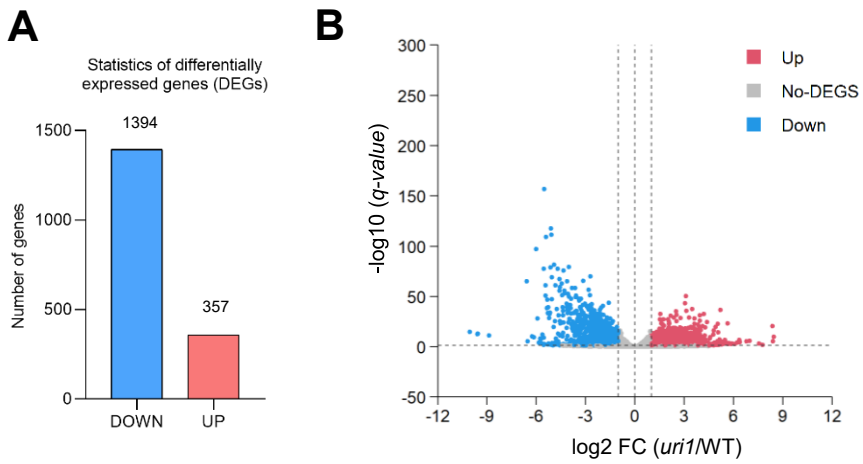

Figure 16. Transcriptomic analysis of *uri1-1* and WT seedlings. **A.** Differentially expressed genes (DEGs) silenced (1394) and induced (357) in *uri1-1* compared to WT. **B.** Volcano plot showing the genes expressed in *uri1-1* (24146). Differential analysis was done with Dr.Tom with default options (Beijing, China). The red and blue dots indicate up-regulated and down-regulated genes, respectively. DEGs were considered when $\log_2$ FC ≥ 1 and *q-value* ≤ 0.05.

We next wondered whether the transcriptomic changes observed in the *uri1-1* mutant reflected activity of the R2TP/PFDL complex or of URI1. In an independent experiment performed in the lab to determine the transcriptomic response to heat stress (part of the PhD work of Alberto Palacios-Abella), we included seedlings of the *uri1-1* mutant along with seedlings of the *tpr5-2* mutant, carrying a hypomorphic allele that affects the RPAP3 subunit of the R2TP complex (Sotta *et al.,* 2016), and of the *pfd2 pfd6* double mutant, deficient in two subunits of the PFD and PFDL complexes obtained by genetic crosses. We obtained the transcriptome of the WT and the three mutant seedlings by RNA-seq. In this case, we applied a less stringent filter to identify DEG (p adj < 0.05 and $\log_2$ FC ± 0.58, instead of $\log_2$ FC ± 1), since the transcriptomic changes in the *tpr5-2* mutant are small. Using this threshold, we identified 3138 DEG (907 up-regulated and 2231 down-regulated) in the *uri1-1* mutant, 6682 DEG (3072 up-regulated and 3610 down-regulated) in the *pfd2 pfd6* mutant, and 558 DEG (156 up-regulated and 402 down-regulated) in the *tpr5-2* mutant compared to WT plants. We next compared the up- and down-regulated DEG between mutants and found that 1745 genes presented similar misregulation in *uri1-1* and *pfd2 pfd6* seedlings, representing a statistically significant overlap (Figure 19A and Supp Table 8). In contrast, the common DEG that were misregulated in the opposite direction were much less. This is compatible in a model where *PFD2*, *PFD6*, and *URI1* act on a common pathway, i.e., the misregulation of these genes would be the consequence of a defective PFDLc. The comparison with the *tpr5-2* mutant rendered a less clear result. Although the overlap was statistically significant, there was no clear trend that genes were misregulated in the same direction (Figure 19B, Supp Table 8).

Figure 17. Gene ontology enrichment among genes that are differentially expressed in *uri1-1* mutant. Bubble plot showing "Biological process" categories overrepresented in *uri1-1* mutant when log2 FC ≥ 1 and *q value* ≤ 0.05. The size of the points match with the number of genes enriched in this category (bigger means more genes). *q-value* is represented by colour. Rich ratio of a particular GO term refers to its enrichment in *uri1-1* DEGs set compared with the reference genome background set. All the GO are included in Supp Table 6.

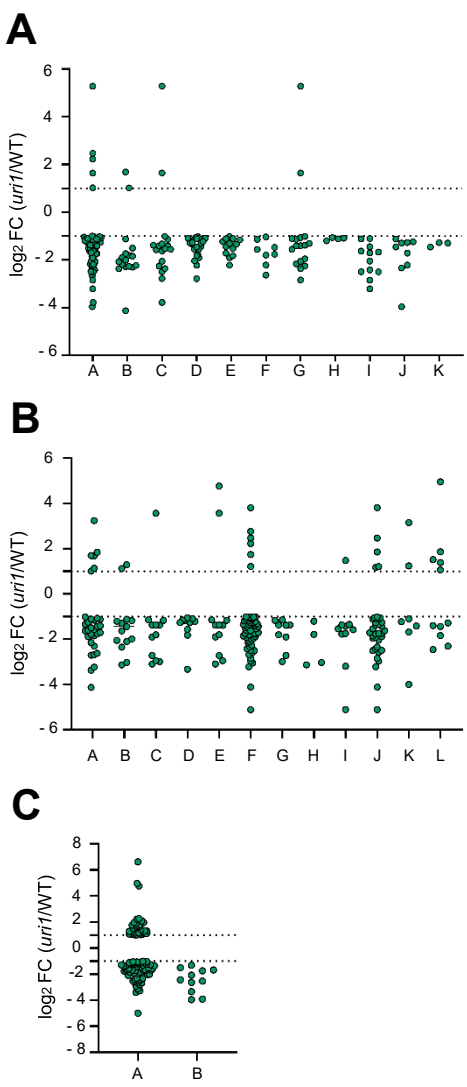

A. Cell wall organization (66 DEGs)
B. Plant-type cell wall organization (17 DEGs)
C. Cell wall modification (18 DEGs)
D. Plant-type secondary cell wall organization (23 DEGs)
E. Xylan biosynthetic process (13 DEGs)
F. Lignin catabolic process (8 DEGs)
G. Pectin catabolic process (17 DEGs)
H. Positive regulation of secondary cell wall biogenesis (4 DEGs)
I. Cell wall biogenesis (12 DEGs)
J. Cellulose biosynthetic process (9DEGs)
K. Cell wall thickening (3 DEGs)

A. Hydrogen peroxide catabolic process (32 DEGs)
B. Sterol metabolic process (14 DEGs)
C. Diterpenoid biosynthetic process (12 DEGs)
D. Suberin biosynthetic process (10 DEGs)
E. Terpenoid biosynthetic process (12 DEGs)
F. Carbohydrate metabolic process (57 DEGs)
G. Sesquiterpene biosynthetic process (9 DEGs)
H. Triterpenoid metabolic process (4 DEGs)
I. Glucosinolate catabolic process (10 DEGs)
J. Metabolic process (36 DEGs)
K. Triterpenoid biosynthetic process (7 DEGs)
L. Toxic catabolic process (11 DEGs)

A. Defence response (90 DEGs)
B. Root hair elongation (11 DEGs)

Figure 18. Multiple genes involved in cell wall, defence, root hair development and secondary metabolism are differentially expressed in *uri1-1*. **A.** Relative expression of several genes involved in different processes related to cell wall. **B.** Relative expression of several genes involved in secondary metabolism. **C.** Relative expression of several genes involved in defence and root hair elongation. Relative expression is represented as $\log_2$ FC (*uri1*/WT). Number genes are showed in Supp Table 7.

When we compared the three transcriptomes together found that *uri1-1*, *tpr5-2*, and *pfd2 pfd6* mutants shared 117 DEG, most of them being affected by mutations in the same direction (Figure 20A and 20B). These results suggest that URI1 performs a considerable part of its

functions independently of the PFDL complex, as there were a considerable number of DEG that did not overlap with the *pfd2 pfd6* mutant. However, the overlap with *pfd2 pfd6* still is considerable, indicating that part of URI1 function is exerted as subunit of the PFDL complex. The overlap of *uri1-1* or *pfd2 pfd6* mutants with *tpr5-2* mutant is small owing to the small number of DEG in this mutant (Figure 19B), which makes difficult to draw conclusions. Nevertheless, the set of common DEG for the three mutants behave similarly in each of them, suggesting that their misregulation may be a consequence of defective activity of the R2TP/PFDLc, which according to the GO analysis could had an influence on biotic stress responses (Figure 20C). These results also suggest that the percentage of URI1, PFD2, and PFD6 activities dedicated to the R2TP/PFDL complex is less compared to the activity dedicated to the PFDL. From these results, it can also be deduced that the PFDL complex and the R2TP complex largely fulfil separate functions, as described in animals (von Morgen *et al*., 2015).

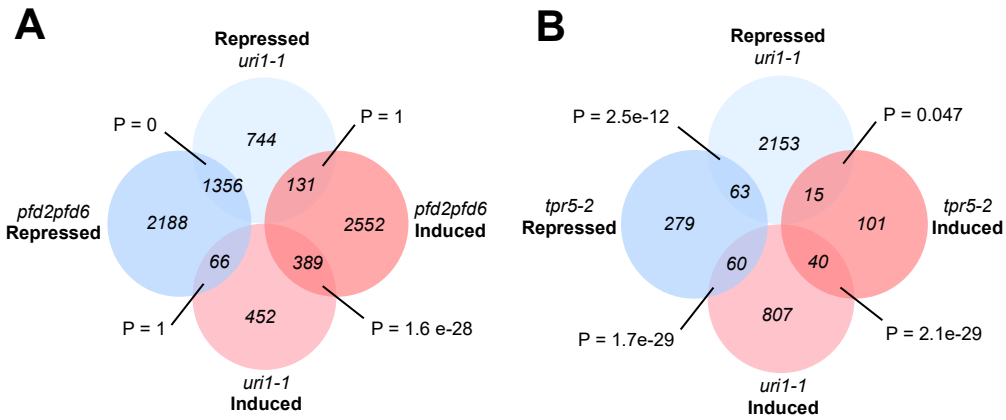

Figure 19. URI1 shares downstream DEGs with PFD2, PFD6 and TPR5. **A.** Venn diagram showing the overlap of upregulated and downregulated in *uri1-1* and *pfd2pfd6* DEGs. **B.** Venn diagram showing the overlap between upregulated and downregulated in *uri1-1* and *tpr5-2* DEGs. Statistical significance of the overlaps is represented by the Fisher's exact test.

URI1 prevents cell differentiation.

We have shown that URI1 is required for cell proliferation and tissue development in the root and shoot. To test in an alternative way whether URI1 is necessary for tissue differentiation and de-novo organogenesis, we analysed how the *in vitro* callus formation and de-novo shoot regeneration were affected by the *uri1-1* mutation. Hypocotyls from 7-day-old etiolated seedlings were separated from cotyledons and root (Wu *et al.,* 2022). The excised hypocotyls were then incubated for 30 days in the dark on CIM media to produce calli. After 30 days in the dark, calli were transferred to SIM media and incubated in LD media for a further 30 days to induce shoot production (Figure 21).

Whereas WT produced calli from excised hypocotyls, the capacity was reduced in *uri1-1* mutant hypocotyls, which produced smaller calli (Figure 22A), with more than two-fold decreased in fresh weight when compared to WT (Figure 22B). This suggests that URI1 activity is required for callus formation from *Arabidopsis* hypocotyls, and therefore to keep the proliferative capacity of these undifferentiated cells. URI1 activity might be necessary keep cells in an undifferentiated state and proliferating. To test the possible role of URI1 in de-novo shoot organogenesis, we induced shoot formation in calli produced from WT and *uri1-1* mutant hypocotyls (Figure 21).

Interestingly, calli produced from *uri1-1* mutant hypocotyls were greener than those of the WT (Figure 23A). Although we did not observe the formation of shoots, the green color indicated that the differentiation into shoots started earlier in the mutant calli, which suggests that URI1 negatively regulates de-novo shoot organonegesis in *Arabidopsis*. To try identifying the molecular

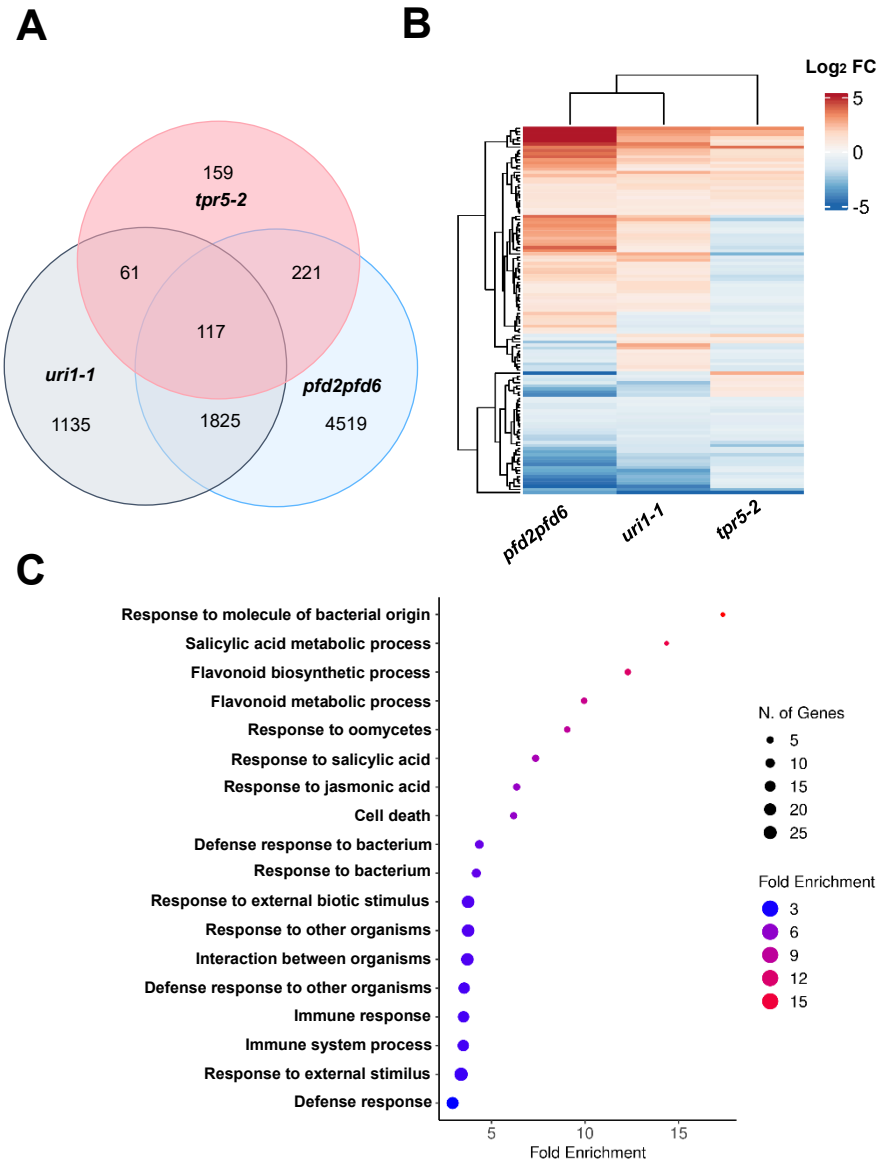

Figure 20. URI1-dependent transcriptome is more similar to PFD2/PFD6-dependent transcriptome. A. Venn diagram showing the overlap of DEGs in *uri1*-1, *pfd2pfd6* and *tpr5-2* mutants. **B.** Heatmap showing the hierarchical clustering of the DEGs which are common between *uri1*-1, *pfd2pfd6* and *tpr5-2* represented as $\log_2$ FC. **C.** Bubble chart of GO terms enriched in the DEGs that are shared between *uri1*-1, *pfd2pfd6* and *tpr5-2*. The size of the points match with the number of genes enriched in this category (bigger means more genes). Fold enrichment is represented by colour. Fold enrichment is a valuable metric for identifying differentially expressed genes and understanding which genes are most affected by the experimental conditions being studied.

basis underlying the possible role of URI1 in this developmental process, we performed RNA-seq analyses on WT and *uri1-1* calli in shoot inducing media. *uri1-1* had 3992 DEG ($log_2FC \geq 1$ and a q-value ≤ 0.05), 2730 down-regulated and 1262 up-regulated when compared with WT (Figure 23B-C, Supp table 9).

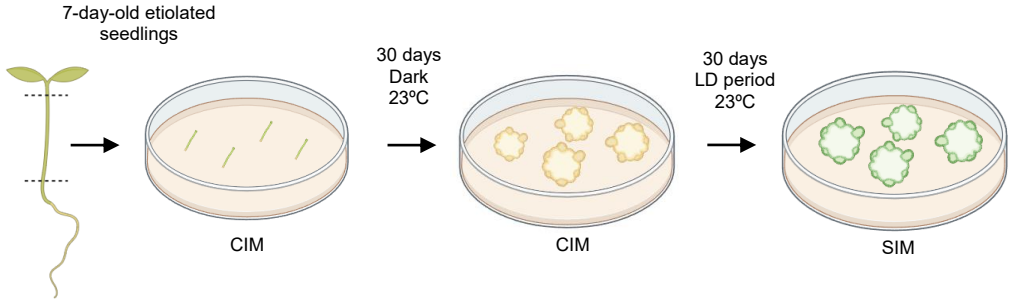

Figure 21. Workflow showing obtaining of calli using 7-day-old etiolated seedlings. Calli Induction Media (CIM) and SIM (Shoot Induction Media) were prepared as explained in Material & Methods section. Excised hypocotyls were incubated during 30 days under dark in CIM and then transferred to SIM during 30 days and under LD conditions.

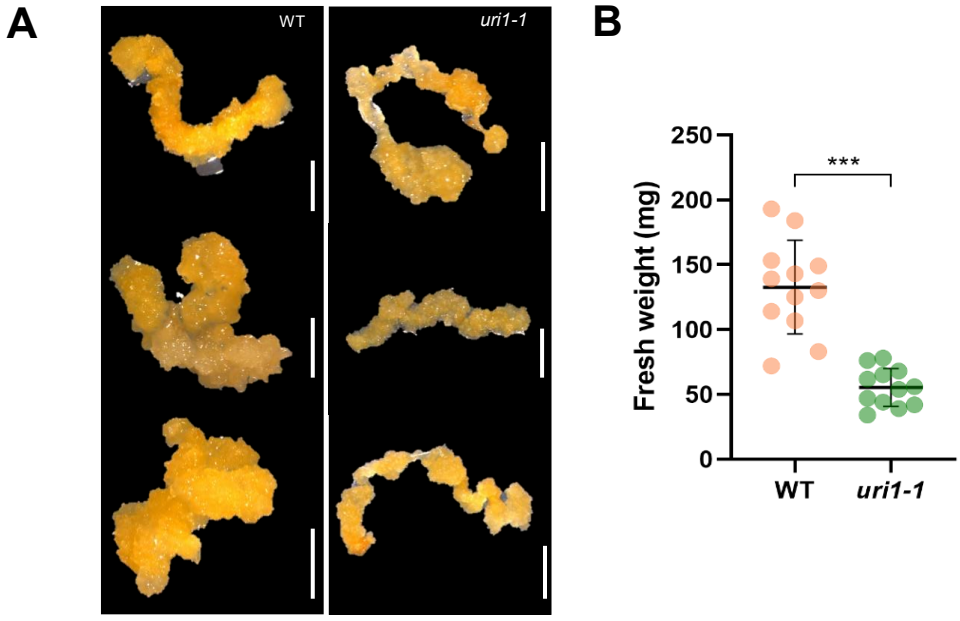

Figure 22. Callus production is defective in *uri1-1*. A. Callus formation in WT and *uri1-1* grown in callus inducing medium. Scale bar 2 mm. **B.** Fresh weight (mg) in WT and *uri1-1* calluses showing a statistically significant reduction (t-test) in *uri1-1* compared to WT. t-test were done to determine that differences between groups in both light regimes are significant using APA style (0.12 (ns), 0.033 (*), 0.002 (**) and 0.001 (***)).

To understand the biological processes underlying the URI1-dependent transcriptome in de-novo organogenesis, we performed a GO enrichment analysis on the *uri1-1* DEG. This analysis showed that multiple processes related to cellular proliferation, tissue differentiation, and photosynthesis were enriched (Figure 24), supporting the hypothesis that URI1 is a regulator of de-novo organogenesis in *Arabidopsis*.

Altogether, these data indicate that URI1 is required for proliferation of undifferentiated tissue, whereas it negatively regulates differentiation/de-novo organogenesis in plants. This agrees to a certain extent with observations in mammals, where URI1 is considered an oncogene and is highly expressed in tumours (Gu *et al.,* 2015; Herranz-Montoya *et al.,* 2021). Moreover, URI1 promotes liver tumorigenesis (Tummala *et al*., 2014) and its overexpression enhances

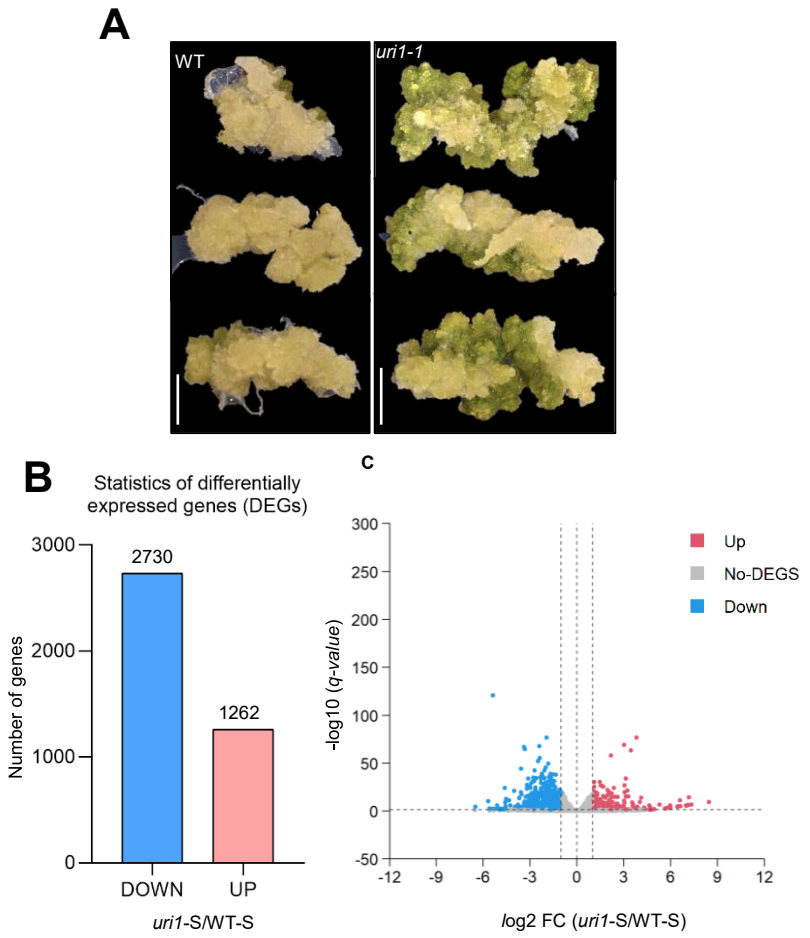

Figure 23. De-novo shoot organogenesis is promoted in *uri1-1*. A. De-novo shoot organogenesis in WT and uri1-1 grown in shoot induction medium. Scale bar 5 mm **B.** Down- (2730) and upregulated (1262) DEGs in uri1-1 in callus grown in shoot induction medium obtained after RNA-seq analysis. **C.** Volcano plot of DEGs in uri1-1 callus compared with WT callus grown in shoot induction media (23758). Differential analysis was done with Dr. Tom (DESeq2 anaylisis), with default options. The red and blue dots indicate induced and repressed genes, respectively. DEGs were considered when log2 FC ≥ 1 and *q-value* ≤ 0.05.

cancer cell survival by inhibiting apoptosis (Ji *et al*., 2019). It is therefore plausible that URI1 acts as a conserved pan-eukaryotic regulator of cellular proliferation and differentiation.

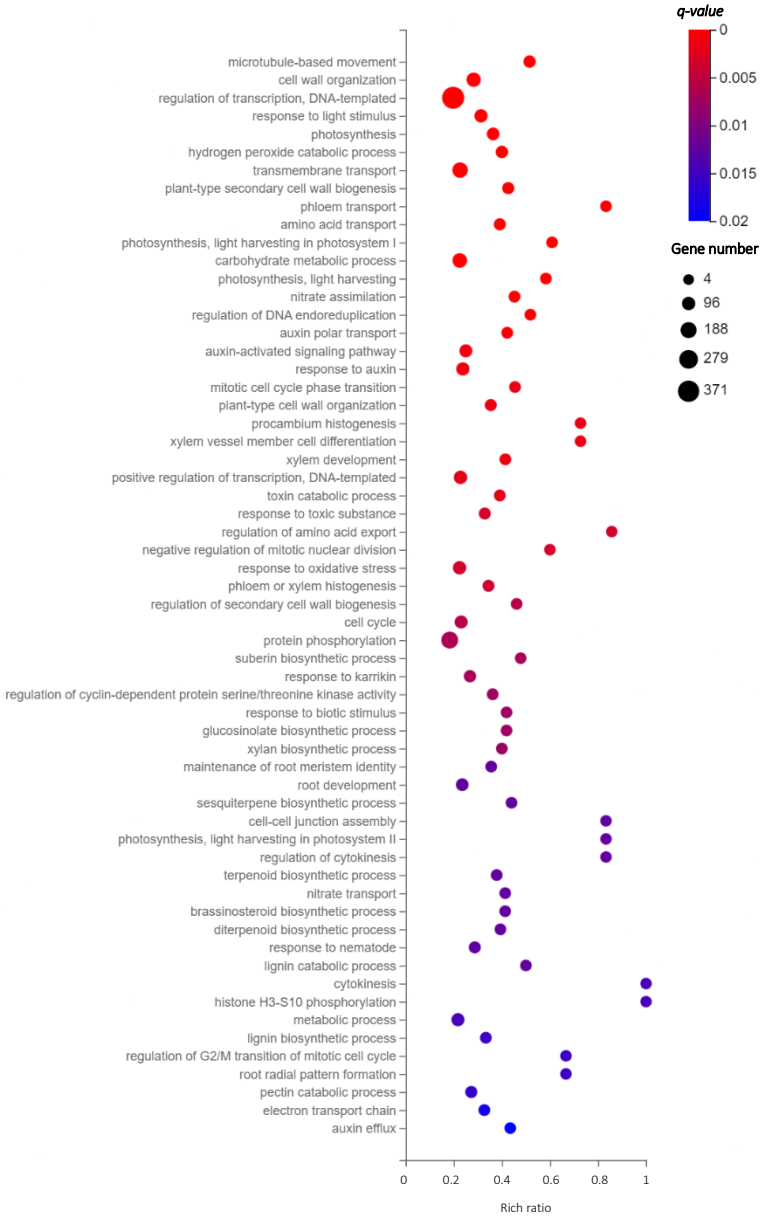

Figure 24. Several biological processes including developmental programs related with plant organogenesis are enriched in *uri1-1* DEGs. Bubble chart showing GO enrichment analysis reveals a multitude of processes that are altered in *uri1-1* compared with WT growing in shoot induction medium. Bubbles are colour-coded according to *q-value* and their size is relative to the gene number. Rich ratio shows the enrichment of each GO term.

Supplemental figures

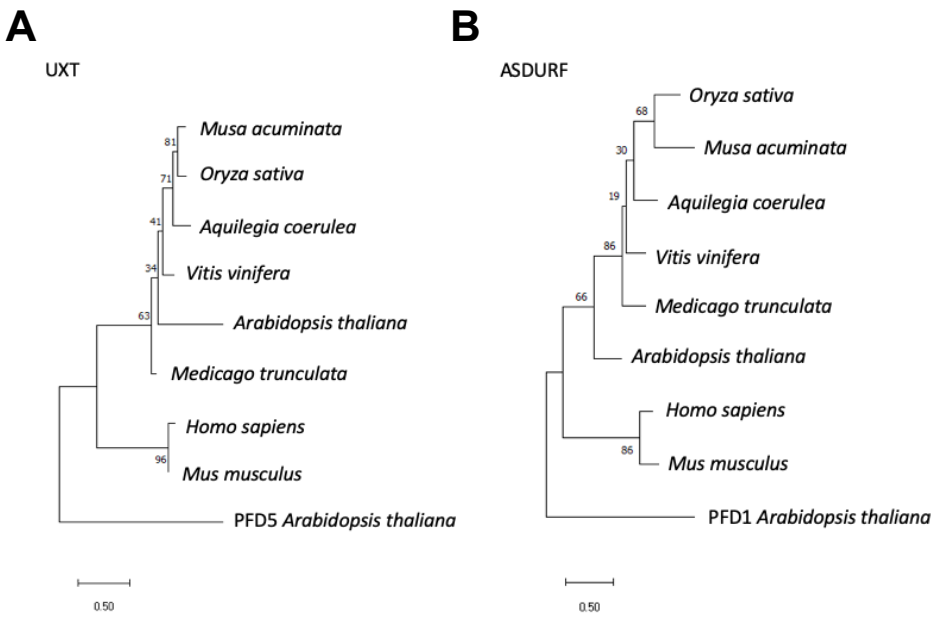

Supp Figure 1. The proteins encoded by *At1g26660* and *At1g49245* genes are the likely orthologs of UXT and ASDURF. A. Phylogenetic analysis of UXT and **B.** ASDURF proteins from various plant species, humans and mouse. Numbers in branches are maximum likelihood bootstrap values from one thousand replicates. The scale bar refers to the evolutive distance. *Arabidopsis* PFD5 and PFD1 were used as outliers.

Supplemental tables

All supplemental tables are available online at: http://plasticity.ibmcp.csic.es/tools.html

REFERENCES

Bai, F., & Demason, D. A. (2008). Hormone interactions and regulation of PsPK2::GUS compared with DR5::GUS and PID::GUS in *Arabidopsis thaliana*. American journal of botany, 95(2), 133–145.

Benbahouche, Nel H., Iliopoulos, I., Török, I., Marhold, J., Henri, J., Kajava, A. V., Farkaš, R., Kempf, T., Schnölzer, M., Meyer, P., Kiss, I., Bertrand, E., Mechler, B. M., & Pradet-Balade, B. (2014). Drosophila Spag is the homolog of RNA polymerase II-associated protein 3 (RPAP3) and recruits the heat shock proteins 70 and 90 (Hsp70 and Hsp90) during the assembly of cellular machineries. The Journal of biological chemistry, 289(9), 6236–6247.

Berg, M., Rogers, R., Muralla, R., & Meinke, D. (2005). Requirement of aminoacyl-tRNA synthetases for gametogenesis and embryo development in *Arabidopsis*. The Plant journal : for cell and molecular biology, 44(5), 866–878.

Blanco-Touriñán, N., Esteve-Bruna, D., Serrano-Mislata, A., Esquinas-Ariza, R. M., Resentini, F., Forment, J., Carrasco-López, C., Novella-Rausell, C., Palacios-Abella, A., Carrasco, P., Salinas, J., Blázquez, M. Á., & Alabadí, D. (2021). A genetic approach reveals different modes of action of prefoldins. Plant physiology, 187(3), 1534–1550.

Boulon, S., Pradet-Balade, B., Verheggen, C., Molle, D., Boireau, S., Georgieva, M., Azzag, K., Robert, M. C., Ahmad, Y., Neel, H., Lamond, A. I., & Bertrand, E. (2010). HSP90 and its R2TP/Prefoldin-like cochaperone are involved in the cytoplasmic assembly of RNA polymerase II. Molecular cell, 39(6), 912–924.

Delgermaa, L., Hayashi, N., Dorjsuren, D., Nomura, T., Thuy, leT. T., & Murakami, S. (2004). Subcellular localization of RPB5-mediating protein and its putative functional partner. Molecular and cellular biology, 24(19), 8556–8566.

Dorjsuren, D., Lin, Y., Wei, W., Yamashita, T., Nomura, T., Hayashi, N., & Murakami, S. (1998). RMP, a novel RNA polymerase II subunit 5-interacting protein, counteracts transactivation by hepatitis B virus X protein. Molecular and cellular biology, 18(12), 7546–7555.

Erb, M., & Kliebenstein, D. J. (2020). Plant Secondary Metabolites as Defenses, Regulators, and Primary Metabolites: The Blurred Functional Trichotomy. *Plant physiology*, *184*(1), 39–52.

Gstaiger, M., Luke, B., Hess, D., Oakeley, E. J., Wirbelauer, C., Blondel, M., Vigneron, M., Peter, M., & Krek, W. (2003). Control of nutrient-sensitive transcription programs by the unconventional prefoldin URI. Science (New York, N.Y.), 302(5648), 1208–1212.

Gu, Y., Deng, Z., Paredez, A. R., DeBolt, S., Wang, Z. Y., & Somerville, C. (2008). Prefoldin 6 is required for normal microtubule dynamics and organization in *Arabidopsis*. Proceedings of the National Academy of Sciences of the United States of America, 105(46), 18064–18069.

Gu, J., Liang, Y., Qiao, L., Lu, Y., Hu, X., Luo, D., Li, N., Zhang, L., Chen, Y., Du, J., & Zheng, Q. (2015). URI expression in cervical cancer cells is associated with higher invasion capacity and resistance to cisplatin. American journal of cancer research, 5(4), 1353–1367.

Herranz-Montoya, I., Park, S., & Djouder, N. (2021). A comprehensive analysis of prefoldins and their implication in cancer. iScience, 24(11), 103273.

Houry, W. A., Bertrand, E., & Coulombe, B. (2018). The PAQosome, an R2TP-Based Chaperone for Quaternary Structure Formation. Trends in biochemical sciences, 43(1), 4–9.

Ji, Y., Shen, J., Li, M., Zhu, X., Wang, Y., Ding, J., Jiang, S., Chen, L., & Wei, W. (2019). RMP/URI inhibits both intrinsic and extrinsic apoptosis through different signaling pathways. International journal of biological sciences, 15(12), 2692–2706.

Ju, Y., Liu, C., Lu, W., Zhang, Q., & Sodmergen (2016). *Arabidopsis* mitochondrial protein slow embryo development1 is essential for embryo development. Biochemical and biophysical research communications, 474(2), 371–376.

Lee, K. H., Minami, A., Marshall, R. S., Book, A. J., Farmer, L. M., Walker, J. M., & Vierstra, R. D. (2011). The RPT2 subunit of the 26S proteasome directs complex assembly, histone dynamics, and gametophyte and sporophyte development in *Arabidopsis*. The Plant cell, 23(12), 4298–4317.

Li, E., Bhargava, A., Qiang, W., Friedmann, M. C., Forneris, N., Savidge, R. A., Johnson, L. A., Mansfield, S. D., Ellis, B. E., & Douglas, C. J. (2012). The Class II KNOX gene KNAT7 negatively regulates secondary wall formation in *Arabidopsis* and is functionally conserved in Populus. *The New phytologist*, *194*(1), 102–115.

López-Juárez, Z. M., Aguilar-Henonin, L., & Guzmán, P. (2021). The ATXN2 Orthologs *CID3* and *CID4*, Act Redundantly to In-Fluence Developmental Pathways throughout the Life Cycle of *Arabidopsis thaliana*. *International journal of molecular sciences*, *22*(6), 3068.

Mita, P., Savas, J. N., Djouder, N., Yates, J. R., 3rd, Ha, S., Ruoff, R., Schafler, E. D., Nwachukwu, J. C., Tanese, N., Cowan, N. J., Zavadil, J., Garabedian, M. J., & Logan, S. K. (2011). Regulation of androgen receptor-mediated transcription by RPB5 binding protein URI/RMP. *Molecular and cellular biology*, *31*(17), 3639–3652.

Parusel, C. T., Kritikou, E. A., Hengartner, M. O., Krek, W., & Gotta, M. (2006). URI-1 is required for DNA stability in *C. elegans*. Development (Cambridge, England), 133(4), 621–629.

Sachs, T. (1991). Pattern Formation in Plant Tissues. Cambridge University.

Serra, L., & Robinson, S. (2020). Plant cell divisions: variations from the shortest symmetric path. Biochemical Society transactions, 48(6), 2743–2752.

Sotta, N., Shantikumar, L., Sakamoto, T., Matsunaga, S., & Fujiwara, T. (2016). TPR5 is involved in directional cell division and is essential for the maintenance of meristem cell organization in *Arabidopsis thaliana.* Journal of experimental botany, 67(8), 2401–2411.

Swaraz, A. M., Park, Y. D., & Hur, Y. (2011). Knock-out mutations of *Arabidopsis* SmD3-b induce pleotropic phenotypes through altered transcript splicing. Plant science: an international journal of experimental plant biology, 180(5), 661–671.

Tummala, K. S., Gomes, A. L., Yilmaz, M., Graña, O., Bakiri, L., Ruppen, I., Ximénez-Embún, P., Sheshappanavar, V., Rodriguez-Justo, M., Pisano, D. G., Wagner, E. F., & Djouder, N. (2014). Inhibition of de novo NAD(+) synthesis by oncogenic URI causes liver tumorigenesis through DNA damage. Cancer cell, 26(6), 826–839.

von Morgen, P., Hořejší, Z., & Macurek, L. (2015). Substrate recognition and function of the R2TP complex in response to cellular stress. Frontiers in genetics, 6, 69.

Wu, L. Y., Shang, G. D., Wang, F. X., Gao, J., Wan, M. C., Xu, Z. G., & Wang, J. W. (2022). Dynamic chromatin state profiling reveals regulatory roles of auxin and cytokinin in shoot regeneration. Developmental cell, 57(4), 526–542.e7.

Xu, C., Luo, F., & Hochholdinger, F. (2016). LOB Domain Proteins: Beyond Lateral Organ Boundaries. *Trends in plant science*, *21*(2), 159–167.

Yang, Y., Liu, F., Liu, L., Zhu, M., Yuan, J., Mai, Y. X., Zou, J. J., Le, J., Wang, Y., Palme, K., Li, X., Wang, Y., & Wang, L. (2022). The unconventional prefoldin RPB5 interactor mediates the gravitropic response by modulating cytoskeleton organization and auxin transport in *Arabidopsis*. Journal of integrative plant biology, 64(10), 1916–1934.

Zhao, Q., Leung, S., Corbett, A. H., & Meier, I. (2006). Identification and characterization of the *Arabidopsis* orthologs of nuclear transport factor 2, the nuclear import factor of ran. Plant physiology, 140(3), 869–878.

CHAPTER II.

THE PREFOLDIN-LIKE PROTEIN URI1 EXHIBITS CHARACTERISTICS OF INTRINSICALLY DISORDERED PROTEINS

The results from Chapter 1 indicate that URI1 is involved in diverse processes in *Arabidopsis*, most likely due to its ability to interact with many different proteins. We have found that this versatility in the function of URI1 is also observed in its orthologs from yeast and humans, however, the molecular basis is unknown. In this chapter, we have investigated the reason for this versatility.

URI1 has an intrinsically disordered region

The interactions of the URI1 protein with other subunits of the complex in humans occur via its PFD domain (Mita *et al*., 2013). In *Arabidopsis*, the *uri1-1* mutation leads to a G-to-R change at position 90 within the PFD domain, resulting in a weakened interaction with PFD6 (Yang *et al*., 2022). This observation suggests that the PFD domain plays a crucial role in the interaction in *Arabidopsis*. As mentioned in the Introduction, unlike other PFD or PFDL proteins, URI1 is larger and contains a C-terminal extension downstream of the PFD domain. Using AlphaFold, we generated the predicted structure of URI1 (Figure 1A) (Jumper *et al*., 2021). The algorithm showed high confidence in predicting the position of the residues forming the PFD domain (dark blue regions in Figure 1A and dark green regions in the plot of predicted alignment errors in Figure 1B). However, the confidence in the prediction of the position of most residues in the C-terminal extension was low (yellow and orange regions in Figure 1A and light green regions in the plot in Figure 1B). Analysis of the URI1 sequence using various protein disorder prediction algorithms, such as FoldIndex (Prilusky *et al*., 2005), IupedL, IupredS and SPOT-disorder summarised in DEPICTER (Barik *et al*., 2023), and AlphaFold-disorder included in MobiDB (Piovesan *et al*., 2023), showed that the C-terminal extension of URI1 is predicted to be disordered (Figure 1C, Figure 2A-B). The predicted disorder in URI1, expressed as a percentage of disordered residues, ranges from 65.5% to 83.6%, depending on the algorithm used. Consequently, URI1 is a partially disordered protein with a well-structured region at the N-terminus, the PFD domain, followed by an intrinsically disordered region (IDR).

We then investigated whether the presence of the IDR is a conserved feature of URI1. Using AlphaFold and the same disorder prediction tools used for URI1 in *Arabidopsis*, we analysed the orthologs of URI1 in humans and yeast. The structure predictions generated by AlphaFold showed that both human URI and yeast Bud27 have a well-defined PFD domain at the N-terminus followed by a predominantly unstructured region (Figure 3A-B; Figure 4A-B). Notably, the disorder predictors for both proteins revealed the presence of an IDR that encompassed the region at the C-terminus of the PFD domain (Figure 3C; Figure 4C). Despite the limited sequence homology in the C-terminal extension of URI1 in *Arabidopsis*, humans and yeast (Gstaiger *et al*., 2003), it was identified as an IDR in all three cases. This observation suggests that the unfoldability of this part of the protein has a functional significance, while the sequence may contribute to species-specific properties, such as interactions with certain partners.

Experimental findings from yeast and humans have provided substantial evidence supporting the crucial role of the region encompassing the IDR in URI/Bud27 function (Djouder *et al*., 2007; Deplazes *et al*., 2009; Mirón-García *et al*., 2013; Burén *et al*., 2016). Notably, complementation analyses in yeast involving deleted versions of Bud27 have demonstrated that the region downstream of the PFD domain, corresponding to the IDR, is sufficient to alleviate translational defects (Deplazes *et al*., 2009) and temperature sensitivity (Mirón-García *et al*., 2013) in Δuri/bud27 cells. Subsequently, we investigated whether *Arabidopsis* URI1 exhibits characteristics typical of proteins with IDRs. Our focus was directed towards examining the

capacity of URI1 to interact with other proteins, the stability of the URI1 protein, and the effects for the plant resulting from the overaccumulation of URI1.

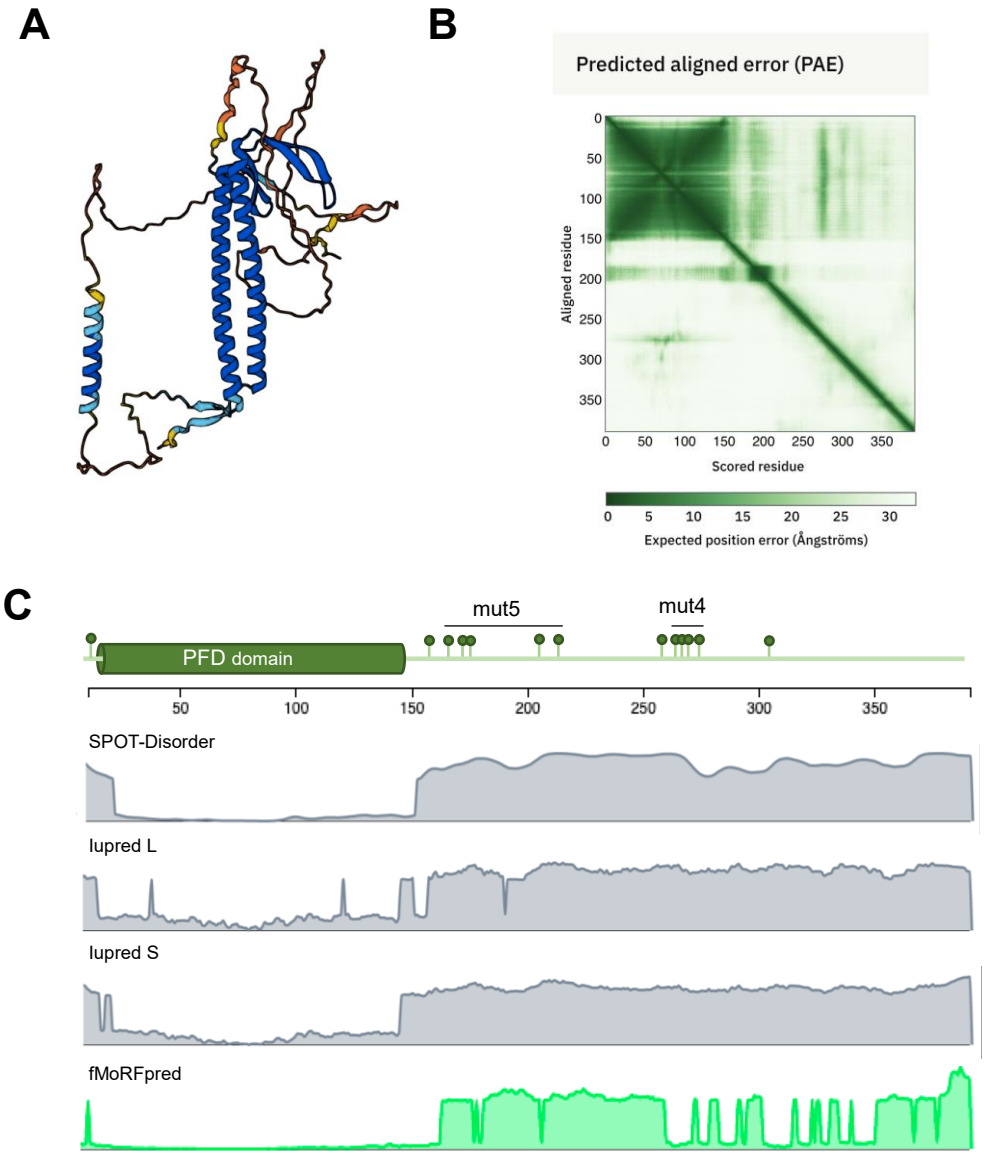

Figure 1. URI1 is predicted to be a partially disordered protein. **A.** The AlphaFold-predicted structure of URI1, where colours represent model confidence: dark blue (very high), light blue (high), orange (low), and yellow (very low). **B.** The PAE plot measures the confidence in the relative position of two residues in Angstroms (ranging arbitrarily between 0 and 31), with smaller distances indicating higher confidence. **C.** Plots display disorder (grey) and MoRF (green) propensity profiles in URI1 predicted by SPOT-Disorder, Iupred L, Iupred S, and fMoRFpred.The numeric line at the top indicates residue positions in the protein. The scheme of URI1 is depicted at the top of the panel, with green lollypops indicating residues phosphorylated *in vivo*.

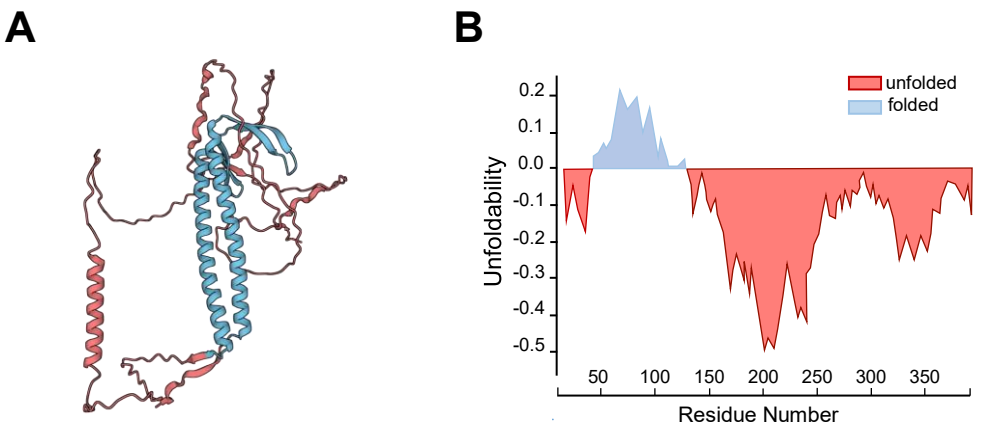

Figure 2. The URI1 protein is partially disordered. **A.** 3D structure of URI1 predicted by AlphaFold. The part of the protein predicted to be folded is colored in blue, while the disordered/unfolded regions appear in red. **B.** Output graph from the preFold analysis using the FoldIndex algorithm, showing the predicted folded (blue) and unfolded (red) regions of URI1.

URI1 has an extensive interactome

IDRs give proteins the versatility and adaptability to interact with a variety of different partners (Sun *et al*., 2013). The ability of IDRs to confer binding promiscuity and plasticity is attributed to small regions known as molecular recognition features (MoRFs), also referred to as short linear motifs or linear interacting peptides. These MoRFs can adopt different conformations when binding to different interaction partners (Yan *et al*., 2016). Analysis of *Arabidopsis* URI1 using the fMoRFpred algorithm incorporated in DEPICTER (Barik *et al*., 2020) predicted the presence of MoRFs in the IDR, particularly in the region extending from residues 150 to 250 and at the C-terminus (Figure 1C). A similar analysis identified numerous MoRFs in the IDRs of human and yeast URI1/Bud27 (Figure 3C; Figure 4C). This study suggests that the IDR of URI1 in *Arabidopsis* confers it the ability to bind promiscuously to partners, a property shared by URI of the three species.

In Chapter 1, we showed that URI1 interacts *in vivo* with a relatively large number of partners, 135, when following a strict cut-off criterion for identification, i.e. only proteins present in the three replicates, with minimum of two unique peptides in at least one of them and absent in the control line were considered (the number of interactors would be 194 if proteins represented by at least one unique peptide in each of the three replicates instead of considering two) (Figure 5A; Chapter I - Supp Table 4). We then investigated whether URI/Bud27 exhibits similar promiscuity in yeast and humans. We used the list of URI interactors in human HEK 293T cells identified by AP-MS (Cloutier *et al*., 2020). The list of yeast Bud27 interactors, identified by various experimental approaches, was obtained from the Saccharomyces Genome Database (Wong *et al*., 2023). URI has 142 and 117 partners in humans and yeast, respectively (Cloutier *et al*., 2020; Wong *et al*., 2023), suggesting that both are promiscuous proteins. However, the number of interactors for the partner of *Arabidopsis* URI1, UXT, was comparatively lower (Figure 5A-B; Chapter I - Supp Table 4). In contrast to URI1, UXT is predominantly an ordered protein consisting almost exclusively of the α-type PFD domain (Chapter I - Figure 9A). These results suggest that the

promiscuity of *Arabidopsis* URI1 in establishing protein-protein interactions is likely mediated by the IDR region rather than the PFD domain. This property is probably influenced by the presence of numerous MoRFs within the IDR.

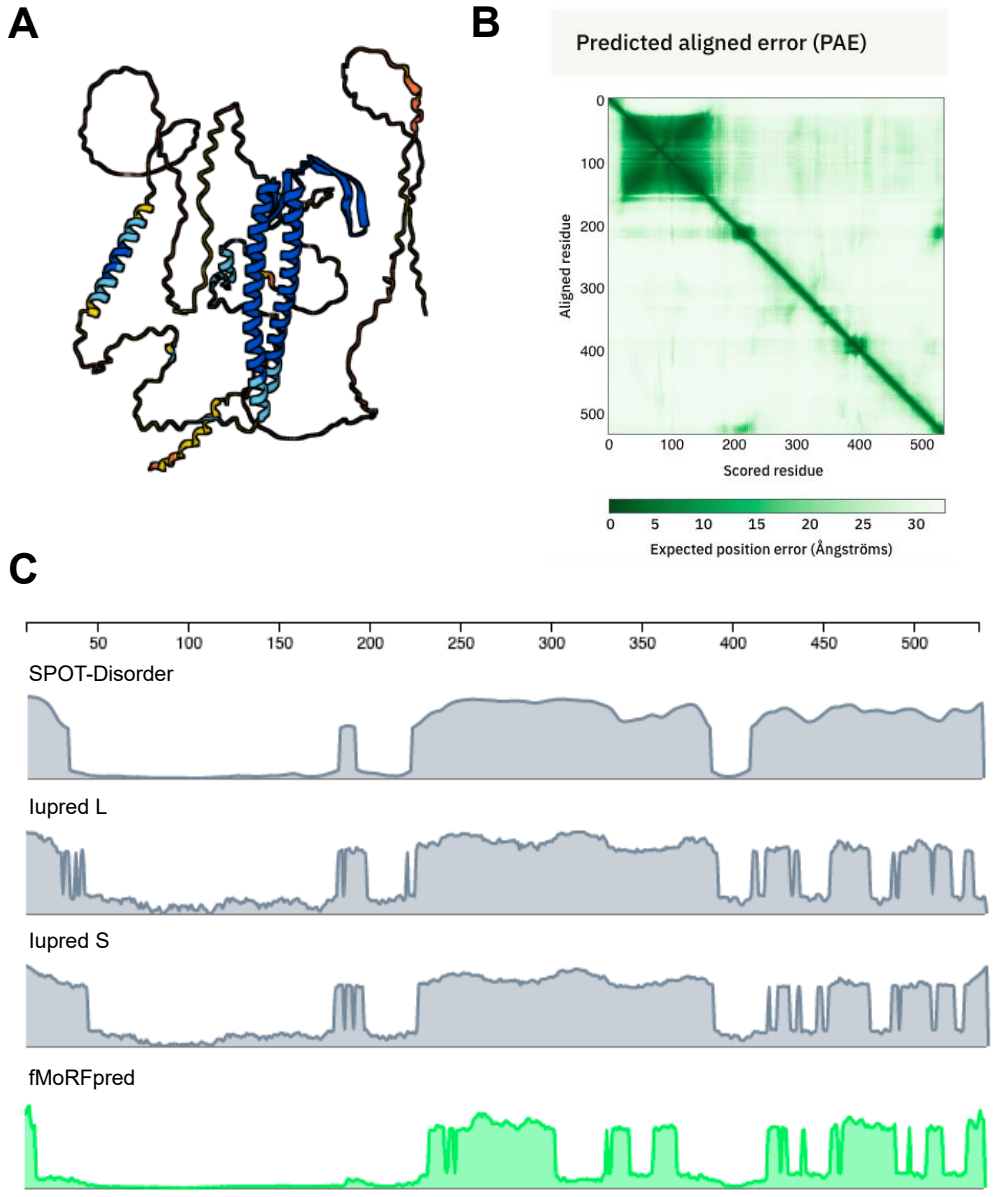

Figure 3. Human URI is predicted to be a partially disordered protein. **A.** The AlphaFold-predicted structure of URI, where colours represent model confidence: dark blue (very high), light blue (high), orange (low), and yellow (very low). **B.** The PAE plot measures the confidence in the relative position of two residues in Angstroms (ranging arbitrarily between 0 and 31), with smaller distances indicating higher confidence. **C.** Plots display disorder (grey) and MoRF (green) propensity profiles in URI predicted by SPOT-Disorder, Iupred L, Iupred S, and fMoRFpred. The numeric line at the top indicates residue positions in the protein.

A higher preference for interactions between disordered proteins was found in humans (Shimizu and Toh, 2009). To investigate whether URI1 preferentially interacts with disordered proteins, we determined the unfoldability value for each of the URI1 interactors using FoldIndex and compared it with the value calculated for a list containing the same number of randomly selected proteins (Supp Table 1). Positive values correspond to preferentially folded proteins,

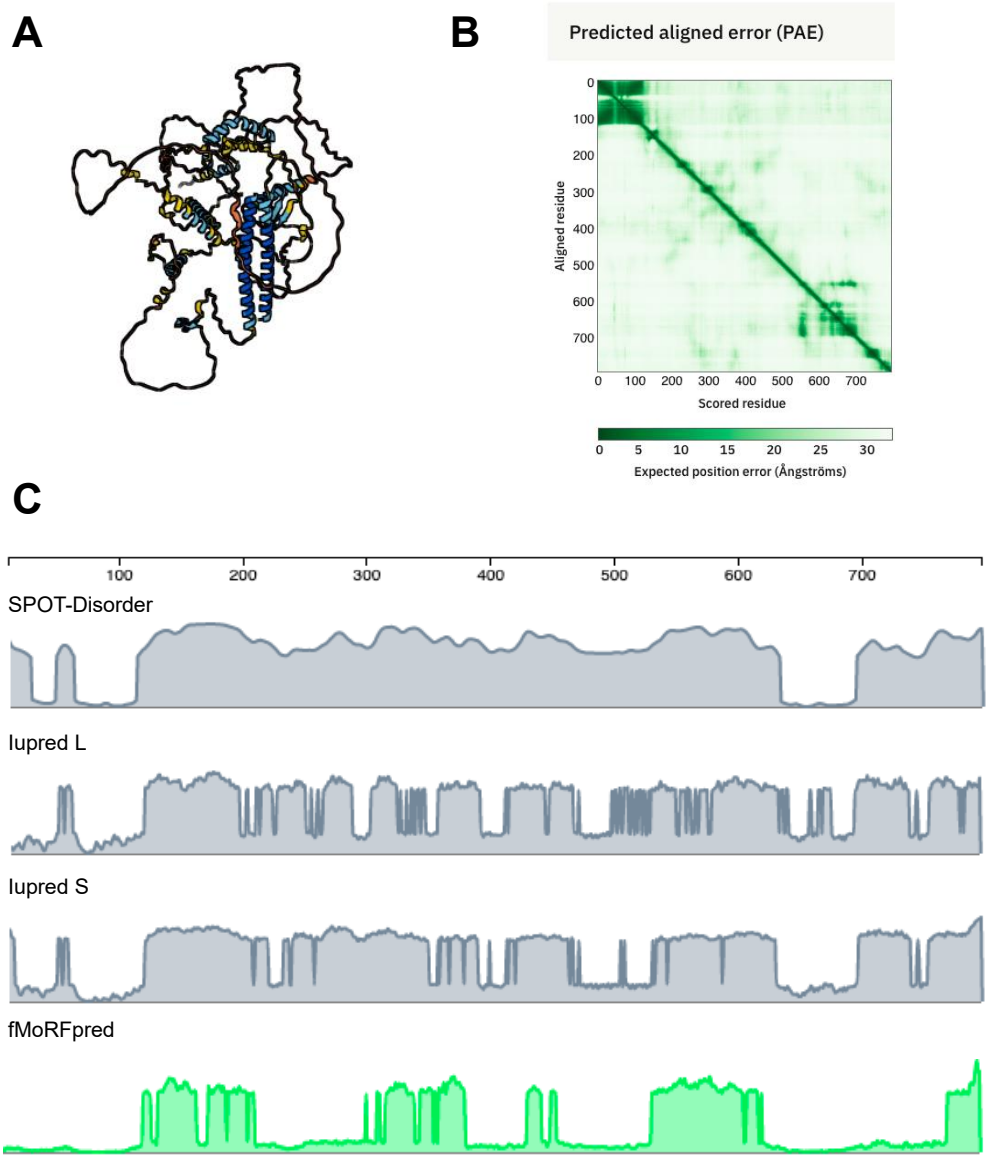

Figure 4. Bud27 is predicted to be a partially disordered protein. A. The AlphaFold-predicted structure of Bud27, where colours represent model confidence: dark blue (very high), light blue (high), orange (low), and yellow (very low). **B.** The PAE plot measures the confidence in the relative position of two residues in Angstroms (ranging arbitrarily between 0 and 31), with smaller distances indicating higher confidence. **C.** Plots display disorder (grey) and MoRF (green) propensity profiles in URI/Bud27 predicted by SPOT-Disorder, Iupred L, Iupred S, and fMoRFpred. The numeric line at the top indicates residue positions in the protein.

while negative values correspond to predicted disordered proteins; the lower the value, the more disordered (Prilusky *et al*., 2005).

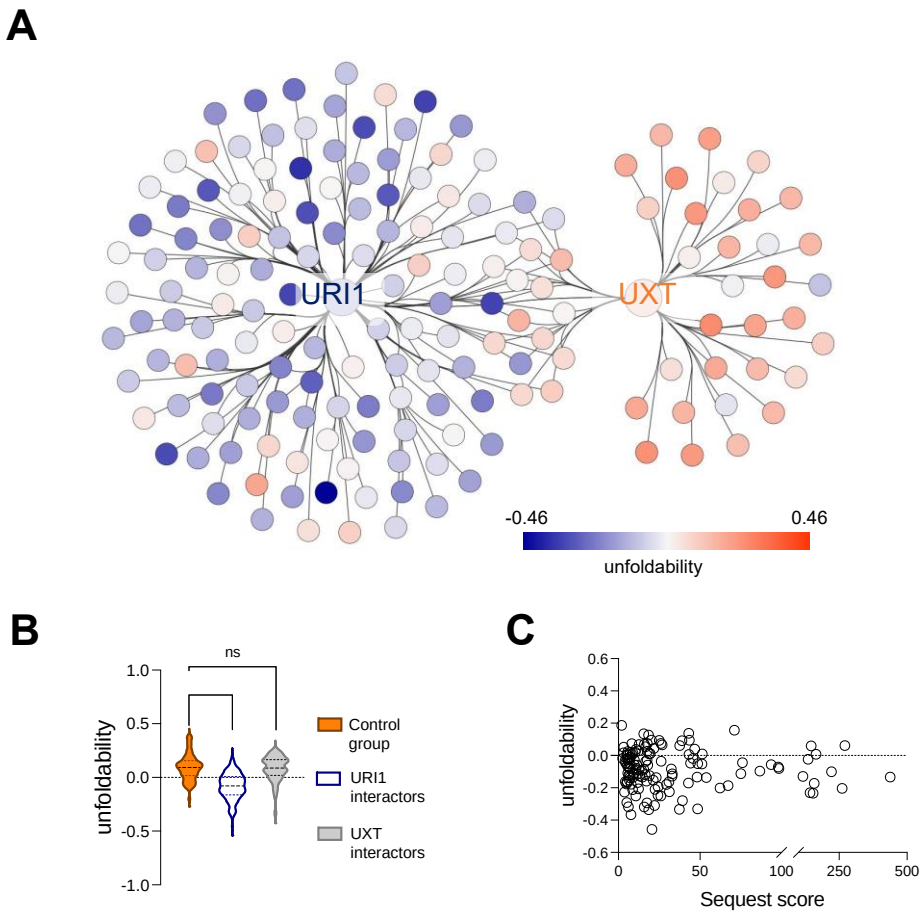

Figure 5. URI1 is a promiscuous protein that preferentially interacts with disordered proteins. A. Visualization of the URI1 and UXT interacting network generated by Cytoscape. The node color indicates the unfoldability, as depicted in the scale bar. Six UXT interactors have not been included in the network, as we did not retrieve their unfoldability values from the analysis with preFold. **B.** Violin plots showing the unfoldability value for a group of randomly selected *Arabidopsis* proteins (control group; n=135), URI1 interactors (n=135), and UXT interactors (n=51). Dotted lines within the violins represent the median and the first and third quartiles. ****, $P < 0.0001$; ns, non-significant. **C.** Scatter plot representing the unfoldability value and Score Sequest HT for each URI1 interactor.

For example, the unfoldability value of SERRATE (SE), an URI1 interactor from *Arabidopsis* that has characteristics of disordered proteins (Li *et al*., 2020), is -0.133, while the value for URI1 is -0.099 (Supp Table 2). The mean value of unfoldability of URI1 interactors in *Arabidopsis* was negative and significantly lower than that of the control group (Figure 5A, B) indicating a greater prevalence of disordered proteins or proteins with one or more IDRs among URI1 interactors in *Arabidopsis.*

We then investigated whether this feature of URI1 in *Arabidopsis* is conserved in humans and yeast or whether it is species-dependent. Analogous to *Arabidopsis* URI1, we determined the value of unfoldability for each URI1 partner in each species using FoldIndex. In contrast to *Arabidopsis* URI1, the mean unfoldability value for human URI1 interactors matched that of the control list, both being positive (Figure 6). The average unfoldability value of URI/Bud27 interactors was positive, but significantly lower than that of the control list (Figure 6). In contrast to *Arabidopsis* URI1, these results suggest that, at least under the physiological conditions under which human and yeast URI interactomes were determined, URI from these two organisms does not selectively interact with disordered proteins. Our analyses suggest that the composition of URI1 interactomes likely depends on the species-specific sequence of URI1, including IDR, and it is not solely determined by the unfoldability of the IDR.

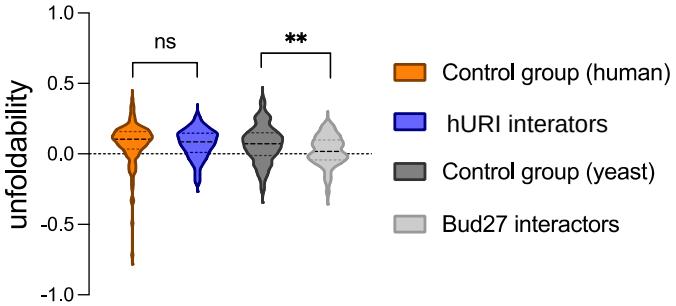

Figure 6. Human URI and yeast Bud27 preferentially interact with ordered proteins. Violin plots showing the unfoldability value for a group of randomly selected human (control group human; n=132) and yeast (control group yeast; n=114) proteins, human URI interactors (hURI; n=132), and yeast Bud27 interactors (Bud27; n=114). Dotted lines within the violins represent the median and the first and third quartiles. **, $P < 0.01$; ns, non-significant.

Having established the propensity of *Arabidopsis* URI1 to interact with disordered proteins, we aimed to determine whether the extent of unfoldability of each partner influences the strength of the interaction. To this end, we plotted the unfoldability value against the average score Sequest HT (Supp Table 3) (Eng *et al*., 1994) for each of them in the three replicates, which we used as a proxy to measure the strength of the interaction. As shown in Figure 5C, no correlation was apparent between these two parameters, suggesting that the degree of disorder of the partner does not seem to determine the strength of its interaction with URI1 in *Arabidopsis.*

In contrast to *Arabidopsis* URI1, the average unfoldability value for UXT interactors was positive and similar to that of the control group of proteins (Figure 5A-B). The specific prevalence of disordered proteins in URI1 partners suggests that URI1 establishes these interactions alone and not as part of the PFDL complex. This is supported by the limited overlap between URI1 and UXT interactors in *Arabidopsis*, as shown in Figure 5A-B. Nevertheless, we cannot rule out the possibility that URI1 interacts with its partners as a part of the PFDL, and that the failure to identify a larger number of UXT interactors may be due to technical limitations of immunoprecipitation.

The interactome of URI1 revealed that proteins were mainly associated with RNA binding, nucleic acid binding, and mRNA binding (Chapter I - Figure 7, Chapter I - Supp Table 4). This observation is consistent with studies showing that RNA-binding proteins and spliceosome components are predominantly disordered in mammals (Castello *et al*., 2012; Korneta and Bujnicki, 2012; Zhao *et al*., 2021), suggesting a functional connection between URI1 and RNA transactions based on the disorder of URI1 and its RNA binding partners. We propose that URI1, supported by the capabilities conferred by the IDR, can act on these partners in various ways,

either autonomously or as part of the PFDL complex in *Arabidopsis* (Van Der Lee *et al*., 2014). Thus, URI1 could serve several functions: (i) as a chaperone that helps achieve the final conformation of the partner; (ii) as an effector protein that modulates partner activity, as evidenced by interaction with the phosphatase PP1γ via a region within the URI IDR in humans (Djouder *et al*., 2007); or (iii) as an assembler that helps in the assembly of protein complexes (Houry *et al*., 2018).

URI1 is an unstable protein likely degraded via 20S proteasome

The involvement of disordered or partially disordered proteins in regulatory pathways and their propensity to form protein-protein interactions means that the amount of these proteins must be tightly controlled (Gsponer *et al*., 2008). Thus, disordered or partially disordered proteins tend to be unstable, short-lived proteins (Gsponer *et al*., 2008). We investigated whether this was the case for URI1 by conducting *in vitro* cell-free degradation assays.

For this purpose, we transiently expressed either *Arabidopsis* HA-URI1 or GFP in the leaves of *N. benthamiana* and incubated the protein extracts for different time points at 30ºC in the presence of the protein synthesis inhibitor cycloheximide (CHX). We then analysed the protein levels of HA-URI1 and GFP by Western blot. As shown in Figure 7A-B, the *Arabidopsis* HA-URI1 levels decreased within the first minutes of incubation, while the GFP level remained unchanged. This result indicates that *Arabidopsis* URI1 is susceptible to rapid degradation, suggesting that it is an unstable protein. We then investigated whether URI1 is degraded via the proteasome pathway. Incubation of protein extracts with the proteasome inhibitor MG-132 resulted in a delay in the degradation of HA-URI1, suggesting that the proteasome is at least partially involved in the degradation (Figure 7A-B).

Many disordered proteins are directly degraded by the 20S core proteasome without requiring the proteasome 19S lid, which is responsible for unfolding the target proteins (Opoku-Nsiah and Gestwicku, 2018). This process is independent of protein ubiquitination. The 20S proteasome also degrades partially disordered proteins, as shown for the *Arabidopsis* protein SE (Li *et al*., 2020). To determine whether *Arabidopsis* URI1 can also be degraded via 20S proteasome, we conducted the *in vitro* cell-free degradation assays in the presence of CHX and PYR41, an inhibitor of the ubiquitin-activating enzyme E1. As shown in Figure 7C-D, the decay of HA-URI1 protein levels were not affected by PYR-41, suggesting that it occurs independent of ubiquitination via 20S proteasome. The degradation of the URI1 protein was also observed when conducted the *in vitro* cell-free degradation assays with recombinant URI1 fused to maltose binding protein (MBP), which was expressed and purified from *E. coli* (Figure 8A). The degradation of the recombinant MBP-URI1 was delayed by treatment with MG-132 but not with PYR41, suggesting that, like HA-URI1 expressed in *N. benthamiana* leaves, the recombinant version was degraded via the core 20S proteasome (Figure 8B-C).

IDRs are particularly susceptible to post-translational modifications such as phosphorylation, which often alter the stability of the protein (Wright and Dyson, 2015). Several phosphoproteomic analyses have identified 13 *in vivo* phosphorylated Ser/Thr residues in *Arabidopsis* URI1 (Xu *et al*., 2017; Cruz *et al*., 2019; Willems *et al*., 2019), all of which are located within the IDR (Figure 1C; Supp Table 2). We tested whether the phosphorylation of some of these residues had an effect on the protein level of URI1. Therefore, we generated two mutant versions of URI1 in which two clusters of phosphorylated Ser/Thr were replaced by Ala. The replaced residues were Ser^{165}, Ser^{174}, Thr^{178}, Ser^{211} and Ser^{218} in $URI1^{mut5A}$, all of which predicted to be phosphorylated by casein kinase II (CK2; Supp Table 2), and Ser^{262}, Ser^{263}, Ser^{264} and Ser^{268} in

URI1^{mut4A}. We then transiently expressed the WT and mutant versions in *N. benthamiana* leaves and analysed protein levels by Western blot (Figure 7E). Two interesting findings could be derived from this analysis. First, the bands of the mutant versions exhibited faster migration than those of the WT, suggesting that the mutant residues were typically phosphorylated in *N. benthamiana* leaves. This phosphorylation likely contributes to the observed increased molecular weight of YFP-

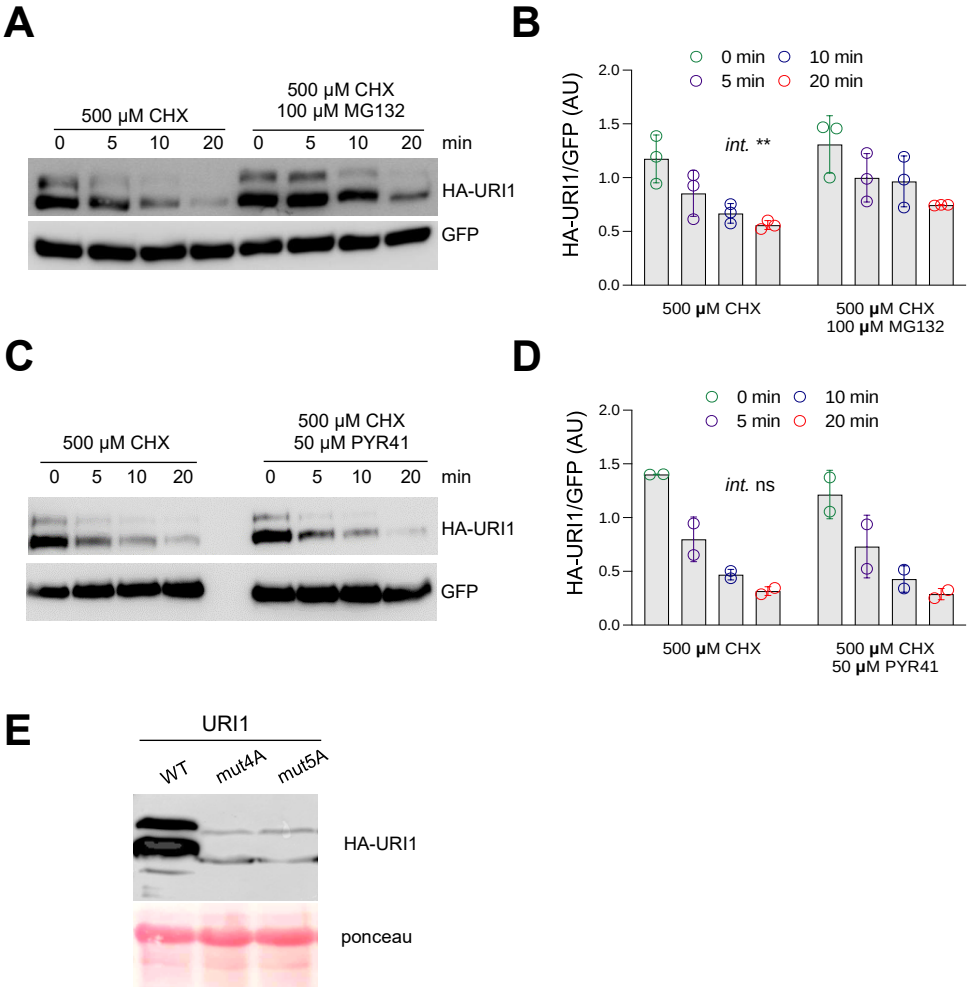

Figure 7. URI1 is an unstable protein. Total proteins from *N. benthamiana* leaves co-expressing HA-URI1 and GFP were used for cell-free degradation assays. Protein extracts were incubated with 500 µM CHX or with 500 µM CHX and 100 µM MG-132 (A, B), or with 500 µM CHX and 50 µM PYR-41 (C, D) for the indicated times. HA-URI1 and GFP levels were determined from three (A, B) and two (C, D) biological replicates by western blot. One representative western blot is shown in (A, C), while the quantifications are shown in (B, D). URI1 normally appears as a double band; the lower band was used for quantification. E. Western blot showing the protein level of the WT and mutant versions of HA-URI1 transiently expressed in leaves of *N. benthamiana*. In (B, D) *Int.* refers to the interaction between treatments assessed by two-way ANOVA; **, $P < 0.01$, ns, non-significant.

URI1 and URI-3xFLAG in the immunoblots. Second, the mutant proteins accumulated to a lesser extent than their WT counterpart, suggesting that phosphorylation of these residues may play a role in maintaining the stability of URI1 in *Arabidopsis*.

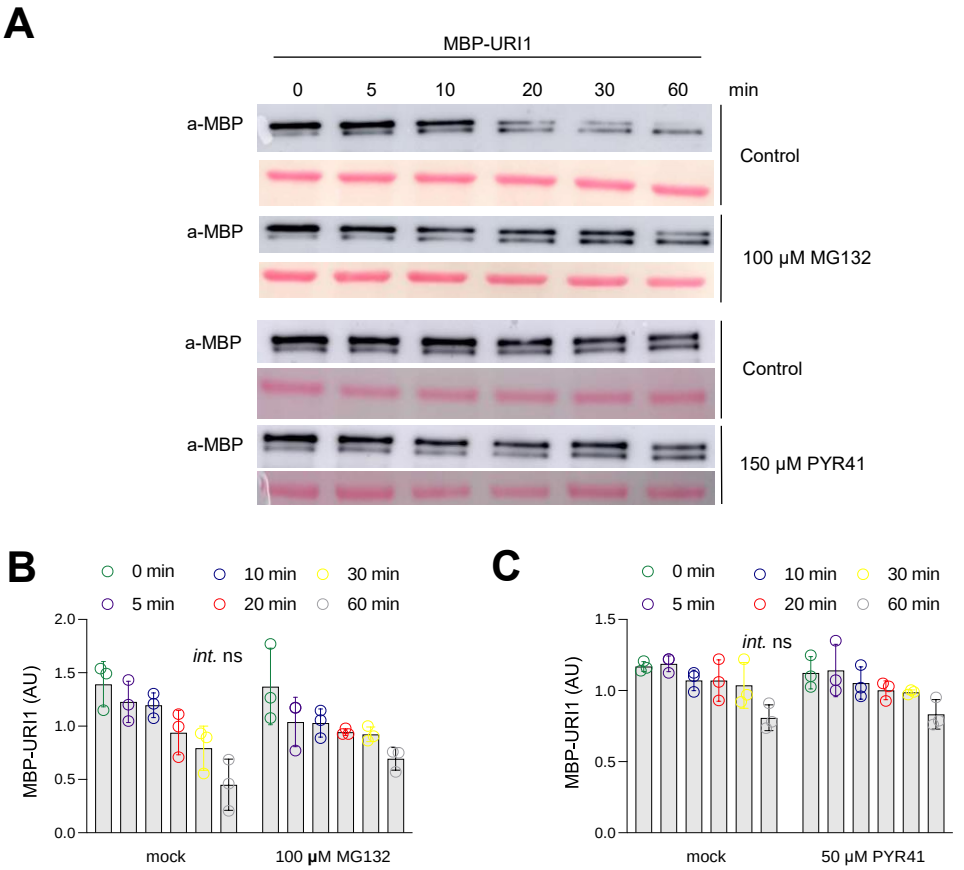

Figure 8. Recombinant MBP-URI1 is likely degraded via the proteasome 20S. **A.** Representative immunoblots illustrating the degradation of MBP-URI1 in cell-free degradation assays, with Ponceau staining of the membranes shown below each immunoblot. Quantification of the upper band, representing MBP-URI1, in three replicates of mock and MG-132 treatment **B.** and mock and PYR-41 treatment **C.** '*Int.*' refers to the interaction between treatments assessed by two-way ANOVA. The effect of the treatments is non-significant (ns), despite a tendency towards the stabilization of MBP-URI1 observed after treatment with MG-132.

Overaccumulation of URI1 may interfere with its function.

To assess the effects of URI1 overaccumulation in plants, we generated several transgenic *Arabidopsis* lines expressing an YFP-URI1 fusion under the control of the constitutive *35S* promoter. These lines exhibited varying degrees of developmental and growth alterations, including the appearance of twin stems (Figure 9A), changes in phyllotaxis (Figure 9B) and extreme dwarfism with a bushy appearance, possibly due to internode shortening associated with additional branching (Figure 9C-D). The phenotype of homozygous plants of lines 4.9, 6.7, 16.11 and 29.6 was very similar within each line. However, a range of phenotypes was observed in homozygous plants of line 5.3 (Figure 9A). To determine whether the severity of the phenotypes correlated directly with the amount of YFP-URI1, we measured the protein levels in the inflorescences of 25-day-old plants (Figure 10A). Surprisingly, the lines with the most severe phenotype, 5.3 and 6.7, had the lowest YFP-URI1 levels. We ruled out co-suppression of the endogenous URI1 locus as the cause of these phenotypes, as URI1 was overexpressed and the transgene was expressed (Figure 11A-B). The reduced levels of YFP-URI1 in line 5.3 was also

observed in 7-day-old seedlings (Figure 10B). In this case, no correlation was observed between the amount of YFP-URI1 protein and the expression of the transgene (Figure 10B, Figure 11C). None of the transgenic lines showed a distinctive phenotype at the seedling stage (Figure 11D).

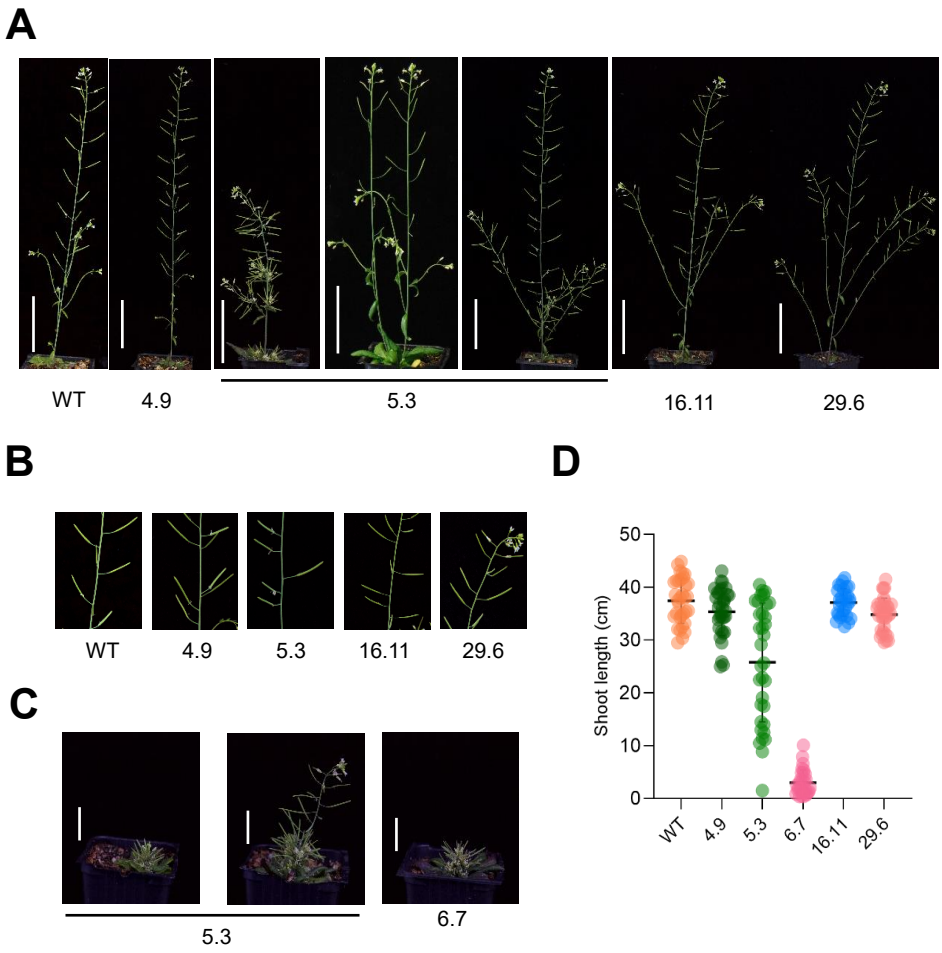

Figure 9. Alteration of URI1 levels causes growth and developmental defects. **A, B, C.** Representative homozygous plants from the indicated lines expressing *35S:YFP-URI1.* Plants were grown under a 16 h light:8 h dark photoperiod at 22 ºC for 25 days. Several plants of line 5.3 are shown, as this line exhibited phenotypes of diverse severity. **B.** Close-up view of the defects in silique arrangement in the transgenic lines. **C.** Dwarf and bushy plants from lines 5.3 and 6.7. **D.** Stem length of 25-day-old plants from the different lines; 28-35 plants per line were used for measurements. The scale bar in **A.** and **C.** is 5 cm and 2 cm, respectively.

Li *et al*. (2020) reported a parallel situation concerning SE, in which excess transgenic SE protein in SE-overexpressing lines led to degradation by the 20S proteasome. The proteasome also degraded endogenous SE, resulting in a similar phenotype of *se* mutants and SE transgenic lines. The authors hypothesised that SE is typically involved in various protein complexes and any non-associated SE fraction is degraded by the 20S proteasome to prevent deleterious effects of excess of this protein. We hypothesised that a similar mechanism might regulate URI1 protein levels in *Arabidopsis*. We explored this possibility by investigating whether overexpression of *YFP-URI1* could trigger the degradation of URI1-3xFLAG in *pURI1:URI1-3xFLAG* x *35S:YFP-URI1* 6.7

and 29.6 F1 seedlings. As shown in Figure 10C, the levels of URI1-3xFLAG were reduced in F1 seedlings co-expressing YFP-URI1 compared to control F1s from the cross with the non-transgenic WT. This would be consistent with the reduced levels of URI1-3xFLAG being caused by the degradation triggered by the overexpression of YFP-URI1, which is also likely to affect endogenous URI1. Thus, URI1 levels may be subject to a control mechanism similar to SE (Li *et al*., 2020). This suggests that the developmental phenotypes shown in Figure 9A were caused by reduced URI1 activity. However, it is worth noting that these developmental phenotypes are not observed in the *uri1-1* mutant (Yang *et al*., 2022), likely reflecting different molecular defects, i.e. a change in the amino acid in the *uri1-1* protein versus a reduced amount of the protein in the transgenic plants, each having different effects on developmental processes.

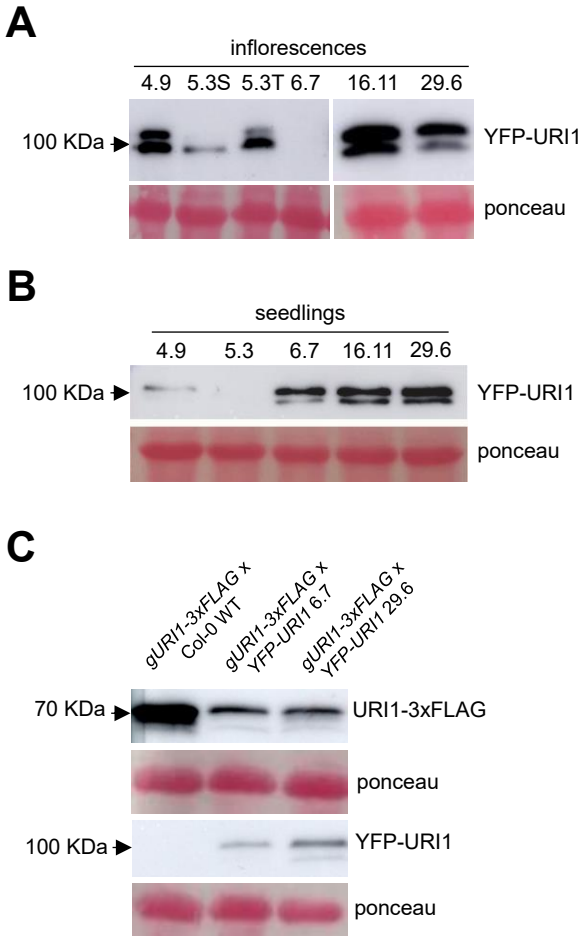

Figure 10. Overexpression of *YFP-URI1* causes URI1 degradation. A. Western blot analysis of YFP-URI1 levels in inflorescences of 25-day-old plants, **B.** and 10-day-old seedlings of the *35S:YFP-URI1* transgenic lines. In A, 5.3T and 5.3S refer to the inflorescences of tall and dwarf plants, respectively. **C.** Western blot analysis of URI1-3xFLAG and YFP-URI1 levels in 10-day-old seedlings of the indicated genotypes. Ponceau staining is shown as a loading control.

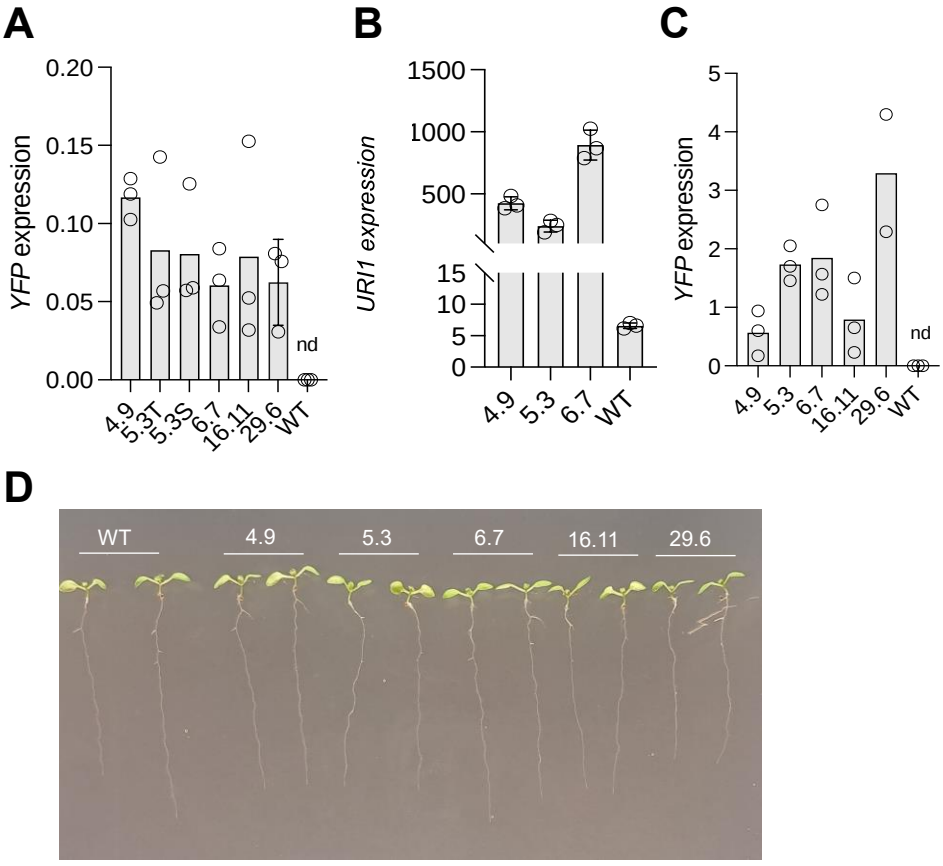

Figure 11. *URI1* is overexpressed in the transgenic lines. A, C. Expression of *YFP* and **B.** *URI1* assessed by RT-qPCR in inflorescences (A) and seedlings (B, C). Each dot represents a biological replicate; nd, non-detected. **D.** Picture of two representative seedlings of the different transgenic lines alongside the wild type.

Supplemental tables

All supplemental tables are available online at: http://plasticity.ibmcp.csic.es/tools.html

REFERENCES

Barik, A., Katuwawala, A., Hanson, J., Paliwal, K., Zhou, Y., and Kurgan, L. (2020). DEPICTER: Intrinsic Disorder and Disorder Function Prediction Server. J. Mol. Biol. 432:3379–3387.

Burén, S., Gomes, A. L., Teijeiro, A., Fawal, M. A., Yilmaz, M., Tummala, K. S., Perez, M., Rodriguez-Justo, M., Campos-Olivas, R., Megías, D., *et al*. (2016). Regulation of OGT by URI in Response to Glucose Confers c-MYC-Dependent Survival Mechanisms. Cancer Cell 30:290–307.

Castello, A., Fischer, B., Eichelbaum, K., Horos, R., Beckmann, B. M., Strein, C., Davey, N. E., Humphreys, D. T., Preiss, T., Steinmetz, L. M., *et al*. (2012). Resource Insights into RNA Biology from an Atlas of Mammalian mRNA-Binding Proteins. Cell 149:1393–1406.

Cloutier, P., Poitras, C., Faubert, D., Bouchard, A., Blanchette, M., Gauthier, M. S., and Coulombe, B. (2020). Upstream ORF-Encoded ASDURF Is a Novel Prefoldin-like Subunit of the PAQosome. J Proteome Res 19:18–27.

Cruz, E. R., Nguyen, H., Nguyen, T., and Wallace, I. S. (2019). Functional analysis tools for post-translational modification: a post-translational modification database for analysis of proteins and metabolic pathways. Plant J. 99:1003–1013.

Deplazes, A., Möckli, N., Luke, B., Auerbach, D., and Peter, M. (2009). Yeast Uri1p promotes translation initiation and may provide a link to cotranslational quality control. EMBO J. 28:1429–41.

Djouder, N., Metzler, S. C., Schmidt, A., Wirbelauer, C., Gstaiger, M., Aebersold, R., Hess, D., and Krek, W. (2007). S6K1-Mediated Disassembly of Mitochondrial URI/PP1γ Complexes Activates a Negative Feedback Program that Counters S6K1 Survival Signaling. Mol. Cell 28:28–40.

Eng, J., McCormack, A., and Yates, J. (1994). An approach to correlate tandem mass spectral data of peptides with amino acid sequences in a protein database. J Am Soc Mass Spectrom 5:976–989.

Gsponer, J., Futschik, M. E., Teichmann, S. A., and Babu, M. M. (2008). Tight regulation of unstructured proteins: from transcript synthesis to protein degradation. Science (80-.). 322:1365–1369.

Gstaiger, M., Luke, B., Hess, D., Oakeley, E. J., Wirbelauer, C., Blondel, M., Vigneron, M., Peter, M., and Krek, W. (2003). Control of nutrient-sensitive transcription programs by the unconventional prefoldin URI. Science (80-.). 302:1208–1212

Houry, W. A., Bertrand, E., and Coulombe, B. (2018). The PAQosome , an Chaperone for Quaternary Structure Formation R2TP core PIH1D1 POLR2E PFDL module. Trends Biochem. Sci. 43:4–9

Jumper, J., Evans, R., Pritzel, A., Green, T., Figurnov, M., Ronneberger, O., Tunyasuvunakool, K., Bates, R., Žídek, A., Potapenko, A., Bridgland, A., Meyer, C., Kohl, S. A. A., Ballard, A. J., Cowie, A., Romera-Paredes, B., Nikolov, S., Jain, R., Adler, J., Back, T., … Hassabis, D. (2021). Highly accurate protein structure prediction with AlphaFold. Nature, 596(7873), 583–589.

Korneta, I., and Bujnicki, J. M. (2012). Intrinsic Disorder in the Human Spliceosomal Proteome. PLoS Comput Biol 8:1002641

Li, Y., Sun, D., Ma, Z., Yamaguchi, K., Wang, L., Zhong, S., Yan, X., Shang, B., Nagashima, Y., Koiwa, H., *et al*. (2020). Degradation of SERRATE via ubiquitin-independent 20S proteasome to survey RNA metabolism. Nat. Plants 6:970–982.

Mirón-García, M. C., Garrido-Godino, A. I., García-Molinero, V., Hernández-Torres, F., Rodríguez-Navarro, S., and Navarro, F. (2013). The prefoldin bud27 mediates the assembly of the eukaryotic RNA polymerases in an rpb5-dependent manner. PLoS Genet 9:e1003297.

Mita, P., Savas, J. N., Ha, S., Djouder, N., Yates, J. R., 3rd, & Logan, S. K. (2013). Analysis of URI nuclear interaction with RPB5 and components of the R2TP/prefoldin-like complex. PloS one, 8(5), e63879.

Opoku-Nsiah, K. A., and Gestwicki, J. E. (2018). Aim for the core: suitability of the ubiquitin-independent 20S proteasome as a drug target in neurodegeneration. Transl. Res. 198:48–57.

Piovesan, D., Del Conte, A., Clementel, D., Monzon, A. M., Bevilacqua, M., Aspromonte, M. C., Iserte, J. A., Orti, F. E., Marino-Buslje, C., and Tosatto, S. C. E. (2023). MobiDB: 10 years of intrinsically disordered proteins. Nucleic Acids Res. 51:D438–D444.

Prilusky, J., Felder, C. E., Zeev-Ben-Mordehai, T., Rydberg, E. H., Man, O., Beckmann, J. S., Silman, I., & Sussman, J. L. (2005). FoldIndex: a simple tool to predict whether a given protein sequence is intrinsically unfolded. Bioinformatics (Oxford, England), 21(16), 3435–3438.

Shimizu, K., and Toh, H. (2009). Interaction between Intrinsically Disordered Proteins Frequently Occurs in a Human Protein-Protein Interaction Network. J. Mol. Biol. 392:1253–1265.

Sun, X., Rikkerink, E. H. A., Jones, W. T., and Uversky, V. N. (2013). Multifarious roles of intrinsic disorder in proteins illustrate its broad impact on plant biology. Plant Cell 25:38–55

Van Der Lee, R., Buljan, M., Lang, B., Weatheritt, R. J., Daughdrill, G. W., Dunker, A. K., Fuxreiter, M., Gough, J., Gsponer, J., Jones, D. T., *et al*. (2014). Classification of intrinsically disordered regions and proteins. Chem. Rev. 114:6589–6631.

Willems, P., Horne, A., Van Parys, T., Goormachtig, S., De Smet, I., Botzki, A., Van Breusegem, F., and Gevaert, K. (2019). The Plant PTM Viewer, a central resource for exploring plant protein modifications. Plant J. 99:752–762.

Wong, E. D., Miyasato, S. R., Aleksander, S., Karra, K., Nash, R. S., Skrzypek, M. S., Weng, S., Engel, S. R., and Cherry, J. M. (2023). Saccharomyces genome database update: Server architecture, pan-genome nomenclature, and external resources. Genetics 224:1–6.

Wright, P. E., and Dyson, H. J. (2015). Intrinsically disordered proteins in cellular signalling and regulation. Nat. Rev. Mol. Cell Biol. 16:18–29.

Xu, S. L., Chalkley, R. J., Maynard, J. C., Wang, W., Ni, W., Jiang, X., Shin, K., Cheng, L., Savage, D., Huhmer, A. F., *et al*. (2017). Proteomic analysis reveals O-GlcNAc modification on proteins with key regulatory functions in *Arabidopsis*. Proc Natl Acad Sci U S A 114:E1536–E1543.

Yan, J., Dunker, A. K., Uversky, V. N., and Kurgan, L. (2016). Molecular recognition features (MoRFs) in three domains of life. Mol. Biosyst. 12:697–710.

Yang, Y., Liu, F., Liu, L., Zhu, M., Yuan, J., Mai, Y. X., Zou, J. J., Le, J., Wang, Y., Palme, K., Li, X., Wang, Y., & Wang, L. (2022). The unconventional prefoldin RPB5 interactor mediates the gravitropic response by modulating cytoskeleton organization and auxin transport in *Arabidopsis*. Journal of integrative plant biology, 64(10), 1916–1934.

Zhao, B., Katuwawala, A., Oldfield, C. J., Hu, G., Wu, Z., Uversky, V. N., and Kurgan, L. (2021). Intrinsic Disorder in Human RNA-Binding Proteins. J. Mol. Biol. 433:167229.

CHAPTER III.

URI1, A POTENTIAL NOVEL SIGNALLING PROTEIN IN *ARABIDOPSIS THALIANA*

URI1 in the response to abiotic stress

In Chapter 1, a significant enrichment of genes related to the stress response was observed in the RNA-seq analysis of the *uri1-1* mutant (Chapter I – Figure 17). Our aim for this chapter was to investigate the involvement of URI1 at the molecular and physiological level in the plant in response to different stress factors.

To investigate the molecular behaviour of URI1 in response to stress, we determined the levels of *URI1* by RT-qPCR, the levels of the URI1 protein using the *pURI1:URI1-3xFLAG* line by Western analysis, and its subcellular localization using the *pURI1:URI1-GFP* in the confocal microscope. All stress treatments were performed on 5-day-old seedlings that had germinated and grown under continuous light. They were then transferred to liquid MS medium supplemented with 100 mM NaCl (salt stress), 300 mM mannitol (osmotic stress) or 1 mM H_2O_2 (oxidative stress) (Figure 1). As a control, the seedlings were kept in liquid MS medium.

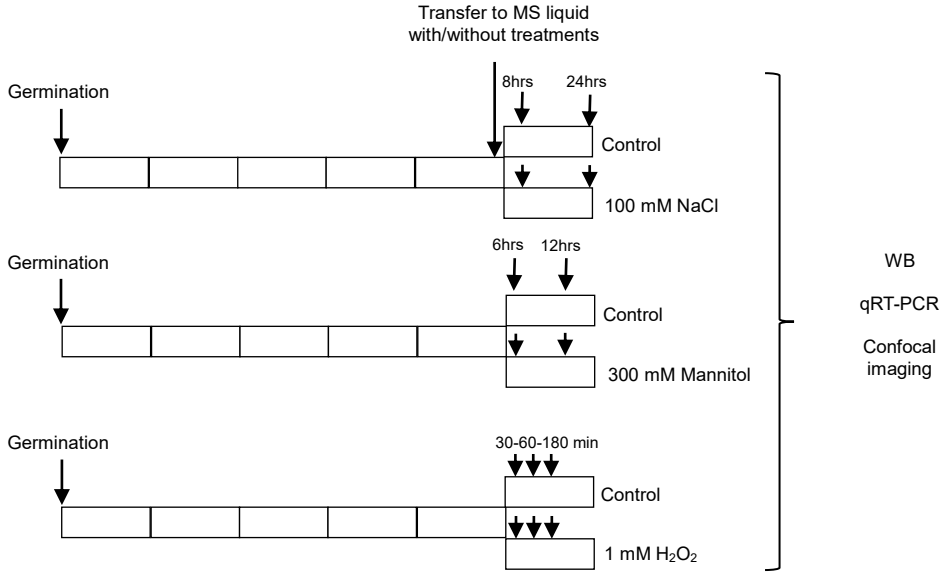

Figure 1. Workflow done to determine URI1 behaviour under different abiotic stresses. 5 day-old-seedlings from WT, pURI1:URI1-3xFLAG and pURI1:URI1-GFP were treated with 100 mM NaCl, 300 mM manitol and 1 mM H2O2. Samples were taken at the marked time points in order to perform confocal imaging, Western blot and qRT-PCR.

Regarding *URI1* mRNA levels and URI1-3xFLAG protein, we did not detect significant differences in either of the treatments analysed. As control to be sure that the treatments were effective, we selected genes from the literature that showed a substantial response, with *NCED3* serving as a control for salt stress (Figure 2A, Nishiyama *et al.,* 2011), *RD26* as a control for osmotic stress (Figure 2B, Fujii *et al* 2011) and Z*AT10* as a control for oxidative stress (Figure 2C, Mittler *et al.,* 2006). In all three cases, there was an increase in gene expression after treatment of the plants with these stressors, while no induction of *URI1* was observed. The same was true for URI1-3xFLAG, whose levels remained unaltered under all conditions. Next, we determined whether heat stress affects *URI1* gene expression or protein levels. To investigate this, we exposed 6-day-old seedlings to 37ºC in the dark for three hours. The experimental setup is depicted in Figure 4A. Neither *URI1* mRNA nor the protein levels were altered in response to the treatment (Figure 4B and 4C). In this case, we used the *HSP70* gene as a control, which showed

a clear induction immediately after the heat shock and whose expression was normalised during the recovery phase at 22ºC. Thus, we can conclude that *URI1* gene expression and URI1 protein levels are not affected by salt, osmotic, oxidative or heat stress.

We did observe, however, a partial change in the subcellular localization of URI1-GFP in root cells in response to these stressors. A fraction of URI1-GFP was located in cytoplasmic granules after osmotic or oxidative stress was applied (see the inset in Figure 3). Similarly, we also observed the formation of aggregates in the cytoplasm of the root cells after exposing the plants to heat shock for 3 hours (Figure 4D). Compared to osmotic or oxidative stress (Figure 3), the presence of URI1-GFP in cytoplasmic granules was observed in more cells, suggesting a more homogeneous response.

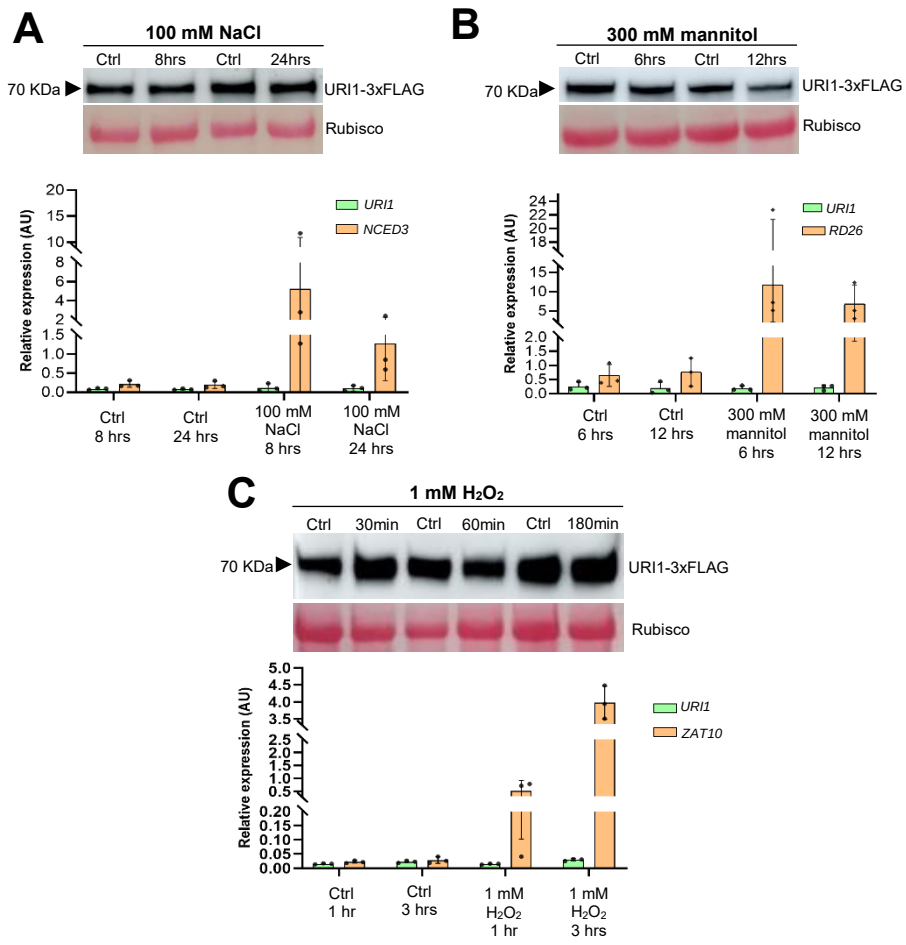

Figure 2. URI1 remains stable after abiotic stress. URI1-3xFLAG protein levels and URI1 levels were not altered after treatment with: **A.** 100 mM NaCl, **B.** 300 mM mannitol and **C.** 1 mM H2O2. LPT3 were used as a positive control for NaCl treatment. RD26 were use as positive control for mannitol treatment. HSP17 were used as positive control for H2O2 treatment. Time points of each treatment are marked on the western blot and qPCR graphics.

The aggregates observed after osmotic, oxidative and heat stress may correspond to stress granules (SGs) or processing bodies (P-bodies) (Protter *et al.,* 2016; Luo *et al.,* 2018). Eukaryotic organisms tend to present aggregates under various stress scenarios. This serves as

an adaptive mechanism to maintain the right balance between protection, degradation and translation of mRNA in stressful situations. These aggregated particles dissolve as soon as the stress subsides, during the recovery phase (Kedersha *et al.,* 2005). This mechanism would prevent cells from investing energy into often counterproductive protein translation under stress conditions. SGs are a universally conserved mechanism in response to environmental stresses. In plants, they are triggered by heat shock and salinity among others (Kosmacz *et al.,* 2019; Maruri-López *et al.,* 2021 and Gutierrez-Beltrán *et al*., 2015). Nonetheless, P-bodies exist in the cell in normal conditions, while its number and size increase after a stress is applied. In plants, both biotic and abiotic stress factors provoke the enlargement of P-bodies (Weber *et al.,* 2008). Although the presence of URI1 in cytoplasmic granules has not been described in any organism, it has been observed that URI1 plays a role in various stress situations in animals. It has been associated with various types of cancer, including uterine (Wang *et al*., 2015), ovarian (Theurillat *et al*., 2011), gastric (Leung *et al*., 2006) and esophageal (Lin *et al*., 2000) cancers. Recent studies in mice suggest that URI1 levels may play a critical role in promoting oncogenic or tumour suppressive functions. This is based on its ability to directly interact with and regulate the activity of various proteins, including transcription factors (Tummala *et al.*, 2014), enzymes (Zhang *et al*., 2018, Burén *et al.,* 2016) and tumour suppressors (Yart *et al.*, 2005). Our results suggest that URI1 in *Arabidopsis* is also able to react differently to stress. In this regard, further studies are needed to determine how stresses promote the presence of URI1 in SG/P-bodies in plants and whether this is conserved in other eukaryotes.

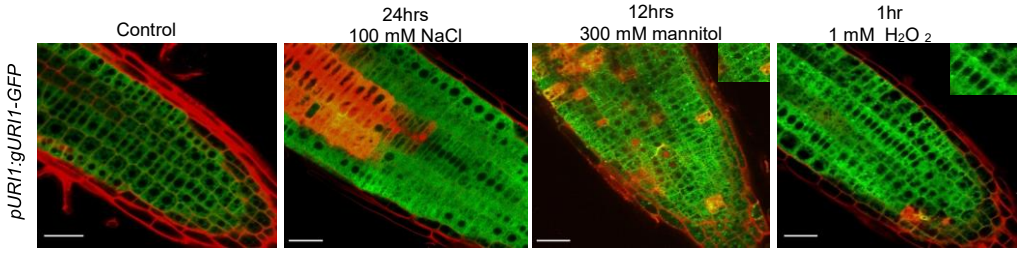

Figure 3. URI1-GFP is relocalized into granules after mannitol and H_2O_2 treatment. URI1-GFP is relocalized into granules in the cytoplasm after osmotic (during 12 hours) and oxidative stress (during 1 hour) exposure. Scale bar 50 µm.

URI1 protein is affected by available sugar levels

The RNA-seq analysis (Chapter I) showed that the *uri1-1* mutant has alterations in several metabolic pathways, both in primary and secondary metabolism. The category carbohydrate metabolism attracted our attention (Figure 17 – Chapter I), as it is key to provide energy to the cells and the involvement of URI in energy stress has been demonstrated in mammals and yeast (Gstaiger *et al*., 2003 and Djouder *et al.,* 2007). Thus, a significant repression of genes within this category was observed (Figure 18 – Chapter I). This prompted us to investigate a possible role of URI1 in energy stress in *Arabidopsis*.

We first investigated whether the levels of URI1 were sensitive to sugar availability. To this end, we used *Arabidopsis* PSB-D cell suspensions expressing *p35S:GS-URI1*. We subjected the cell suspensions to the growing protocol depicted in the Figure 5A. PSB-D cells were grown in darkness in MSMO medium containing a 3% sucrose. After 3 days, the culture was divided. One part continued to grow in fresh MSMO with sucrose, while the other half was washed three times with MSMO without sucrose and then allowed to grow in MSMO without sucrose for 24 hours to provoke energy stress cause by starvation (Figure 5A).

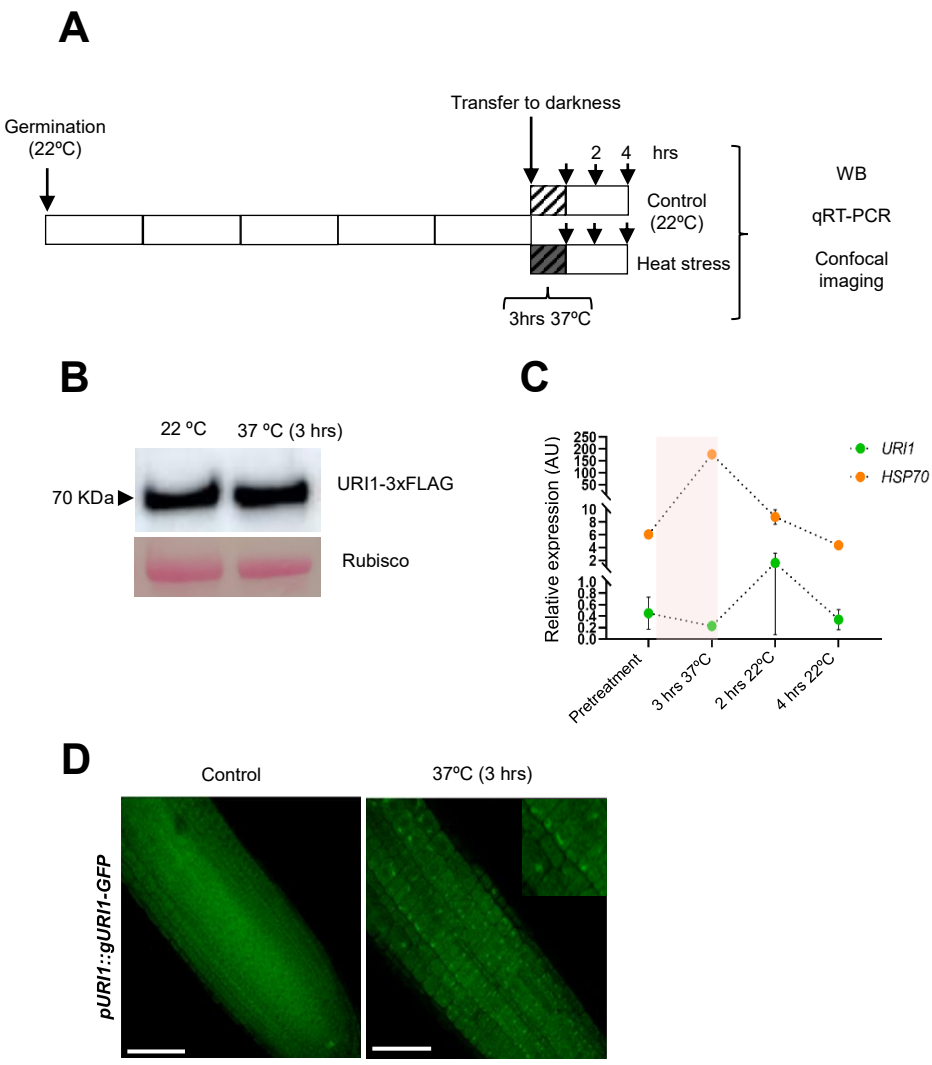

Figure 4. Heat-shock exposure promotes changes in URI1. **A.** Workflow performed during the heat-shock exposure. 5 day-old-seedlings were treated 2h at 37ºC under the dark. Seedlings were recovered 4 h at 22ºC under light conditions. This samples were used to: **B**. Western blot, to determine URI1-3xFLAG protein after 3 hours of heat-shock treatment, **C.** determine URI1 levels by qRT-PCR. HSP70 were used as positive control, being induced after 3h at 37ºC, **D.** Confocal imaging, to determine URI1-GFP location. URI1-GFP is relocated into granules after 3 h at 37ºC on the cytoplasm. Scale bar 50 µm.

In this way, we observed that the level of GS-URI1 was reduced after 24 hours of sugar deprivation (Figure 5B). Given that the protein fusion was expressed under the constitutive *35S* promoter, this result suggests that the reduced level of GS-URI1 is the consequence of post-transcriptional regulation. We then determined whether this regulation was also observed in *Arabidopsis* seedlings. We subjected seedlings of the *pURI1:URI1-3xFLAG* line to sugar starvation following the protocol depicted in Figure 5C. Seedlings were grown in MS medium with 1% sucrose for 3 days and then transferred them to MS medium with 1% sucrose (as a control) or MS medium

without sucrose under darkness conditions. Samples were taken every 24 hours for 2 days. URI1-3xFLAG levels increased slightly after 48 hours the control media. In contrast, after 24 hours without sucrose, a decrease of URI1-3xFLAG levels was observed compared to the control (Figure 5D). The decrease of URI1-3xFLAG level was gradual, as it was lower after 48 hours without sucrose (Figure 5D).

The reduction in URI1 levels observed in seedlings was lower than that in the cell suspensions, suggesting that sugar deprivation was more effective in the latter. To provoke greater sugar deprivation in the seedlings, we decided to combine growth in minimal medium with the use of 2-deoxyglucose (2-DG) or 3-(3,4-dichlorophenyl)-1,1-dimethylurea (DCMU), as these two compounds are most commonly used for this purpose. 2-DG, a non-metabolizable glucose analogue, which disrupts glycolysis by targeting hexokinase enzyme, the rate-limiting step in glycolysis (Xiong *et al.,* 2013). DCMU, on the other hand, inhibits photosystem II (PSII) by blocking the electron transport chain, which also causes energy stress in the plant (Xiong *et al.,* 2013). We grew the seedlings expressing URI1-3xFLAG on MS + 1% sucrose, which were transferred to minimal MS medium after two days. This medium contains the necessary salts to maintain the

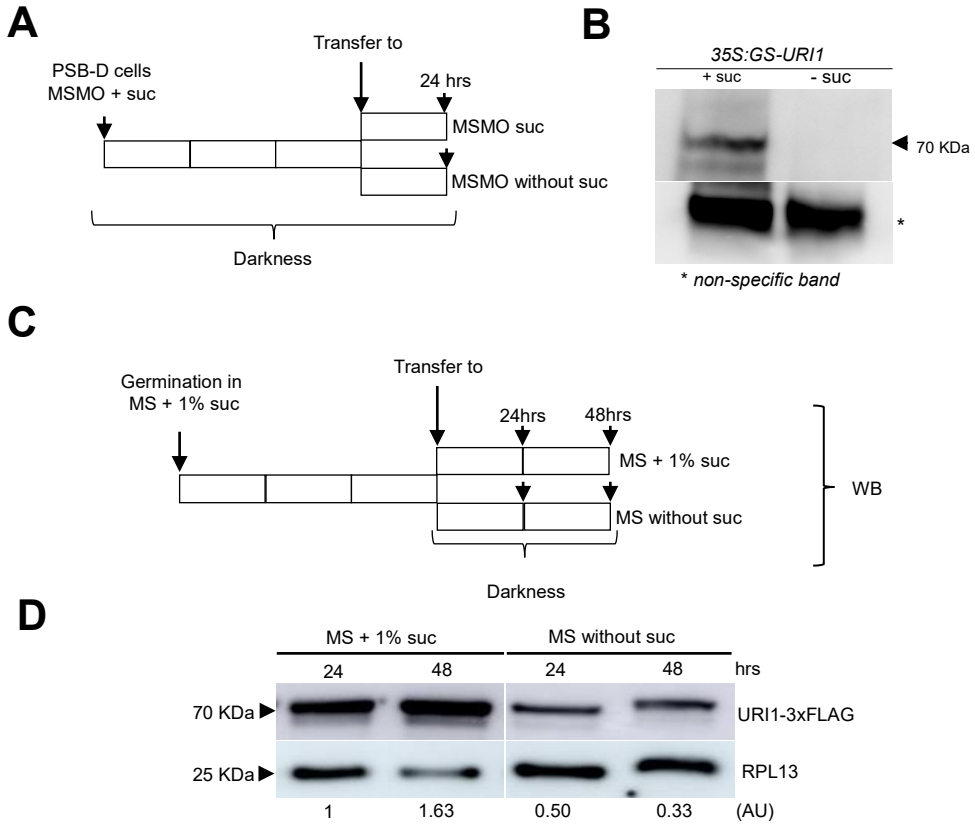

Figure 5. URI1 protein responds to sugar availability. A. Workflow performed using *Arabidopsis* cell cultures expressing *p35S:GS-URI1*. B. Western blot showing GS-URI1 levels in presence and absence of sucrose. C. Workflow used to determine URI1-3xFLAG levels in *Arabidopsis*. D. Protein levels of URI1-3xFLAG determined by western blot after starving induction. RPL13 was used as loading control. Proteins were quantified using ImageJ and URI1-3xFLAG/RPL13 ratio calculated. Point 24 hrs MS + 1% suc was used as URI1-3xFLAG reference expression.

osmotic functions of the plant, but no carbon source. Subsequently, after four days, the seedlings were transferred to different conditions: MS minimal, MS + 90 mM sucrose, MS minimal + 5 mM

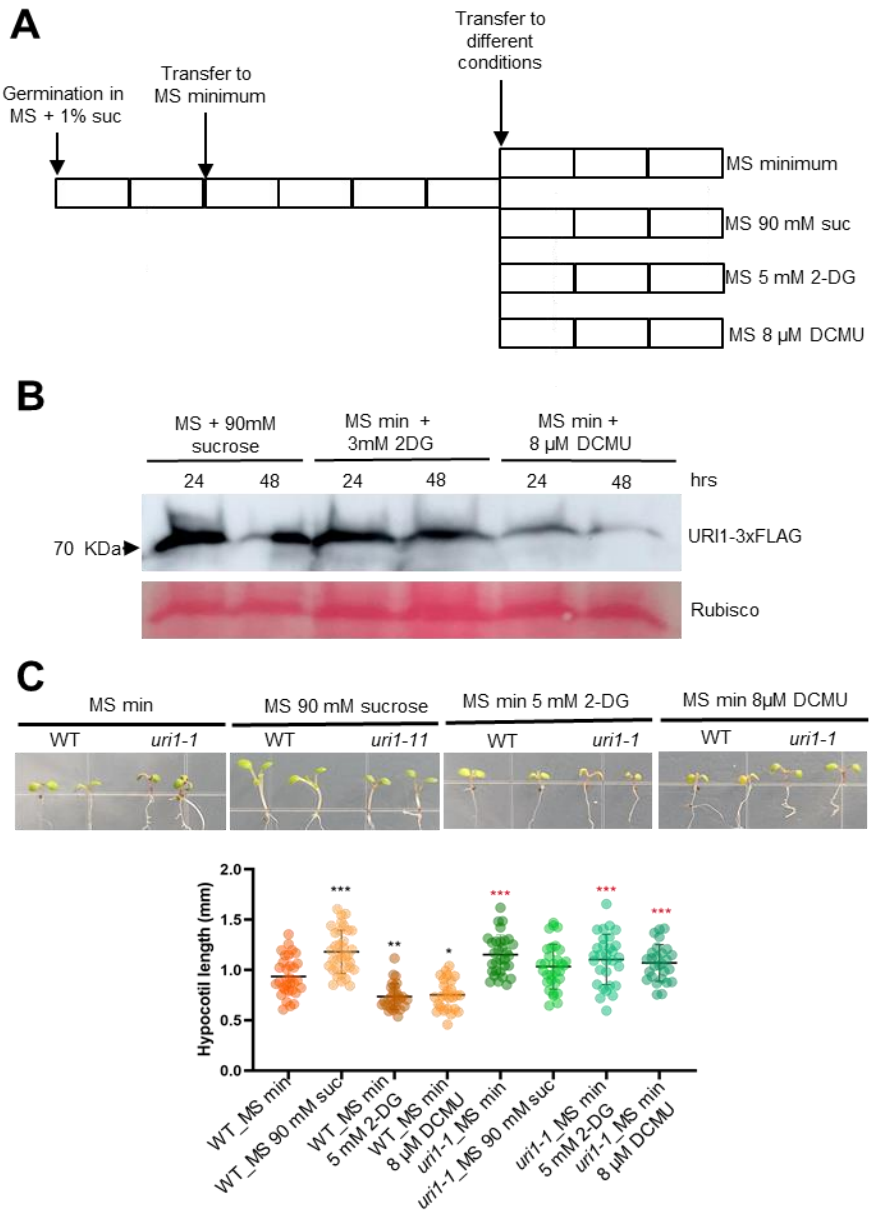

Figure 6. Hypocotils of *uri1-1* mutant respond to induced chemical starvation. **A.** Workflow followed to treat 6 day-old-seedlings with different sugar conditions. **B.** URI1-3xFLAG protein levels are lower when chemical starving induced. Western blot showing URI1-3xFLAG protein (70 KDa). Ponceau staining was used as loading control. **C.** Hypocotyl treated with MS minimal, MS 90 mM sucrose, MS minimal + 5 mM 2-DG and MS minimal + 8 µM DCMU. Quantification of hypocotyl length after treatments. Black asterisks represent statistical significance of WT under each condition compared with WT control. Red asterisks represent statistical significance of *uri1-1* mutant under each condition compared with WT under same condition. Statistical significance used; p value=0,12 (ns), p value = 0,033 (*), p value = 0,002 (**), p value < 0,001 (***).

2DG and MS minimal + 8 µM DCMU and maintained under these conditions for three days (Figure 6A). Treated seedlings were harvested and analysed by western blot to determine the levels of the URI1-3xFLAG fusion protein. We observed that the URI1-3xFLAG level decreased slightly 48 hours after the addition of 2-DG (Figure 6B). The same trend was observed in seedlings treated with DCMU, although the effect was stronger (Figure 6B). Taken together, these results suggest that level of URI1 protein is positively regulated by sugar (sucrose) in both cell suspensions and *Arabidopsis* seedlings. Considering that URI is involved in energy stress signalling downstream of sugar in animals and yeast (Gstaiger *et al.,* 2003 and Djouder *et al.,* 2007), our results suggest that URI1 may also function as a signalling protein in energy stress pathways in plants.

Next, we investigated the possible involvement of URI1 in the response to sugar by analyzing hypocotyl length in WT and *uri1-1* seedlings subjected to the same growth protocol (Figure 6A). Several findings can be derived from this analysis. First, although the difference was not significant, the *uri1-1* mutant tended to grow less than the WT in the presence of 90 mM sucrose. Second, and more importantly, the *uri1-1* mutant grew more in MS minimal medium and in the presence of 2-DG and DCMU than the WT, especially in the presence of DCMU (Figure 6C). This genetic analysis suggests that URI1 plays a negative role in the signalling pathway that regulates hypocotyl elongation and seedling growth -according to the aspect of cotyledons- in response to sugar availability.

In plants, as in other eukaryotes, the protein kinase TOR is a central regulator of intracellular energy state (Xiong *et al.,* 2014; Dobrenel *et al.,* 2016). In recent years, numerous studies have focused on TOR and its regulation. It has been observed that TOR controls ribosome biogenesis, translation initiation and elongation processes by phosphorylating its substrates, such as ribosomal S6 kinase (S6K) (Xiong *et al.,* 2012; Xiong *et al.,* 2017). Previous studies have shown that phosphorylation of ribosomal protein S6 (RPS6) relies primarily on the TOR-S6K signalling module (Meyuhas *et al.,* 2015). RPS6 phosphorylation is stimulated by the availability of nutrients (Xiong *et al.,* 2017 and Xiong *et al.,* 2013*)*. In addition, in plants cultivated under light-dark cycles, the rate of RPS6 phosphorylation was observed to be higher during the light period (Turkina *et al.,* 2011), which is also related to photosynthetic activities (Boex-Fontvieille *et al.,* 2013). In this way, the phosphorylation of RPS6 is used as a readout of the TOR activity, being RPS6 more phosphorylated when TOR is more active.

Considering the relevance of TOR signalling for energy stress signalling (Baena-González *et al.,* 2007 and Dobrenel *et al.,* 2016), the role of URI in the TOR pathway both in animals and yeast (Gstaiger *et al.,* 2003; Djouder *et al.,* 2007; Gutiérrez-Santiago *et al*., 2022), and our results, we investigated whether URI1 participates in the TOR pathway in *Arabidopsis* as well. To investigate this, we examined if TOR activity was altered by the *uri1-1* mutation. To this end, we grew seedlings of the *uri1-1* mutant and the WT in MS minimal and in MS minimal supplemented with 8 µM DCMU for 48 hours (Figure 7A). We used the phosphorylation of RPS6 (RPS6-P) protein as a readout of TOR activity. Notably, RPS6-P levels were higher in *uri1-1* seedlings compared to the WT seedlings in MS minimal (Figure 7B), suggesting that TOR activity is higher in the mutant. When examining the effects of DCMU, a drastic decrease in RPS6-P was observed after 24 hours in the WT and levels were below the detection limit after 48 hours of treatment. In *uri1-1* seedlings, the reduction was less dramatic. These results confirm that TOR is more active in the *uri1-1* mutant, even under conditions of severe sugar deprivation. This result may explain why the growth of the mutant is less sensitive to the energy stress induced by sugar deprivation (Figure 6C). URI1 could therefore be a regulator of TOR.

URI1 is required for the transcriptional response to energy stress

We have shown that *uri1-1* mutant is more resistant to the energy stress induced by DCMU compared to the WT, supporting the hypothesis that URI1 is involved in the pathway sensing energy stress in *Arabidopsis*. To further test this hypothesis, we performed RNA-seq analysis of 7-day-old WT and *uri1-1* seedlings grown on MS minimal for 5 days and then transferred to MS minimal (as a control) or to MS minimal supplemented with DCMU for 2 days. Consistent with the phenotypes of seedling growth (Figure 6), we observed that the transcriptome of *uri1-1* was generally less affected by DCMU treatment than that of WT. We found 8805 DEGs in WT affected by DCMU (3373 upregulated and 5432 downregulated) (*q value* < 0.05, $|\log_2 FC| > 1$), whereas in *uri1-1* we found 2633 DEGs (1286 upregulated and 1347 downregulated) (Figure 8A and B, Supp Table 1).

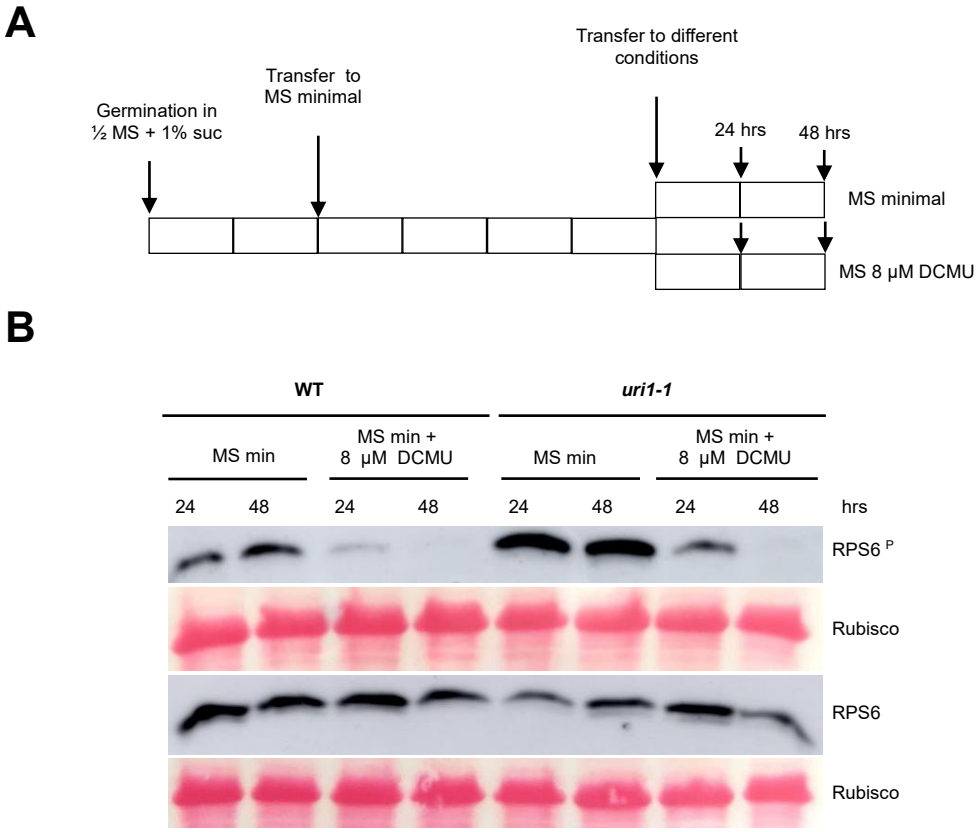

Figure 7. TOR activity in *uri1-1* mutant is upregulated when there is no carbon source. A. Workflow followed to treat 6-day-old seedlings with MS minimal and MS minimal with 8 µM DCMU. **B.** Western blot showing RPS6 and RPS6^P protein levels after different treatment conditions, using WT and *uri1-1* mutant. Ponceau staining was used as loading control.

To determine which categories comprised the affected genes by DCMU in WT and *uri1-1*, we performed a GO enrichment analysis using the BGI's Dr. Tom online tool for genomic analysis. Enrichment analysis based on the biological process was performed with DEGs that had a

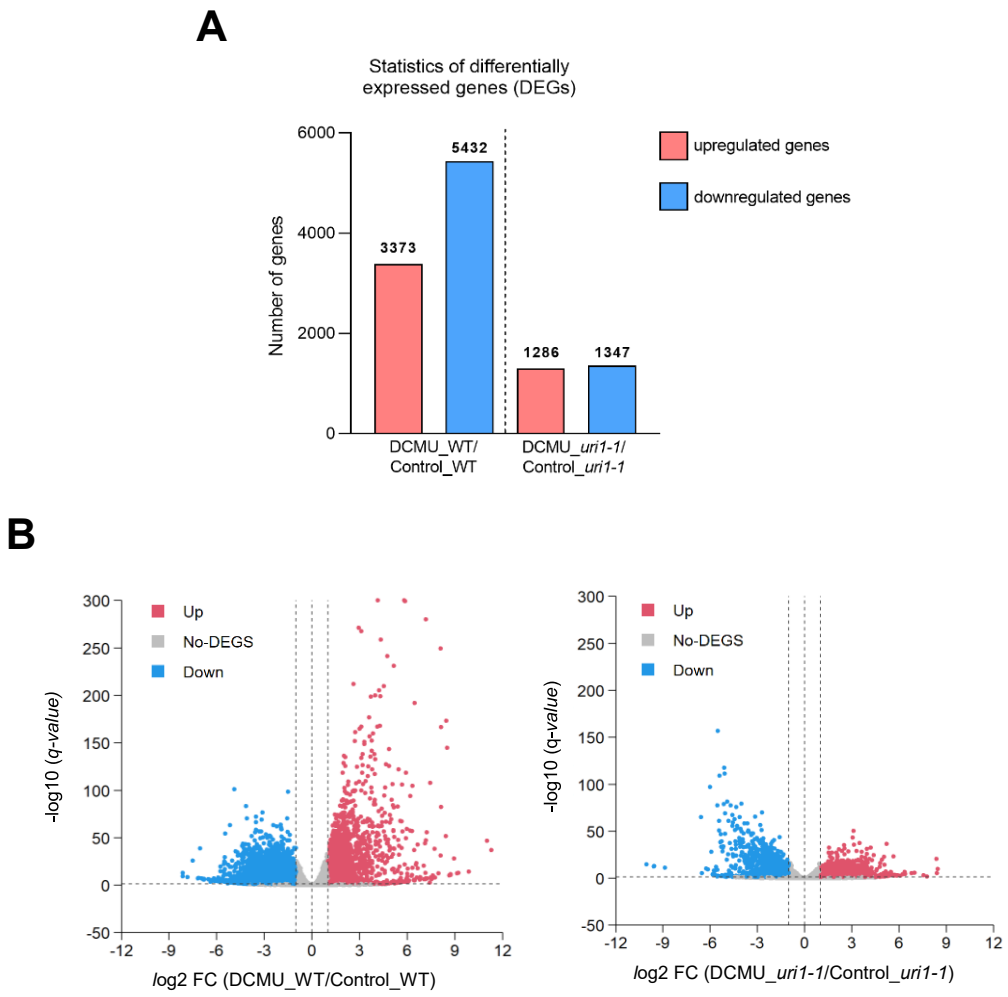

Figure 8. Transcriptomic analysis of *uri1-1* and WT seedlings after DCMU treatment. **A.** DEGs upregulated (3373) and downregulated (5432) after DCMU treatment in WT seedlings compared with DEGs upregulated (1286) and downregulated (1347) after DCMU treatment in *uri1-1* seedlings. **B.** Volcano plots showing the genes expressed in DCMU_WT/Control WT (24355) and DCMU_*uri1*-1/Control_*uri1-1* (24476). Differential analysis was done with Dr. Tom with default options (Beijing, China). The red and blue dots indicate upregulated and downregulated genes, respectively. DEGs were considered when log2 FC ≥ 1 and *q-value* ≤ 0.05. All genes are on Supp Table 1.

|log2FC| ≥ 1 and a *q-value* ≤ 0.05. We plotted the 60 most overrepresented categories (out of 100) with a *q-value* ≤ 0.05 (Figure 9). In the WT, multiple processes related with metabolism, protein phosphorylation, response to different stimuli and cell growth were

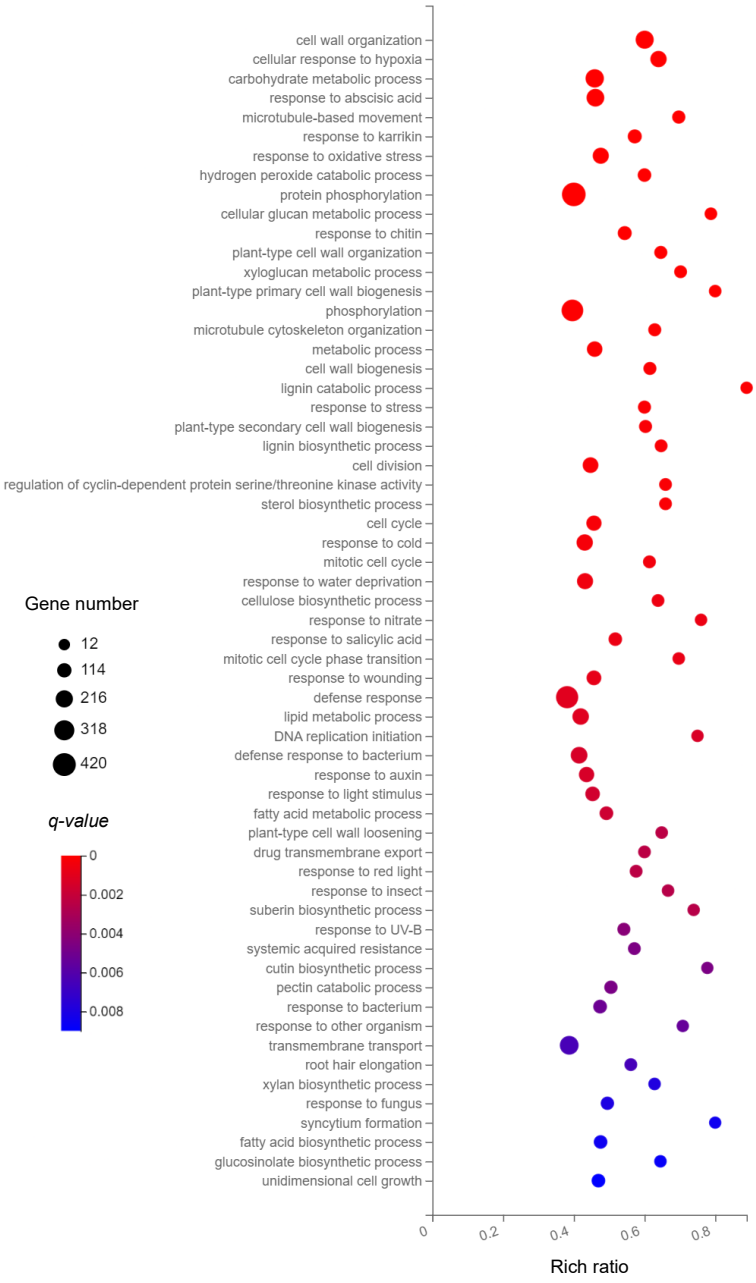

Figure 9. Gene ontology enrichment among genes that are differentially expressed in WT after DCMU treatment. Bubble plot showing "Biological process" of the first 60 categories overrepresented in WT after DCMU treatment when log2 FC ≥ 1 and *q value* ≤ 0.05. The size of the points match with the number of genes enriched in this category (bigger means more genes). *q-value* is represented by colour. Rich ratio of a particular GO term refers to its enrichment in WT DEGs set compared with the reference genome background set. All the GO are included in Supp Table 2.

enriched (Figure 9, Supp Table 2). We then performed the same analysis in the *uri1-1* mutant. After plotting the 60 most overrepresented categories (q-value ≤ 0.05), we found similar affected processes (Figure 10, Supp Table 3), with the most enriched categories being those exhibited DEGs related to cell wall organization, response to various stimuli (e.g., water deprivation, abscisic acid, oxidative stress, cold, among others), lipid and carbohydrate metabolism, etc.

Using a *q-value* < 0.05 and $|\log_2 FC| > 1$ cut-off, we observed 1,070 common upregulated genes in WT and *uri1-1* mutant, and 1,191 common downregulated genes in response to DCMU. In contrast, the common DEGs that were misregulated in the opposite direction were much less (Figure 11). This is an important indication that the *uri1-1* mutation and the treatment with DCMU act on the same transcriptional pathways. Notably, 4,213 downregulated genes by DCMU and 2,280 upregulated genes by DCMU in the WT were not affected in *uri1-1* seedlings. This indicates that URI1 function is required for the plant to fully respond to this inhibitor. The genes that are exclusively altered in the WT (both downregulated and upregulated) belong to categories that are mainly involved in metabolism, similar to the genes shared with the *uri1-1* mutant. The fact that the WT has the same altered categories in both the common and exclusive deregulated genes may suggest that DCMU affects the WT more than the *uri1-1* mutant, possibly because the latter is better adapted to stress. Given our observation that the *uri1-1* mutant has increased TOR activity under control conditions, this could explain why the mutant is more resistant to energy stress.

To better understand the effects of the *uri1-1* mutation on the response to DCMU, we analysed the expression of different DEGs in WT and *uri1-1*, which belong to different biological processes related to primary metabolism (Figure 12, Supp Table 4). Consistent with the results described above, the *uri1-1* mutant had fewer genes related to primary metabolism whose expression is affected by DCMU compared to WT. When comparing the DEGs in the “Carbohydrate metabolic process” we found three times more affected genes in the WT than in the *uri1-1* mutant (Figure 12). Moreover, in biological processes such as the "Reductive pentose-phosphate cycle" and the "Photosynthetic electron transport in photosystem I (PSI)", only genes in *uri1-1* are upregulated (Figure 12), suggesting that *uri1-1* has a compensatory mechanism when the photosystem II (PSII) is disrupted and is therefore more resistant to starvation than WT. Overall, these data are consistent with the hypothesis that URI1 is required for energy stress response in *Arabidopsis.*

Next, we analysed which metabolic pathways were affected in relation to carbohydrate metabolism. In particular, we focussed on glycolysis/gluconeogenesis, fructose metabolism, mannose metabolism, galactose metabolism, starch formation and the pentose phosphate pathway. The latter is necessary for the production of intermediate metabolites that are essential for glycolysis. In plants, which are autotrophic organisms, sugar metabolism must be finely controlled and regulated. Plants have a complex and dynamic carbohydrate metabolism, as they exhibit altered metabolic fluxes and sugar concentrations that change during plant development, not only in response to the environment or stress, but also between day and night (Bläsing *et al.,* 2005; Roitsch., 1999; Smith *et al.,* 2005). Therefore, the integration of environmental signals into metabolism of plants is particularly important as they are sessile organisms. It is important to remember that photosynthesis and carbon metabolism are also involved in sugar signalling.

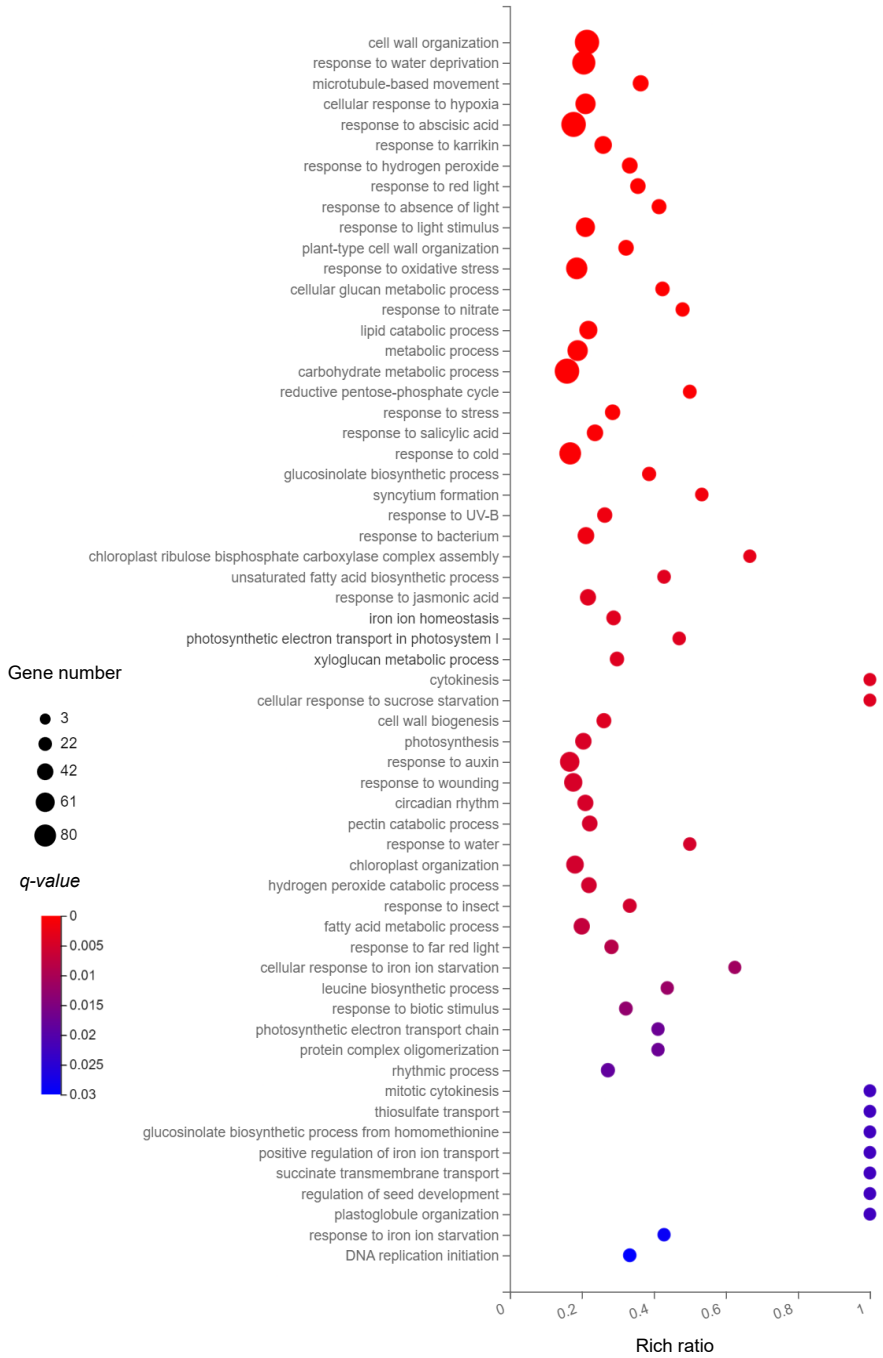

Figure 10. Gene ontology enrichment among genes that are differentially expressed in *uri1-1* after DCMU treatment. Bubble plot showing "Biological process" of the first 60 categories overrepresented in *uri1-1* after DCMU treatment when log2 FC ≥ 1 and *q-value* ≤ 0.05. The size of the points match with the number of genes enriched in this category (bigger means more genes). *q-value* is represented by colour. Rich ratio of a particular GO term refers to its enrichment in WT DEGs set compared with the reference genome background set. All the GO are included in Supp Table 3.

All DEGs identified with a *q-value* < 0.05 and $|\log_2 FC| > 1$ from the RNA-seq analysis were compiled. The list of genes was analysed via Shinny-GO (http://bioinformatics.sdstate.edu/go/) using KEGG databases to localize the DEGs involved within the metabolic pathways. The images were then colour coded with R Studio according to whether the enzymes were upregulated or downregulated.

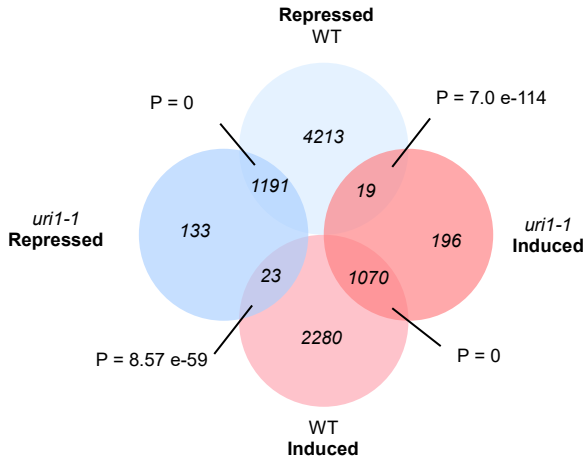

Figure 11. URI1 shares downstream DEGs with WT after DCMU treatment. Venn diagram showing the overlap of upregulated and downregulated in *uri1-1* WT DEGs. Statistical significance of the overlaps is represented by the Fisher's exact test.

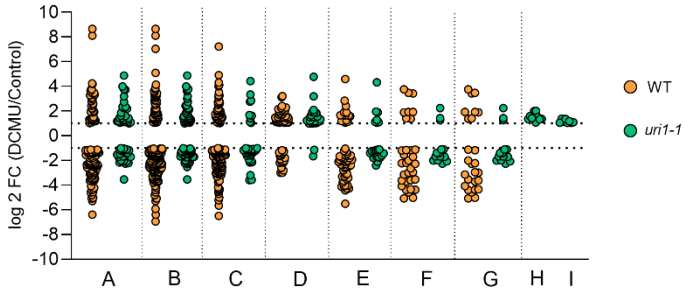

A. Metabolic process (WT: 129 DEG, *uri1-1*: 53 DEG)
B. Carbohydrate metabolic process (WT: 231 DEG, *uri1-1*: 80 DEG)
C. Lipid metabolic process (WT: 164 DEG, *uri1-1*: 38)
D. Photosynthesis (WT: 59 DEG, *uri1-1*: 27 DEG)
E. Hydrogen peroxide catabolic process (WT: 60 DEG, *uri1-1*: 22 DEG)
F. Xyloglucan metabolic process (WT: 33 DEG, *uri1-1*: 14 DEG)
G. Cellular glucan metabolic process (WT: 26 DEG, *uri1-1*: 14 DEG)
H. Reductive pentose phosphate cycle (*uri1-1*: 10 DEG)
I. Photosynthetic electron transport in photosystem I (*uri1-1*: 8)

Figure 12. Multiple genes involved in cell metabolism are differentially expressed in *uri1-1* compared to WT after DCMU treatment. Relative expression of several genes involved in different metabolic processes in DCMU/control. Orange dots represent WT DEGs and green dots represent *uri1-1* DEGs. Enrichment of the genes 'reductive pentose phosphate pathway' and 'photosynthetic electron transport in photosystem I' are only found in the *uri1-1* mutant. The relative expression is shown as log2 FC (DCMU/control) for each genotype. The numbers and names of the genes can be found in Supp Table 4.

The glycolysis/gluconeogenesis pathway is one of the best-known metabolic pathways. It is considered to be a participant in the core metabolic processes, as it is the main pathway for glucose assimilation (Plaxton *et al.,* 1996). When analysing the difference between the *uri1-1* mutant and the WT in glycolysis/gluconeogenesis, we found that the WT in general not only had more affected enzymes after DCMU treatment, but that those that were also affected in the *uri1-1* mutant under the same conditions had a higher level of misregulation in the WT (Figure 13). This pattern was also observed when we analysed fructose and mannose metabolism (Figure 14), galactose metabolism (Figure15), sucrose metabolism and starch formation (Figure 16). With regard to sucrose metabolism and starch formation (Figure 16), it is noteworthy that DCMU treatment resulted in an overall suppression of the metabolic pathway in the WT compared to the *uri1-1* mutant, whereas upregulation was observed in the *uri1-1* mutant, which might provide some clues as to why the *uri1-1* mutant exhibits resistance to DCMU treatment. It is worth noting that the production of trehalose-6P, an inhibitor of SnRK1 kinase (Peixoto *et al*., 2022), can be affected by DCMU in the WT and *uri1-1* mutant in different ways (Figure 16). Although it seems paradoxical, since SnRK1 is active under energy stress, the trehalose-6-P production in the WT is likely enhanced by DCMU, as the expression of the trehalose-6-P synthase step was upregulated and that of trehalose-6P phosphatase was downregulated. In contrast, both steps were upregulated in the mutant, most likely resulting in lower levels of trehalose-6P compared to the WT. This result could be the consequence of a regulatory pathway that prevents excessive activation of SnRK1 kinase. On the other hand, the pentose phosphate pathway plays an essential role in the generation of precursors for nucleic acid synthesis and the provision of NADPH to maintain redox balance and support anabolic responses in cells. Analysis of this pathway showed that the repression of several genes by DCMU in the WT was not observed in the *uri1-1* mutant (Figure 17). In summary, this analysis suggests that the *uri1-1* mutant can withstand DCMU treatment that induces energy stress, in part because certain metabolic pathways are upregulated in it compared to the WT.

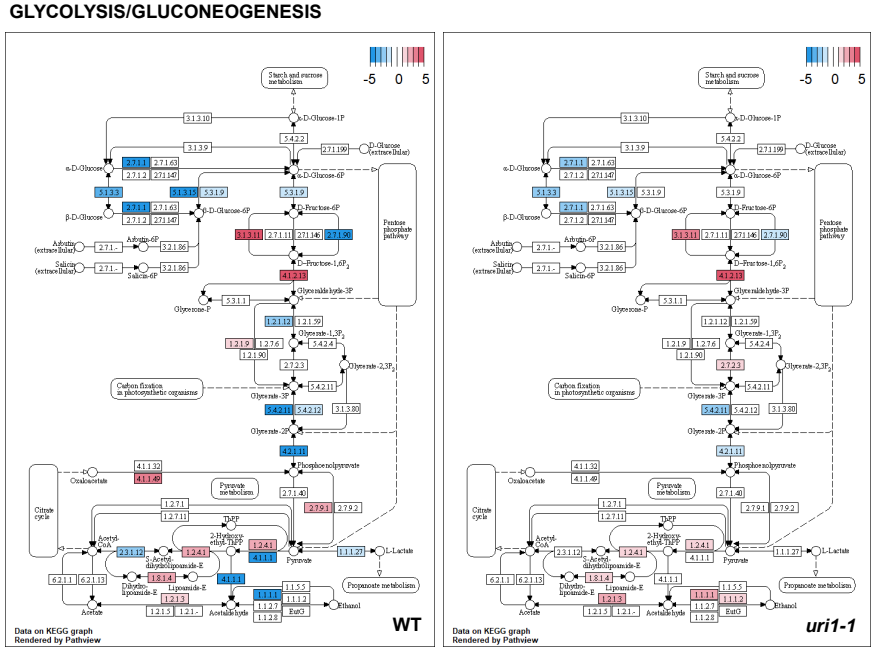

Figure 13. Glycolysis/gluconeogenesis KEGG pathway. The enzymes involved are coded with the KEGG code for each pathway. The colour gradient represents the log2 FC and shows a gradation where blue represents downregulation and red represents upregulation.

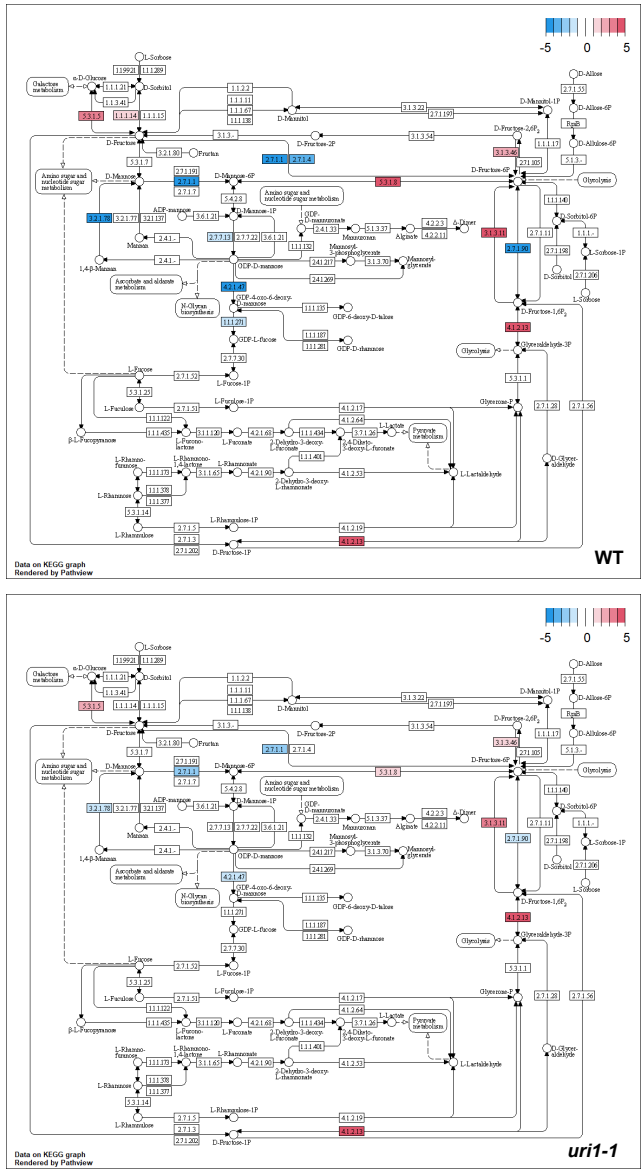

Figure 14. KEGG pathway showing the fructose and mannose metabolism with the enzymes involved. The enzymes are coded with the KEGG code for each pathway. The colour gradient represents the log2 FC and shows a gradation where blue represents down-regulation and red represents up-regulation in DCMU_WT/Control_WT and DCMU_*uri1-1*/Control_*uri1-1*.

GALACTOSE METABOLISM

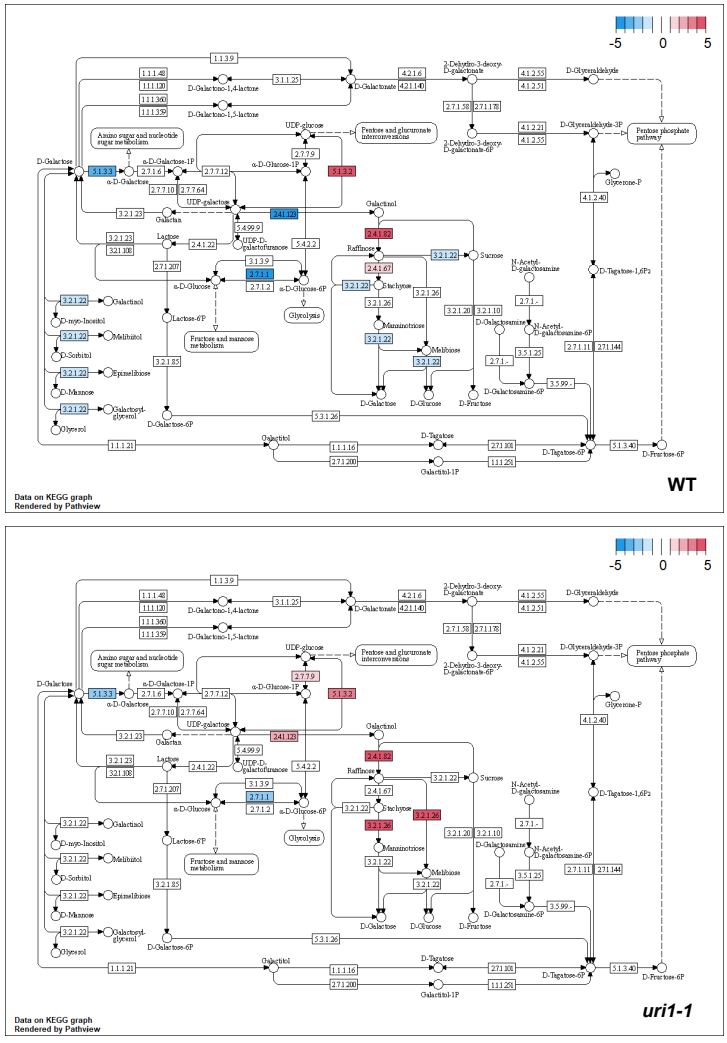

Figure 15. KEGG pathway showing galactose metabolism with the enzymes involved. The enzymes are coded with the KEGG code for each pathway. The colour gradient represents the log2 FC and shows a gradation where blue represents downregulation and red represents upregulation.

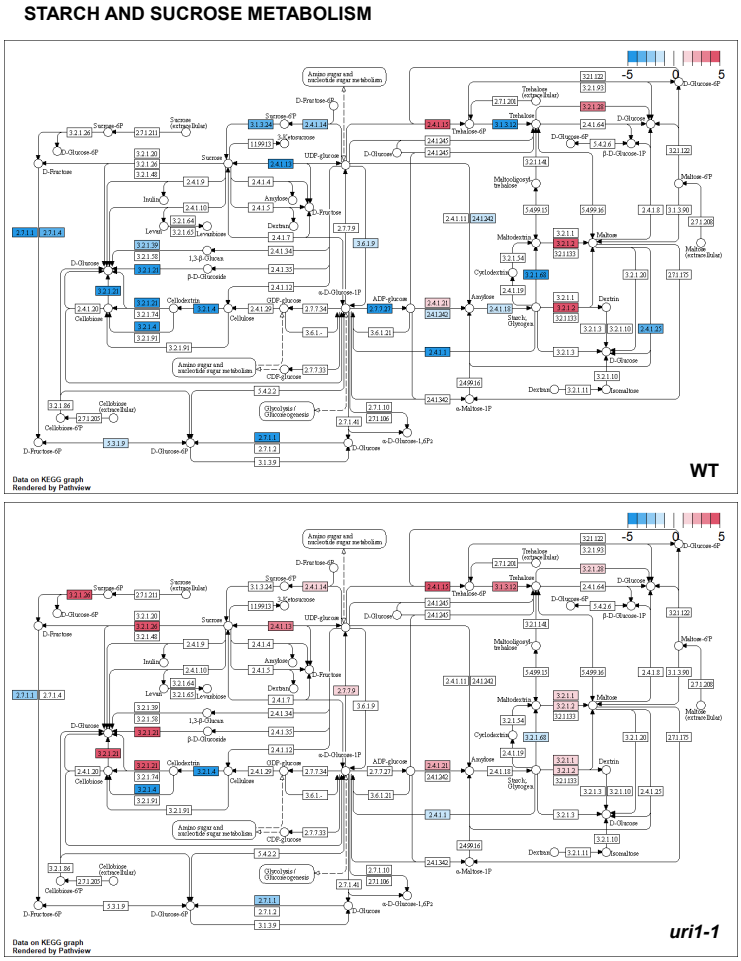

Figure 16. KEGG pathway for the visualisation of starch and sucrose metabolism with the enzymes concerned. The enzymes are coded with the KEGG code for each pathway. The colour gradient represents the log2 FC and shows a gradation where blue represents down-regulation and red represents up-regulation in DCMU_WT/Control_WT and DCMU_*uri1-1*/Control_*uri1-1*.

To determine whether the transcriptional changes observed in response to DCMU are reflected in changes in metabolite levels, we next analysed the levels of primary metabolites in the WT and *uri1-1* seedlings under control conditions and after DCMU treatment. Primary metabolites are abundant and essential for plant growth and development (Fernie *et al*., 2015). Secondary metabolites, which include important groups such as phenols, terpenes and nitrogenous compounds, are often specific to certain plant lineages and help plants interact with the biotic and abiotic environment (Hartmann *et al*., 2007). The primary metabolites were analysed according to the instructions described in the 'Material and Methods' section. We analysed different carbon sources, such as mannitol, glycerol, glucose, sucrose, fructose and myoinositol, different amino acids and derivatives as well as different organic acids involved in primary metabolism, and nitrogen-containing compounds such as putrescine, uracil and urea. When analysing the levels of the different carbon sources, it was found that the DCMU treatment resulted in a general decrease of these sugars in the WT (Figure 18). However, this drastic decrease did not occur in the *uri1-1* mutant; rather, the values remained very similar to the control. When analysing amino acids and

derivatives, DCMU was found to promote the accumulation of certain amino acids, probably because the plant enters an autophagy process that promotes protein degradation. In contrast, the content of amino acids and other derivatives

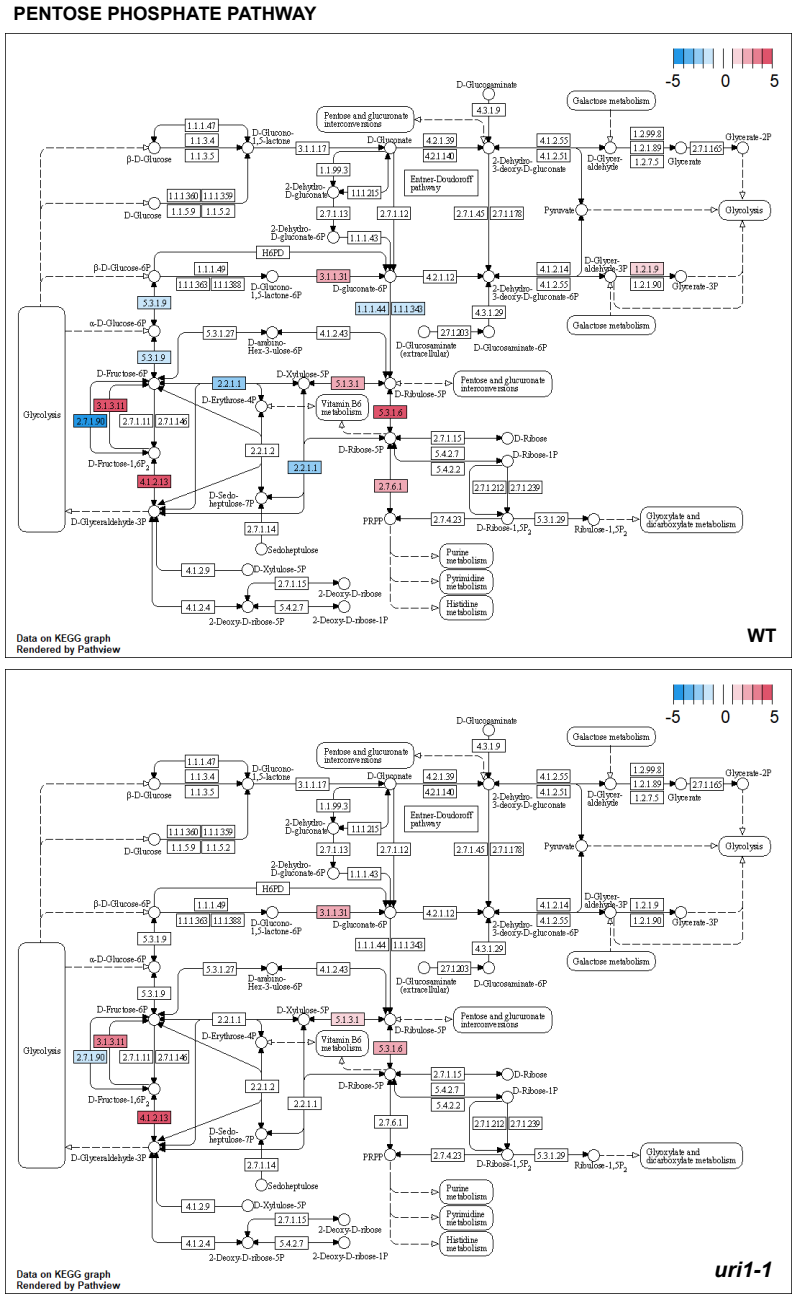

Figure 17. KEGG pathway showing the pentose phosphate pathway with the enzymes involved. The enzymes are coded with the KEGG code for each pathway. The colour gradient represents the log2 FC and shows a gradation where blue represents down-regulation and red represents up-regulation in DCMU_WT/Control_WT (left) and DCMU_*uri1-1*/Control_*uri1-1* (right).

in the *uri1-1* mutant was quite similar when comparing control conditions with DCMU treatment. As for organic acids, we found that the concentration of threonic acid (an intermediate in the pentose phosphate pathway), glyceric acid (an intermediate in glycolysis/gluconeogenesis), fumaric acid (Krebs cycle) and malic acid (Krebs cycle) decreased after DCMU treatment in the WT, but remained stable in the *uri1-1* mutant. In the mutant, the concentration of succinic acid and citric acid, which are both involved in the Krebs cycle, decreased after DCMU treatment.

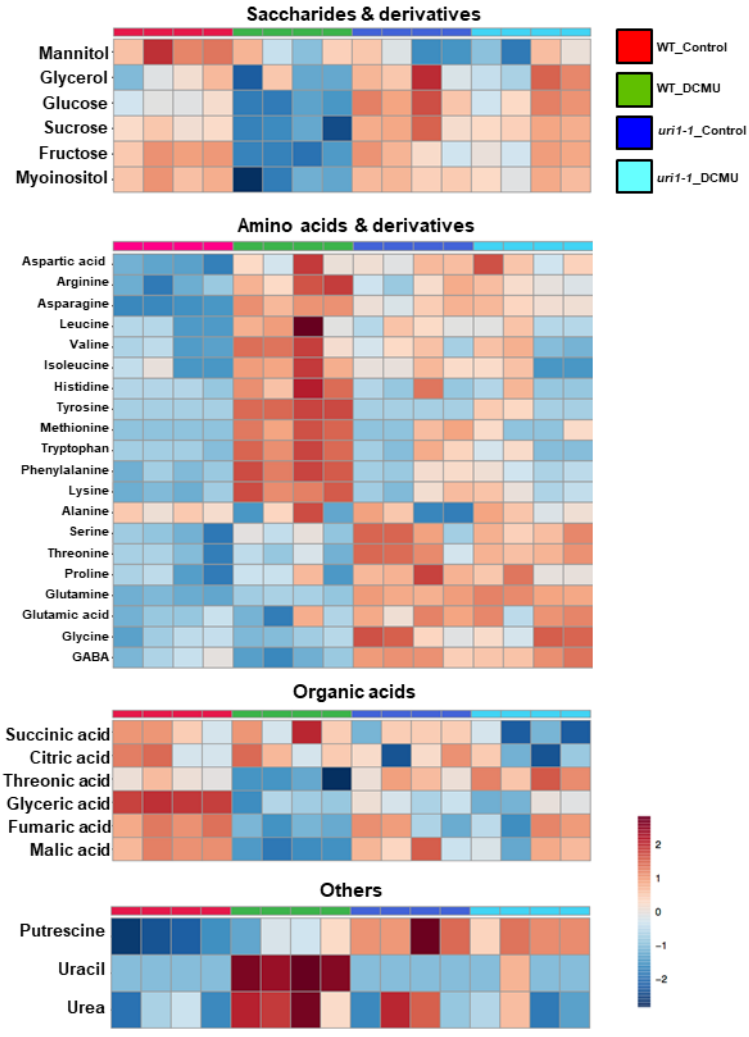

Figure 18. Metabolome of WT and *uri1-1* mutant under control conditions and DCMU treatment. The colour gradients represent the quantification of the metabolites (using arbitrary units). The metabolites analysed were classified into saccharides and derivatives, amino acids, organic acids and others. Four independent replicates were performed and quantified.

The results obtained in the metabolome are consistent with the results of the transcriptome analysis. In the metabolome, it was observed that the WT had lower levels of sugars and derivatives that serve as carbon and energy sources after treatment with DCMU, while the *uri1-1* mutant showed no changes. These sugars are essential metabolites for the generation of cellular energy via various metabolic pathways such as glycolysis/gluconeogenesis, fructose, mannose and galactose metabolism as well as starch and sucrose metabolism. Thus, since all of the above metabolic pathways are impaired in WT after treatment with DCMU, it is logical that there would be a reduction in these metabolites. In fact, the observed reduction in organic acids could also be related to energy production. The organic acids that were impaired in WT after DCMU treatment are involved in glycolysis/gluconeogenesis, cellular respiration and the pentose phosphate pathway, all of which were impaired in the transcriptome.

On the other hand, the increase of certain amino acids in the WT after DCMU treatment could be due to the plant entering an autophagy process when simple sugars are not available for metabolism (Pu *et al*., 2017 and Magen *et al*., 2022). Plant metabolism during autophagy would degrade proteins to simple amino acids, which could be converted to metabolic intermediates of gluconeogenesis (pyruvate and oxaloacetate) by transamination, oxidative deamination by loss of the amino group or by conversion of keto acids to gluconeogenic derivatives to obtain energy (Ren *et al.*, 2014 and Magen *et al*., 2022). When the gluconeogenesis pathway was analysed, it was found to be suppressed in the same way as glycolysis. Amino acids would then accumulate because they do not enter the gluconeogenesis pathway. Thus, since *uri1-1* had a milder effect on metabolism in general, these abrupt changes were not reflected in metabolite levels after DCMU treatment, suggesting that the *uri1-1* mutant must have a previously unknown compensatory mechanism that allows it to maintain metabolism despite treatment with DCMU.

Our results suggest that URI1 plays a role in the response of the plant to energy stress. Here is the evidence that supports our claim: (i) the URI1 protein levels are sensitive to sugars, being reduced upon sugar deprivation; (ii) seedlings of the *uri1-1* mutant grow better than the WT in the presence of compounds that induce energy stress; (iii) the *uri1-1* mutant exhibits higher TOR activity than the WT; and (iv) the transcriptome and metabolome of the *uri1-1* mutant are less affected by energy stress than the WT. This is in line with what has been observed for URI in animals and yeast (Gstaiger *et al.,* 2003 and Djouder *et al.,* 2007). Nevertheless, our results suggest that the mechanisms by which URI1 operates in the energy stress pathways may be different from those reported for animals and yeast, as URI1 in plants may be an upstream regulator of TOR, whereas in yeast and animals it acts downstream of the kinase. For example, phosphorylation of URI by the TOR/S6K1 kinase pathway prevents the interaction of URI1 with the phosphatase PP1γ, which is crucial for controlling excessive growth under nutrient-rich conditions (Djouder *et al.,* 2007). Under other physiological conditions, such as glucose deprivation, the protein kinase PKA phosphorylates URI to prevent its interaction with PP1γ, allowing URI to interact with and inhibit the O-linked N-acetylglucosamine transferase, which alters O-GlcNacylation-dependent signalling pathways (Burén *et al.,* 2016). Thus, the results in this chapter position URI1 as an indicator of cellular nutritional status. Further studies are needed to determine whether URI1 directly or indirectly affects TOR activity and whether URI1 is regulated by other kinases as observed in animals.

Supplemental tables

All supplemental tables are available online at: http://plasticity.ibmcp.csic.es/tools.html

REFERENCES

Baena-González, E., Rolland, F., Thevelein, J. M., & Sheen, J. (2007). A central integrator of transcription networks in plant stress and energy signalling. Nature, 448(7156), 938–942.

Bläsing, O. E., Gibon, Y., Günther, M., Höhne, M., Morcuende, R., Osuna, D., Thimm, O., Usadel, B., Scheible, W. R., & Stitt, M. (2005). Sugars and circadian regulation make major contributions to the global regulation of diurnal gene expression in *Arabidopsis*. The Plant cell, 17(12), 3257–3281.

Boex-Fontvieille, E., Daventure, M., Jossier, M., Zivy, M., Hodges, M., & Tcherkez, G. (2013). Photosynthetic control of *Arabidopsis* leaf cytoplasmic translation initiation by protein phosphorylation. PloS one, 8(7), e70692.

Burén, S., Gomes, A. L., Teijeiro, A., Fawal, M. A., Yilmaz, M., Tummala, K. S., Perez, M., Rodriguez-Justo, M., Campos-Olivas, R., Megías, D., & Djouder, N. (2016). Regulation of OGT by URI in Response to Glucose Confers c-MYC-Dependent Survival Mechanisms. Cancer cell, 30(2), 290–307.

Djouder, N., Metzler, S. C., Schmidt, A., Wirbelauer, C., Gstaiger, M., Aebersold, R., Hess, D., & Krek, W. (2007). S6K1-mediated disassembly of mitochondrial URI/PP1gamma complexes activates a negative feedback program that counters S6K1 survival signalling. Molecular cell, 28(1), 28–40.

Dobrenel, T., Caldana, C., Hanson, J., Robaglia, C., Vincentz, M., Veit, B., & Meyer, C. (2016). TOR Signalling and Nutrient Sensing. Annual review of plant biology, 67, 261–285. https://doi.org/10.1146/annurev-arplant-043014-114648

Fernie, A. R., & Pichersky, E. (2015). Focus Issue on Metabolism: Metabolites, Metabolites Everywhere. Plant physiology, 169(3), 1421–1423.

Fujii H, Verslues PE, Zhu JK (2011). *Arabidopsis* decuple mutant reveals the importance of SnRK2 kinases in osmotic stress responses in vivo. Proc Natl Acad Sci U S A 108: 1717–1722.

González-Sánchez, M. I., González-Macia, L., Pérez-Prior, M. T., Valero, E., Hancock, J., & Killard, A. J. (2013). Electrochemical detection of extracellular hydrogen peroxide in *Arabidopsis* thaliana: a real-time marker of oxidative stress. Plant, cell & environment, 36(4), 869–878.

Gstaiger, M., Luke, B., Hess, D., Oakeley, E. J., Wirbelauer, C., Blondel, M., Vigneron, M., Peter, M., & Krek, W. (2003). Control of nutrient-sensitive transcription programs by the unconventional prefoldin URI. Science (New York, N.Y.), 302(5648), 1208–1212.

Gutierrez-Beltran, E., Moschou, P. N., Smertenko, A. P., & Bozhkov, P. V. (2015). Tudor staphylococcal nuclease links formation of stress granules and processing bodies with mRNA catabolism in *Arabidopsis.* The Plant cell, 27(3), 926–943.

Gutiérrez-Santiago, F., Cintas-Galán, M., Martín-Expósito, M., Del Carmen Mota-Trujillo, M., Cobo-Huesa, C., Perez-Fernandez, J., & Navarro Gómez, F. (2022). A High-Copy Suppressor Screen Reveals a Broad Role of Prefoldin-like Bud27 in the TOR Signalling Pathway in *Saccharomyces cerevisiae*. Genes, 13(5), 748.

Harshavardhan, V. T., Van Son, L., Seiler, C., Junker, A., Weigelt-Fischer, K., Klukas, C., Altmann, T., Sreenivasulu, N., Bäumlein, H., & Kuhlmann, M. (2014). AtRD22 and AtUSPL1,

members of the plant-specific BURP domain family involved in *Arabidopsis* thaliana drought tolerance. PloS one, 9(10), e110065.

Hartmann T. (2007). From waste products to ecochemicals: fifty years research of plant secondary metabolism. Phytochemistry, 68(22-24), 2831–2846.

He, H., Denecker, J., Van Der Kelen, K., Willems, P., Pottie, R., Phua, S. Y., Hannah, M. A., Vertommen, D., Van Breusegem, F., & Mhamdi, A. (2021). The *Arabidopsis* mediator complex subunit 8 regulates oxidative stress responses. The Plant cell, 33(6), 2032–2057.

Kedersha, N., Stoecklin, G., Ayodele, M., Yacono, P., Lykke-Andersen, J., Fritzler, M. J., Scheuner, D., Kaufman, R. J., Golan, D. E., & Anderson, P. (2005). Stress granules and processing bodies are dynamically linked sites of mRNP remodeling. The Journal of cell biology, 169(6), 871–884.

Kosmacz, M., Gorka, M., Schmidt, S., Luzarowski, M., Moreno, J. C., Szlachetko, J., Leniak, E., Sokolowska, E. M., Sofroni, K., Schnittger, A., & Skirycz, A. (2019). Protein and metabolite composition of *Arabidopsis* stress granules. The New phytologist, 222(3), 1420–1433.

Leung, S. Y., Ho, C., Tu, I. P., Li, R., So, S., Chu, K. M., Yuen, S. T., & Chen, X. (2006). Comprehensive analysis of 19q12 amplicon in human gastric cancers. Modern pathology: an official journal of the United States and Canadian Academy of Pathology, Inc, 19(6), 854–863.

Lin, L., Prescott, M. S., Zhu, Z., Singh, P., Chun, S. Y., Kuick, R. D., Hanash, S. M., Orringer, M. B., Glover, T. W., & Beer, D. G. (2000). Identification and characterization of a 19q12 amplicon in esophageal adenocarcinomas reveals cyclin E as the best candidate gene for this amplicon. Cancer research, 60(24), 7021–7027.

Luo, Y., Na, Z., & Slavoff, S. A. (2018). P-Bodies: Composition, Properties, and Functions. Biochemistry, 57(17), 2424–2431.

Magen, S., Seybold, H., Laloum, D., & Avin-Wittenberg, T. (2022). Metabolism and autophagy in plants-a perfect match. FEBS letters, 596(17), 2133–2151.

Maruri-López, I., Figueroa, N. E., Hernández-Sánchez, I. E., & Chodasiewicz, M. (2021). Plant Stress Granules: Trends and Beyond. Frontiers in plant science, 12, 722643.

Meyuhas O. (2015). Ribosomal Protein S6 Phosphorylation: Four Decades of Research. International review of cell and molecular biology, 320, 41–73.

Mittler, R., Kim, Y., Song, L., Coutu, J., Coutu, A., Ciftci-Yilmaz, S., Lee, H., Stevenson, B., & Zhu, J. K. (2006). Gain- and loss-of-function mutations in Zat10 enhance the tolerance of plants to abiotic stress. *FEBS letters*, *580*(28-29), 6537–6542.

Peixoto, B., & Baena-González, E. (2022). Management of plant central metabolism by SnRK1 protein kinases. Journal of experimental botany, 73(20), 7068–7082.

Plaxton W. C. (1996). The organization and regulation of plant glycolysis. Annual review of plant physiology and plant molecular biology, 47, 185–214.

Protter, D. S. W., & Parker, R. (2016). Principles and Properties of Stress Granules. Trends in cell biology, 26(9), 668–679.

Pu, Y., Soto-Burgos, J., & Bassham, D. C. (2017). Regulation of autophagy through SnRK1 and TOR signalling pathways. Plant signalling & behavior, 12(12), e1395128.

Ren, C., Liu, J., & Gong, Q. (2014). Functions of autophagy in plant carbon and nitrogen metabolism. Frontiers in plant science, 5, 301.

Roitsch T. (1999). Source-sink regulation by sugar and stress. Current opinion in plant biology, 2(3), 198–206.

Smith, A. M., Zeeman, S. C., & Smith, S. M. (2005). Starch degradation. Annual review of plant biology, 56, 73–98.

Theurillat, J. P., Metzler, S. C., Henzi, N., Djouder, N., Helbling, M., Zimmermann, A. K., Jacob, F., Soltermann, A., Caduff, R., Heinzelmann-Schwarz, V., Moch, H., & Krek, W. (2011). URI is an oncogene amplified in ovarian cancer cells and is required for their survival. Cancer cell, 19(3), 317–332.

Tummala, K. S., Gomes, A. L., Yilmaz, M., Graña, O., Bakiri, L., Ruppen, I., Ximénez-Embún, P., Sheshappanavar, V., Rodriguez-Justo, M., Pisano, D. G., Wagner, E. F., & Djouder, N. (2014). Inhibition of de novo NAD(+) synthesis by oncogenic URI causes liver tumorigenesis through DNA damage. Cancer cell, 26(6), 826–839.

Turkina, M. V., Klang Årstrand, H., & Vener, A. V. (2011). Differential phosphorylation of ribosomal proteins in *Arabidopsis* thaliana plants during day and night. PloS one, 6(12), e29307.

Wang, Y., Garabedian, M. J., & Logan, S. K. (2015). URI1 amplification in uterine carcinosarcoma associates with chemo-resistance and poor prognosis. American journal of cancer research, 5(7), 2320–2329.

Weber, C., Nover, L., & Fauth, M. (2008). Plant stress granules and mRNA processing bodies are distinct from heat stress granules. The Plant journal: for cell and molecular biology, 56(4), 517–530.

Xiong, F., Zhang, R., Meng, Z., Deng, K., Que, Y., Zhuo, F., Feng, L., Guo, S., Datla, R., & Ren, M. (2017). Brassinosteriod Insensitive 2 (BIN2) acts as a downstream effector of the Target of Rapamycin (TOR) signalling pathway to regulate photoautotrophic growth in *Arabidopsis*. The New phytologist, 213(1), 233–249.

Xiong, Y., & Sheen, J. (2012). Rapamycin and glucose-target of rapamycin (TOR) protein signalling in plants. The Journal of biological chemistry, 287(4), 2836–2842.

Xiong, Y., & Sheen, J. (2014). The role of target of rapamycin signalling networks in plant growth and metabolism. Plant physiology, 164(2), 499–512. https://doi.org/10.1104/pp.113.229948

Xiong, Y., McCormack, M., Li, L., Hall, Q., Xiang, C., & Sheen, J. (2013). Glucose-TOR signalling reprograms the transcriptome and activates meristems. Nature, 496(7444), 181–186.

Yart, A., Gstaiger, M., Wirbelauer, C., Pecnik, M., Anastasiou, D., Hess, D., & Krek, W. (2005). The HRPT2 tumor suppressor gene product parafibromin associates with human PAF1 and RNA polymerase II. Molecular and cellular biology, 25(12), 5052–5060.

Zhang, F., Hu, X., Gu, Y., Bian, H., Xu, Z., Wang, Q., Chen, J., Lu, Y., Sun, L., Zheng, Q., & Gu, J. (2018). URI knockdown induces autophagic flux in gastric cancer cells. American journal of cancer research, 8(10), 2140–2149.

GENERAL DISCUSSION

Cellular homeostasis relies on intricate protein interactions that act at the core of a myriad of signalling and regulatory pathways, in most cases involving multiprotein complexes. One protein complex that acts as a nexus of multiprotein complexes and that is poorly understood in plants is the PFDLc. This poses several questions that span from the putative conserved role of this complex in eukaryotes to the endogenous and exogenous signals that modulate its activity. Understanding these questions will allow us to decipher how the PFDLs operate in plants and maybe in other eukaryotes. Furthermore, the functional characterisation of these proteins in plants can break new grounds for biotechnological approaches to improve plant fitness and resilience by modulating their interactions with specific proteins.

The discovery of PFDLs in the early 2000s led to research in yeast and mammals, focussing mainly on the function of Bud27/URI. The versatility of Bud27/URI became apparent as it interacted with many proteins involved in different processes, suggesting pleiotropic functions. In both yeasts and mammals, Bud27/URI played a crucial role in cytoplasmic assembly of RNA polymerases (Mirón-García *et al.,* 2013; Cloutier and Coulombe, 2010) and contributed to the regulation of transcription and transcription elongation through interactions with various complexes (Mirón-García., *et al*; 2014; Cuevas-Bermúdez *et al.*, 2023; Mita *et al.*, 2011; Millan-Zambrano *et al.*, 2013; Yart *et al*., 2005; Herranz-Montoya *et al.,* 2021). In yeasts, the involvement of Bud27 extended to translation processes and the influence on ribosomal components and biogenesis (Deplazes *et al.,* 2009; Martínez-Fernandez *et al.*, 2020). Complexity increased in mammals, where URI together with R2TP formed the PAQsome complex (Houry *et al.,* 2018), which stabilises the assembly of macromolecular complexes, including RNA polymerases (Cloutier and Coulombe, 2010), snoRNPs (Zhao *et al.*, 2008; Boulon *et al.*, 2008; Machado-Pinilla *et al.,* 2012), U5 snRNP (Cloutier *et al.,* 2017; Malinova *et al.,* 2017), PIKKs (Horejsi *et al.,* 2010; Izumi *et al.,* 2012) and the TSC complex (Cloutier *et al.,* 2017; Malinova *et al.,* 2017). In particular, the PAQsome has shown a role in regulating mTOR activity (Woodford *et al.*, 2017) and plays a crucial role in the assembly of macrocomplexes, especially under stress conditions (Houry *et al.,* 2018). The complex functions of URI emphasise its importance in cellular processes and provide insights into molecular mechanisms in both yeast and mammalian systems.

When we started this PhD, there was no available information about the PFDL complex in plants. Considering the research done in yeast and mammals, particularly with URI, we wondered about its function in plants and to what extent it was conserved. The results obtained in this PhD thesis have allowed us to clarify some of the questions originally posed. We have found that the URI1 protein is present in *Arabidopsis* and that it is part of the PFDL complex. The strong overlap of misregulated genes in both *uri1-1* and *pfd2 pfd6* mutant seedlings indicates that at least part of the functions performed by URI1 are as part of PFDLc. One feature of URI1 that caught our attention was that it is found mainly in the cytoplasm and to a lesser extent in the nucleus, as observed for the orthologs in yeast and mammals. This observation contrasts with the results of Yang *et al.,* 2022, who reported that URI1 is exclusively located in the cytoplasm. They reasoned that the amino acid sequence of URI1 in *Arabidopsis* lacks a nuclear localisation signal (NLS) and it was therefore not surprising that URI1 was found exclusively in the cytoplasm. However, it is noteworthy that Yang *et al.* determined nuclear localisation exclusively by confocal microscopy of *Arabidopsis* root cells using *pURI1*:*URI1-GFP* lines. Considering that URI1 probably enters the nucleus to fulfil certain functions and is subsequently recycled to the cytoplasm, the probability of finding URI1 in the nucleus might depend on the specific cellular state in which this process takes place. Under our experimental conditions, we demonstrated that URI1 can be localised in the nucleus by confocal microscopy, after transient expression of the protein fused to YFP in *N. benthamiana* leaves and in the root of *Arabidopsis* seedlings expressing the *pURI1:URI1-GFP*, and also by cell fractionation using seedlings of the *pURI1:URI1-3xFLAG* line. Interestingly, we

found that the domain that promotes the entry of the protein into the nucleus is the PFD domain. This suggests that there is either a non-canonical NLS region in the amino acid sequence of the PFD domain or that the domain itself is sufficient to interact with a partner that then transports it into the nucleus.

Our AP-MS experiments with URI1 and UXT as baits allowed us to demonstrate the presence of the PFDL complex in *Arabidopsis*. In addition, we also found RPAP3 subunit of the R2TP cochaperone complex as an interactor, suggesting that the PAQsome, formed by the PFDL and the R2TP subcomplexes, is present in plants. One of the conserved functions of URI1 as part of R2TP/PFDLc could therefore be the assembly of macromolecular complexes and thus contribute to protein homeostasis. Indeed, we found that URI1 has a rather extensive interactome, interacting with a relatively high number of proteins. When we analysed the interactors based on GO enrichment and categorise them according to biological processes, we found that they are mainly related to mRNA processing, mRNA metabolism and RNA splicing. Many of the partners may interact with URI1 as part of the R2TP/PFDL complex, while others may do it with the subunit alone. How the impaired interactions with partners contribute to the observed phenotypes in the *uri1-1* mutant awaits further investigations. In some cases, the phenotypes are likely to be indirect effects resulting from the impairment in the assembly of client complexes, although in other may reflect the direct involvement of URI1 in certain physiological processes. For example, the defects observed in the root apical meristem could be a consequence of a defect in microtubule assembly, as also observed in the *pfd6* mutant (Gu *et al*., 2006 and Yang *et al*., 2022).

The URI1 protein has features that make it different from the other PFDLs. In Chapter 2, we found that the region of URI1 located at the C-terminal part of the PFD domain is predicted to be disordered, as feature conserved in the human and yeast orthologs. Thus, this feature of URI1 has been maintained throughout evolution, indicating its importance for protein function. In fact, complementation analyses in yeast with deleted variants of URI/Bud27 have shown that the region corresponding to the IDR is sufficient to mitigate the translation defects (Deplazes *et al*., 2009) and temperature sensitivity (Mirón-García *et al*., 2013) observed in Δ*uri/bud27* cells. Two properties often observed in IDPs or in proteins with IDRs, i.e. the promiscuity for interaction with partners and instability (Haynes *et al*., 2006; Dyson and Wright, 2005), are present in URI1.

In humans, IDPs preferentially interact with other IDP or proteins with IDRs (Shimizu and Toh, 2009). We confirmed that a significant percentage of URI1 interactors tend to be disordered or have IDR regions. However, this feature was not conserved in humans and yeast, suggesting that the composition of the interactome is strain-specific and dependent on the specific sequence of the URI1/URI/Bud27 protein, including the IDR sequence. The involvement of IDP or proteins with IDR regions in regulatory pathways, coupled with their promiscuity in interacting with different proteins, suggests that their levels must be tightly controlled (Gsponer *et al*., 2008; Popelka H, 2020). We found that *Arabipdopsis* URI1 is an unstable protein and it is degraded by the core of the proteasome independently of ubiquitination, also described for the degradation of the SE protein in Arabidopsis (Li *et al*., 2020), a protein with IDR regions in *Arabidopsis*.

IDRs are particularly accessible to post-translational modifications (PTMs) such as phosphorylation, which in many cases alters the stability of the protein (Wright and Dyson, 2015; Zhou *et al*., 2018). Several phosphorylated residues have been reported for URI1 *in vivo*, all located as Ser/Thr in the IDR region (Xu *et al.,* 2017; Cruz *et al*., 2019; Willems *et al*., 2019). We have observed that URI1 is also phosphorylated in *Arabidopsis* and that phosphorylation of these residues likely promote URI1 stabilisation. It is tempting to speculate that CK2, a Ser/Thr kinase with high and constitutive activity conserved in eukaryotes (Wang *et al.,* 2022a), is one of the kinases that contribute to keeping URI1 phosphorylated and stable, because several *in vivo*

phosphorylated Ser/Thr on URI1 have been reliably predicted as target sites of CK2. It has been suggested that interaction with partners can stabilise disordered proteins (Li *et al.*, 2020). Phosphorylation of residues within the IDR could enhance the interaction of URI1 with its partners and thus contribute to its stabilisation. This could be through a mechanism involving phosphorylation-induced folding of the disordered region that mediates the interaction (Bah *et al.,* 2015). Alternatively, it could directly influence stability by preventing URI1 from being degraded by the proteasome. An example related to the latter scenario, albeit with the opposite outcome, is the phosphorylation of the partially disordered protein SE by PRP4KA in *Arabidopsis*, which triggers the degradation of SE (Wang *et al*., 2022b).

One piece of information that suggested that the levels of URI1 are tighly regulated came from the analysis *URI1*-overexpressing plants. We observed that the lines with severe phenotypes had lowest levels of YFP-URI1. When we analysed mRNA levels in these lines and correlated them with protein levels, the correlation was not linear. More mRNA did not necessarily lead to higher protein levels. A similar situation was reported for SE (Li *et al.*, 2020). The excess of transgenic SE protein in the *SE* overexpressing lines triggered its degradation by the 20S proteasome, which also degraded the endogenous SE resulting in a similar phenotype of *se* mutants and *SE* transgenic lines. Li *et al.* (2020) proposed that SE is normally part of different protein complexes and any fraction of SE not associated with a complex is degraded by the 20S proteasome to prevent undesirable effects of the excess of this partially disordered protein. SE, like other proteins with disordered regions, can be protected from degradation by masking the unfolded region if it is part of a complex, or by undergoing a folding-upon-interaction transition (Asher *et al*., 2006). We propose that a similar mechanism could operate to control URI1 protein levels. This suggest that the developmental phenotypes observed were caused by the reduced URI1 activity rather than overaccumulation. These developmental phenotypes, however, are not observed in the *aturi-1* mutant (Yang *et al.*, 2022). This likely reflects the different molecular nature of the defects, i.e. a change in amino acid in the uri1-1 protein compared to a reduced level of the protein in the transgenic plants, which have a different effect on the developmental processes involving URI1.

In the third chapter, we investigated whether URI1 is involved in stress responses. This was prompted by our observations that a significant enrichment of genes related to the stress response was found in the RNA-seq analysis of the *uri1-1* mutant (Chapter I). Interestingly, when we exposed plants to different stress situations (osmotic, saline, oxidative, thermal and energy stress), we observed significant changes in URI1 abundance or subcellular localization in response to some of them. For example, we observed that URI1-GFP relocalizes into granules in the cytoplasm after osmotic, oxidative and especially heat stress, without affecting the transcript or protein levels. These granules are probably stress granules or P-bodies, which are formed mainly by mRNAs, whose translation has been stalled in response to stress, and by proteins, many of them RNA-binding proteins. The current view is that these granules act as storage places where mRNAs are kept during stress and that resume translation after the stress is over and granules dissolved (Chantarachot *et al*., 2018). Given the presence of the other PFDLs in granules (Alberto Palacios-Abella and Alabadí, unpublised results) and the proposed role for them in protein homeostasis, we propose that URI1 exerts an active role there, and that it is not simply sequestered. The role of URI1 and the other PFDLs in these structures is being investigated in the PhD thesis of Alberto Palacios.

In the case of energy stress caused by sugar deprivation, we have observed that URI1 responds to the availability of sugar. Specifically, the plant requires a certain level of sugar to maintain the URI1 protein level post-transcriptionally. Two pieces of evidence support this claim: (i) URI1 protein levels are reduced in *Arabidopsis* cell suspensions and seedlings after sucrose

deprivation, and (ii) *URI1* is expressed in the cell suspensions under the constitutive promoter *35S*. This behaviour is like that of URI/Bud27 in yeast subjected to starvation, where there is a steady decrease in the protein as cells experience energy stress (Gstaiger *et al*., 2003). These results and the misregulation of carbohydrate metabolism genes observed in the *uri1-1* mutant suggest that URI1 may be involved in the pathway controlling the response to energy stress in *Arabidopsis*. Indeed, we have demonstrated the involvement of URI1 in the response to this stress by showing that in the presence of specific inhibitors of glycolysis (2DG) and photosynthesis (DCMU), the hypocotyls of the *uri1-1* mutant elongated more, and the seedlings appeared healthier. These results suggest that URI1 exerts a negative role in the pathway that promotes growth. Thus, the positive effect of sugar on URI1 levels could therefore serve as a mechanism to prevent excessive growth. In addition, we observed that the flowering time of the *uri1-1* mutant is influenced by light conditions, showing early flowering under LD conditions and late flowering under SD conditions. It is known that in several plant species, including *Arabidopsis*, there is an accumulation of sucrose in the phloem sap and SAM prior to flower induction (Corbesier *et al.,* 1998 and Yoon *et al.*, 2021). Thus, we have observed that the *uri1-1* mutant has higher sucrose concentrations compared to the WT, even under control conditions, and this could be one of the reasons that promote early flowering under long-day conditions. Further experiments are needed to determine whether URI1 is necessary for flowering and whether it is dependent on the circadian cycle.

Considering the importance of TOR in nutrient signalling, we investigated its possible functional relationship with URI1. Our results suggest that URI1 is likely to be an upstream regulator of TOR activity. We observed that the activity of TOR, as measured by phosphorylation of the ribosomal protein RPS6, was higher in the *uri1-1* mutant than in the WT mutant. This may explain why the *uri1-1* mutant is less sensitive to energy stress induced by sugar deprivation and position URI1 as a potential negative regulator of TOR. This relationship is different of the one reported for animals and yeast, where URI1 acts downstream of the master kinase (Gstaiger *et al.,* 2003; Djouder *et al.,* 2007). Whether the regulation of TOR by URI1 is direct or indirect is a question that requires further investigation. The relationship of URI1 with TOR could also go beyond this regulation. URI1 is part of the R2TP/PFDL complex (Palacios-Abella and Alabadí, unpublished results), which is involved in the formation of TORC homodimers required for TOR activation in animals and most likely also in plants (Brunkard *et al.,* 2020). Thus, although it seems paradoxical, URI1 could have a positive effect on TOR by supporting the assembly of TORC and also a negative role by regulating TOR activity.

Consistent with the growth phenotypes, RNA-seq analysis showed that the transcriptome of the *uri1-1* mutant seedlings was less impaired than that of the WT after DCMU treatment. For example, genes involved in carbohydrate metabolism were less repressed in the *uri1-1* mutant compared to the WT. Interestingly, when we analysed sucrose metabolism and starch formation, and genes involved in photosynthesis, we observed induction of enzymes related to this process in the *uri1-1* mutant after treatment. This could explain why the *uri1-1* mutant is able to withstand the stress. The upregulation of photosynthetic genes could potentially lead to higher availability of energy through the Calvin cycle. Combined with the ability to produce more starch and metabolize sucrose faster, more energy could be available for plant growth, making *uri1-1* better adapted to the stress.

In summary, our results show that the PFDL complex is present in *Arabidopsis* and that URI1 is one of its subunits. URI1 exhibits features of intrinsically disordered proteins thanks to the IDR located downstream of the PFD domain. These features include promiscuity to establish protein-protein interactions and instability of the protein. URI1 instability could allow the plant to precisely control the amount of URI1, for example in response to sugar availability, so that isolated

protein that is not incorporated into functional protein complexes is degraded to prevent unwanted effects. These properties could be reflected in the activity of URI1, both as part of the PFDL complex and as an independent subunit. Our interactome analysis suggests a possible role for URI1 in RNA metabolism, likely exerted as an independent subunit via the promiscuity of the IDR. URI1 could also recruit interactors to the complex via the IDR and limit the formation of the complex under those physiological conditions where URI1 becomes unstable and thus limiting. We hypothesize that the instability of URI1 is regulated by environmental changes and endogenous signals via phosphorylation and dephosphorylation of residues in the IDR, which likely influences the interaction of URI1 with its partners. This regulation of URI1 could potentially serve as a mechanism to control downstream pathways, both dependent and independent of the PFDL complex, for instance the transfer of the nutritional status to the TOR signalling pathway.

In addition to the results proposed by Yang *et al*. (2022), which showed that URI1 regulates gravitropism by modulating the distribution of auxins through PIN2 trafficking in the root and contributes to PIN1 recycling depending on the PFD complex, we updated the model for URI1 action in *Arabidopsis* (Figure 1). In *Arabidopsis*, like in animals, URI1 is part of the PFDL complex, which associates with the R2TP likely participating in the assembly of protein complex (PhD project by Alberto Palacios). Thus, URI1 as part of the R2TP/PFDLc in *Arabidopsis* could assist in the formation of large protein complexes such as nuclear RNAPs (PhD project by Laura Hernández), snRNPs involved in splicing or ribosomal RNA biogenesis and large protein kinases of the PIKK family, such as TOR.

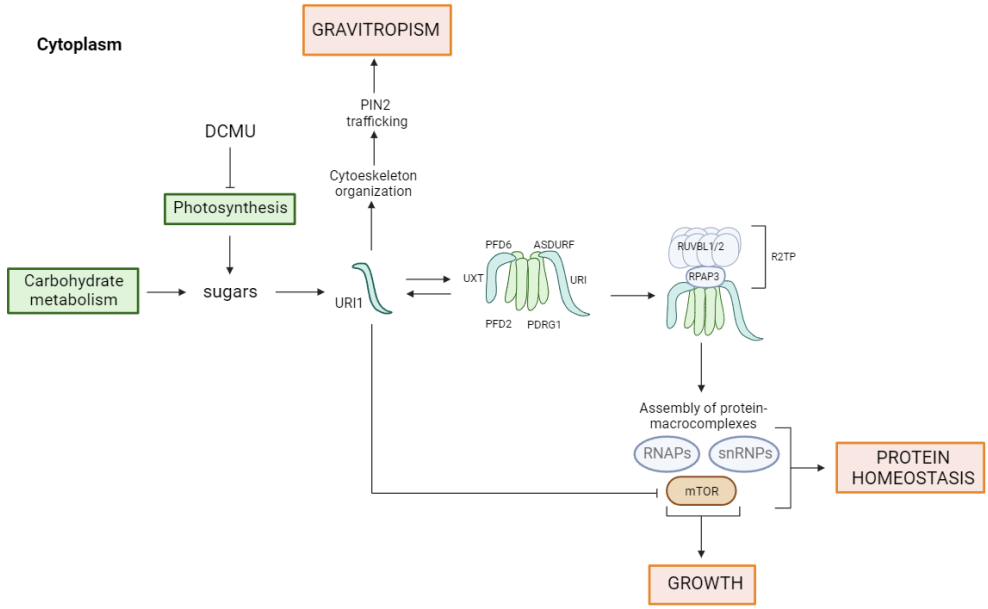

Figure 1. Proposed model for URI1 in *Arabidopsis*. URI1 regulates the organisation of the cytoskeleton and also the intracellular transport of the auxin efflux carrier PIN2, which is necessary to establish the asymmetry of auxin accumulation in the root to respond to gravitropic stimuli (Yang *et al*., 2022). On the other hand, URI1, which is incorporated into the PFDLc together with R2TP, presumably maintains the homeostasis of cellular proteins by promoting the assembly of macromolecular protein complexes such as RNAPs, PIKK (mTOR) and snRNPs. In addition, URI1 acts as a negative regulator of mTOR and influences cell growth.

REFERENCES

Asher G, Reuven N & Shaul Y (2006). 20S proteasomes and protein degradation "by default." *BioEssays* **28**, 844–849.

Bah A, Vernon RM, Siddiqui Z, Krzeminski M, Muhandiram R, Zhao C, Sonenberg N, Kay LE & Forman-Kay JD (2015). Folding of an intrinsically disordered protein by phosphorylation as a regulatory switch. Nature 519, 106–109.

Boulon, S., Marmier-Gourrier, N., Pradet-Balade, B., Wurth, L., Verheggen, C., Jady, B.E., Rothe, B., Pescia, C., Robert, M.C., Kiss, T., *et al*. (2008). The Hsp90 chaperone controls the biogenesis of L7Ae RNPs through conserved machinery. *J.Cell Biol*. 180, 579–595.

Brunkard, J. O., Xu, M., Scarpin, M. R., Chatterjee, S., Shemyakina, E. A., Goodman, H. M., & Zambryski, P. (2020). TOR dynamically regulates plant cell-cell transport. *Proceedings of the National Academy of Sciences of the United States of America*, *117*(9), 5049–5058.

Chantarachot, T., & Bailey-Serres, J. (2018). Polysomes, Stress Granules, and Processing Bodies: A Dynamic Triumvirate Controlling Cytoplasmic mRNA Fate and Function. *Plant physiology*, *176*(1), 254–269.

Cloutier, P., and Coulombe, B. (2010). New insights into the biogenesis of nuclear RNA polymerases? *Biochem.Cell Biol.* 88, 211–221.

Cloutier, P., Poitras, C., Durand, M., Hekmat, O., Fiola-Masson, E., Bouchard, A., Faubert, D., Chabot, B., and Coulombe, B. (2017). R2TP/Prefoldin-like component RUVBL1/RUVBL2 directly interacts with ZNHIT2 to regulate assembly of U5 small nuclear ribonucleoprotein. *Nat. Commun.* 8, 15615.

Corbesier, L., Lejeune, P., & Bernier, G. (1998). The role of carbohydrates in the induction of flowering in *Arabidopsis thaliana*: comparison between the wild type and a starchless mutant. *Planta*, *206*(1), 131–137.

Cruz ER, Nguyen H, Nguyen T & Wallace IS (2019). Functional analysis tools for post-translational modification: a post-translational modification database for analysis of proteins and metabolic pathways. *Plant J* **99**, 1003–1013.

Cuevas-Bermúdez, A., Martínez-Fernández, V., Garrido-Godino, A. I., Jordán-Pla, A., Peñate, X., Martín-Expósito, M., Gutiérrez, G., Govind, C. K., Chávez, S., Pelechano, V., & Navarro, F. (2023). The association of the RSC remodeler complex with chromatin is influenced by the prefoldin-like Bud27 and deter-mines nucleosome positioning and polyadenylation sites usage in Saccharo-myces cerevisiae. *Biochimica et biophysica acta. Gene regulatory mechanisms,* 1867(1), 194995. Advance online publication.

Deplazes, A., Möckli, N., Luke, B., Auerbach, D., & Peter, M. (2009). Yeast Uri1p promotes translation initiation and may provide a link to cotranslational quality control. *The EMBO journal*, *28*(10), 1429–1441.

Djouder, N., Metzler, S. C., Schmidt, A., Wirbelauer, C., Gstaiger, M., Aebersold, R., Hess, D., & Krek, W. (2007). S6K1-mediated disassembly of mitochondrial URI/PP1gamma complexes activates a negative feedback program that counters S6K1 survival signaling. *Molecular cell*, *28*(1), 28–40.

Dyson, H. J., and Wright, P. E. (2005). Intrinsically unstructured proteins and their functions. *Nat. Rev. Mol. Cell Biol.* 6:197–208.

Gsponer, J., Futschik, M. E., Teichmann, S. A., and Babu, M. M. (2008). Tight regulation of unstructured proteins: from transcript synthesis to protein degradation. *Science (80-.).* 322:1365–1369.

Gstaiger, M., Luke, B., Hess, D., Oakeley, E. J., Wirbelauer, C., Blondel, M., Vigneron, M., Peter, M., & Krek, W. (2003). Control of nutrient-sensitive transcription programs by the unconventional prefoldin URI. *Science (New York, N.Y.)*, *302*(5648), 1208–1212.

Gu, Y., Deng, Z., Paredez, A. R., DeBolt, S., Wang, Z. Y., & Somerville, C. (2008). Prefoldin 6 is required for normal microtubule dynamics and organization in *Arabidopsis*. *Proceedings of the National Academy of Sciences of the United States of America*, 105(46), 18064–18069.

Haynes, C., Oldfield, C. J., Ji, F., Klitgord, N., Cusick, M. E., Radivojac, P., Uversky, V. N., Vidal, M., and Iakoucheva, L. M. (2006). Intrinsic disorder is a common feature of hub proteins from four eukaryotic interactomes. *PLoS Comput. Biol.* 2:0890–0901.

Herranz-Montoya, I., Park, S., & Djouder, N. (2021). A comprehensive analysis of prefoldins and their implication in cancer. iScience, 24(11), 103273.

Horejsi, Z., Takai, H., Adelman, C.A., Collis, S.J., Flynn, H., Maslen, S., Skehel, J.M., de Lange, T., and Boulton, S.J. (2010). CK2 phosphodependent binding of R2TP complex to TEL2 is essential for mTOR and SMG1 stability. *Mol.Cell* 39, 839–850.

Houry, W.A., Bertrand, E., and Coulombe, B. (2018). The PAQosome, an R2TP-based chaperone for quaternary structure formation. *Trends Biochem*. Sci. 43, 4–9.

Izumi, N., Yamashita, A., Hirano, H., and Ohno, S. (2012). Heat shock protein 90 regulates phosphatidylinositol 3-kinase-related protein kinase family proteins together with the RUVBL1/2 and Tel2-containing co-factor complex. *Cancer Sci*. 103, 50–57.

Li, Y., Sun, D., Ma, Z., Yamaguchi, K., Wang, L., Zhong, S., Yan, X., Shang, B., Nagashima, Y., Koiwa, H., *et al*. (2020). Degradation of SERRATE via ubiquitin-independent 20S proteasome to survey RNA metabolism. *Nat. Plants* 6:970–982.

Machado-Pinilla, R., Liger, D., Leulliot, N., and Meier, U.T. (2012). Mechanism of the AAA+ ATPases pontin and reptin in the biogenesis of H/ACA RNPs. *RNA* 18, 1833–1845.

Malinova, A., Cvackova, Z., Mateju, D., Horejsi, Z., Abeza, C., Vandermoere, F., Bertrand, E., Stanek, D., and Verheggen, C. (2017). Assembly of the U5 snRNP component PRPF8 is controlled by the HSP90/R2TP chaperones. *J.CellBiol.* 216, 1579–1596.

Martínez-Fernández, V., Cuevas-Bermúdez, A., Gutiérrez-Santiago, F., Garrido-Godino, A. I., Rodríguez-Galán, O., Jordán-Pla, A., Lois, S., Triviño, J. C., de la Cruz, J., & Navarro, F. (2020). Prefoldin-like Bud27 influences the transcription of ribosomal components and ribosome biogenesis in *Saccharomyces cerevisiae*. *RNA (New York, N.Y.)*, *26*(10), 1360–1379.

Millan-Zambrano, G., Rodriguez-Gil, A., Penate, X., de Miguel-Jimenez, L., Morillo-Huesca, M., Krogan, N., and Chavez, S. (2013). The prefoldin complex regulates chromatin dynamics during transcription elongation. *Plos Genet.* 9, e1003776.

Mirón-Garcia, M.C., Garrido-Godino, A.I., Garcia-Molinero, V., Hernandez-Torres, F., Rodriguez-Navarro, S., and Navarro, F. (2013). The prefoldin bud27 mediates the assembly of the eukaryotic RNA polymerases in an rpb5-dependent manner. *PLoS genetics*, 9(2), e1003297.

Mirón-Garcia, M.C., Garrido-Godino, A.I.,Martinez-Fernandez, V., Fernandez-Pevida, A.,Cuevas-Bermudez, A., Martin-Exposito, M.,Chavez, S., de la Cruz, J., and Navarro, F. (2014). The yeast prefoldin-like URI-orthologue Bud27 associates with the RSC nucleosome remodeler and modulates transcription. *Nucl. Acids Res*. 42, 9666–9676.

Mita, P., Savas, J.N., Djouder, N., Yates, J.R., 3rd, Ha, S., Ruoff, R., Schafler, E.D., Nwachukwu, J.C., Tanese, N., Cowan, N.J., *et al*. (2011). Regulation of androgen receptor-mediated transcription by RPB5 binding protein URI/RMP. *Mol.CellBiol*. 31, 3639–3652.

Popelka H. (2020). Dancing while self-eating: Protein intrinsic disorder in autophagy. *Progress in molecular biology and translational science*, *174*, 263–305.

Shimizu, K., and Toh, H. (2009). Interaction between Intrinsically Disordered Proteins Frequently Occurs in a Human Protein-Protein Interaction Network. *J. Mol. Biol.* 392:1253–1265.

Wang G, Gao G, Yang X, Yang X & Ma P (2022a). Casein kinase CK2 structure and activities in plants. *J Plant Physiol* **276**, 153767.

Wang L, Yan X, Li Y, Wang Z, Chhajed S, Shang B, Wang Z, Choi SW, Zhao H, Chen S & Zhang X (2022b). PRP4KA phosphorylates SERRATE for degradation via 20 S proteasome to fine-tune miRNA production in Arabidopsis. *Sci Adv* **8**, eabm8435.

Willems P, Horne A, Van Parys T, Goormachtig S, De Smet I, Botzki A, Van Breusegem F & Gevaert K (2019). The Plant PTM Viewer, a central resource for exploring plant protein modifications. *Plant J* **99**, 752–762.

Woodford, M.R., Sager, R.A., Marris, E., Dunn, D.M., Blanden, A.R., Murphy, R.L., Rensing, N., Shapiro, O., Panaretou, B., Prodromou, C., *et al*. (2017). Tumor suppressor Tsc1 is a new Hsp90 cochaperone that facilitates folding of kinase and non-kinase clients. *EMBO J.* 36, 3650–3665.

Wright, P. E., and Dyson, H. J. (2015). Intrinsically disordered proteins in cellular signalling and regulation. *Nat. Rev. Mol. Cell Biol.* 16:18–29.

Xu SL, Chalkley RJ, Maynard JC, Wang W, Ni W, Jiang X, Shin K, Cheng L, Savage D, Huhmer AF, Burlingame AL & Wang ZY (2017). Proteomic analysis reveals O-GlcNAc modification on proteins with key regulatory functions in Arabidopsis. *Proc Natl Acad Sci U S A* **114**, E1536–E1543.

Yang, Y., Liu, F., Liu, L., Zhu, M., Yuan, J., Mai, Y.-X., Zou, J.-J., Le, J., Wang, Y., Palme, K., Li, X., Wang, Y., and Wang, L. (2022). The unconventional prefoldin RPB5 interactor mediates the gravitropic response by modulating cytoskeleton organization and auxin transport in *Arabidopsis*. *J. Integr. Plant Biol*. 64: 1916–1934.

Yart, A., Gstaiger, M., Wirbelauer, C., Pecnik, M., Anastasiou, D., Hess, D., and Krek, W. (2005). The HRPT2 tumor suppressor gene product parafibromin associates with human PAF1 and RNA polymerase II. *Mol.Cell Biol*. 25, 5052–5060.

Yoon, J., Cho, L. H., Tun, W., Jeon, J. S., & An, G. (2021). Sucrose signaling in higher plants. *Plant science: an international journal of experimental plant biology*, 302, 110703.

Zhao, R., Kakihara, Y., Gribun, A., Huen, J., Yang, G., Khanna, M., Costanzo, M., Brost, R.L., Boone, C., Hughes, T.R., *et al.* (2008). Molecular chaperone Hsp90 stabilizes Pih1/ Nop17 to maintain R2TP complex activity that regulates snoRNA accumulation. *J.Cell Biol*. 180, 563–578.

Zhou, J., Zhao, S., & Dunker, A. K. (2018). Intrinsically Disordered Proteins Link Alternative Splicing and Post-translational Modifications to Complex Cell Signaling and Regulation. *Journal of molecular biology*, *430*(16), 2342–2359.

CONCLUSIONS

1. The PFDL complex is formed in *Arabidopsis* and URI1 is one of its subunits.

2. *Arabidopsis* URI1 has features of intrinsically disordered proteins, which are conserved in the URI1 orthologs of yeast and humans. These features are promiscuity to interact with partners and instability of the protein, so its levels can be tightly controlled by the plant.

3. URI1 participates in the pathway controlling the response of the plant to energy stress as an upstream, negative regulator of TOR.

MATERIALS AND METHODS

In sylico analysis

The sequencences used for the phylogenetic analysis were acquired through a TBLASTN analysis for each species, using data sources from the Phytozome (http://www.phytozome.net/) and NCBI (http://www.ncbi.nlm.nih.gov/) databases. The amino acid sequences of the proteins were used to construct a preliminary maximum likelihood (PhyML) phylogenetic tree using default parameters in NGPPhylofeny.fr (Lemoine et al. 2019 and Goodstein et al. 2012). URI1 tree included representative sequences from S. cerevisiae, C. reinhardtii, P. patens, S. moellendorffii, M. polymorpha, O. sativa, A. thaliana, P. pinaster, S. lycopersicum, D. rerio, M. musculus, H. sapiens, and D. melanogaster. PFD3 from Arabidopsis was used as outliers. UXT and ASFURF trees included representative sequences from M.acuminata, O.sativa, A.coerulea, V.vinifera, A.thaliana, M. truncculata, M.musculus, and H.sapiens. PFD1 and PFD5 from Arabidopsis were used as outliers. To ensure a phylogenetic tree with stronger support, sequences with insertions or missing bases were eliminated from the final alignment. The orthologs of URI1, UXT and ASDURF were aligned separately in MEGA X (Kumar et al. 2018) using MAFFT ver.7 with default parameters (Katoh & Standley, 2013). The alignment was manually curated to verify the presence of conserved domains in URI1, UXT and ASDURF. The Shimodaira-Hasegawa-like approximate likelihood ratio test (SH-like aLRT) was used to calculate the statistical significance. Graphical representations of the phylogenetic trees were created using the webtool Interactive Tree of Life version 6.5.8 (https://itol.embl.de/), and final figures were manually edited.

The 3D structure of each Arabidopsis prefoldin-like protein was determined by homology with the models of *Arabidopsis* canonical prefoldins (Blanco-Touriñán *et al., 2021)* using Modeller (release 10.1) (Webb and Sali, 2016). Similarly, the 3D structure of each human prefoldin-like protein was determined by homology with the human canonical prefoldins (PDB code 6NR8) (Gestaut *et al.,* 2019). The 3D structure of the Arabidopsis and human PFDL complex was assembled using the human PFD complex (PDB code 6NR8) as a template and visualized using PyMOL 2.4 software. The protein disorder was predicted with the online tools DEPICTER (http://biomine.cs.vcu.edu/servers/DEPICTER/) (Barik *et al*., 2020) and MobiDB (https://mobidb.bio.unipd.it/) (Piovesan *et al*., 2023), and with preFold (https://github.com/aretasg/preFold), a tool written in Python and inspired by FoldIndex (Prilusky *et al.,* 2005).

Plant material and growth conditions

Some of the lines that were used in this study *uri1-1* and *uri1-2* (SALK_038314) mutants in the Col-0 background have been described in Yang *et al.* 2022. The pst10814 insertion line of URI1 expressed in the No background, was obtained from RIKEN. Unless otherwise stated, the seeds were surface-sterilised with 70% EtOH with 0.01% Triton X-100 (T8787, Sigma-Aldrich), sown on half-strength Murashige and Skoog (MS, Duchefa Biochemie) media containing 1% (w/v) sucrose, 8 g/L agar (pH 5.7) and stratified for three days at 4ºC in the dark. Seedlings were grown at 22ºC under continuous white light (50-60 $\mu mol \cdot m^{-2} s^{-1}$) for seven days.

Molecular cloning

Within the framework of this thesis, several DNA constructs were generated. To investigate the accumulation and localisation of the URI1 protein, different constructs were cloned using Gateway Technology®. The promoter of *URI1* (1.3 Kb upstream of the ATG) was amplified from genomic DNA by PCR using Fusion High-Fidelity Polymerase (Thermo Fisher Scientific) with attB-containing primers, and introduced into *pDONR207* (Thermo Fisher Scientific) vector using Gateway BP Clonase II Enzyme mix (Thermo Fisher Scientific) to generate *pENTR207-pURI1*. Then, *pENTR207-pURI1* was recombined with *pGWB104* (Ishizaki, Kimitsune *et al*. 2015) to

obtain *pGWB104-pURI1* using Gateway LR Clonase II enzyme mix (Thermo Fisher Scientific). Afterwards, *pGWB104-pURI1* was introduced into *Arabidopsis* plants by *Agrobacterium*-mediated transformation using the floral dip method (modified from Clough and Bent, 1998). Using the same molecular cloning technique and reagents mentioned above, the genomic region of *URI1* including the promoter, introns and exons to STOP codon, was cloned into two destination vectors – a modified *pEarlyGate302 (pEG302)* plasmid containing a 3xFLAG tag downstream of the Gateway cassette and *pGWB107,* to generate *pEG302*-gURI1 and *pGWB107*-gURI1. Both independent constructs were introduced into *Arabidopsis* plants using the floral-dip method.

To generate the overexpression lines, an available *pENTR223-URI1* plasmid containing the CDS of *URI1* was used and recombined with *pEarlyGate104* and *pEarlyGate201* (Earley *et al*. 2006) using Gateway LR Clonase II enzyme mix (Thermo Fisher Scientific) to generate *pEG104-URI1* and *pEG201-URI1*. Subsequently, *pEG104-URI1* was introduced into *Arabidopsis* as previously described but both constructs were used for agroinfiltration of *Nicotiana benthamiana (N. benthamiana)* leaves. Finally, different versions of the URI1 protein regions (PFDD 1bp - 402 bp, ΔPFDD 403bp - 1176bp, and ΔUri1Box 1bp - 1146bp) were amplified from *pENTR223-URI1* by PCR using Fusion High-Fidelity Polymerase (Thermo Fisher Scientific) with attB-containing primers, and introduced into *pDONR207* (Thermo Fisher Scientific) vector using Gateway BP Clonase II enzyme mix (Thermo Fisher Scientific) to generate *pENTR207-URI1-PFDD*, *URI1-ΔPFDD and URI1-ΔUri1Box*. To overexpress the deleted versions of URI1, *pENTR207-URI1-PFDD*, *URI1-ΔPFDD* and *URI1-ΔUri1Box* were recombined with *pEarlyGate104* and *pEarlyGate201* using Gateway LR Clonase II enzyme mix (Thermo Fisher Scientific) to generate *pEG104*-URI1-PFDD, URI1-ΔPFDD, URI1-ΔUri1Box. The deleted versions of *URI1* were used to infiltrate *N. benthamiana* leaves.

The CDSs of $URI1^{mut4A}$ and $URI1^{mut5A}$ were synthesized by Intregrated DNA Technologies (Belgium) and transferred into the *pEarleyGate104* vector by Gateway to create YFP fusions. The WT and the two mutant versions were transiently expressed in *N. benthamiana leaves* as explained below. Protein levels were analyzed by Western blot. All the oligos used for molecular clonning in this work are listed in the Supp Table 1.

Phenotypic analyses

Root measurements

To determine the length of the primary root, Wild-Type (WT) and *uri1-1* roots were measured using 10-day-old seedlings grown on vertical plates in continuous light. First, seeds were sown and germinated as described previously. Three days after germination, the seedlings were transferred to new plates containing half strength MS (Duchefa) media containing 1% (w/v) sucrose, 8 g/L agar (pH 5.7), and grown vertically. At this timepoint, the position of the root tips was marked. After seven days, the root tips were marked and the plates were scanned. The total root length was measured using the NIH ImageJ software (Rueden *et al*. 2017).

Shoot measurements

In order to determine the total shoot length from the lines *p35S::YFP-URI1* 4.9 (4.9), *p35S::YFP-URI1* 5.3 (5.3), *p35S::YFP-URI1*6.7 (6.7), *p35S::YFP-URI1* 16.11 (16.11), *p35S::YFP-URI1* 29.6 (29.6) and WT, the plants were grown in soil (containing a mixture of peat moss, perlite, and vermiculite of 1:1:1 ratio) for 25 days under a long day (LD; 16 hrs light at 22ºC, and 8 hrs dark at 19ºC) photoperiod. The plants were watered twice a week with nutritive solution containing the following ingredients - 0.15 g/L H_3PO_4, 0.82 g/L $Ca(NO_3)_2$, 0.3 g/L KNO_3, 0.35 g/L K_2SO_4, 0.24 g/L

$MgSO_4$, 0.1 g/L micronutrients. The shoot length was measured with a ruler, from the rosette to the last flower of the main shoot.

Tracking of aborted seeds

The seedlings from *uri1-1* and *uri1-2* and pst10814 mutants were sown in soil and stratified for seven days. Subsequently, they were also germinated under long-day conditions. Once the plants had reproduced and had matured siliques, they were dissected and observed under a Leica DMS1000 microscope aborted seeds.

Analysis of flowering time

The seeds from *uri1-1* and WT were sown in soil under LD and short day (SD: 8 hrs light at 22ºC and 16 hrs dark at 19ºC) light regimes. Plants were germinated at LD or SD for each assay. The flowering time was determined by counting the total number of leaves produced before bolting.

GUS staining assays

Seven-day-old plants were fixed in cold acetone for 20 mins, and vacuum-infiltrated with GUS staining solution (50 mM sodium phosphate buffer pH 7.2, 0.5 mM potassium-ferrocyanide, 0.5 mM potassium ferricyanide, 10 mM EDTA, 0.01% Triton X-100 and 1 mM 5-bromo-4-chloro-3-undolyl-β-glucuronic acid) for 15 mins, and then incubated at 37ºC overnight. The tissues were clarified with a series of ethanol solutions, and imaged with a Brightfield filter under a Nikon Eclipse E600 microscope or a Leica DMS 1000 macroscope.

Yeast two-hybrid assays

For yeast two-hybrid (Y2H) analyses, the coding sequence of URI1, UXT, PDRG1, RuvBL1, RuvBL2 full length CDS cloned in *pENTR223* (obtained from the ABRC) was transferred to the *pGADT7-GW* and *pGBKT7-GW* destination vectors using Gateway LR Clonase II enzyme mix (Thermo Fisher Scientific) to produce fusion proteins of the Gal4-activation domain (AD) and GAL4 DNA—binding domain (BD). The RPAP3 CDS was amplified by PCR using Fusion High-Fidelity Polymerase (Thermo Fisher Scientific) with attB-containing primers from an *Arabidopsis* cDNA pool and introduced into *pDONR207* (Thermo Fisher Scientific) using Gateway BP Clonase II enzyme mix (Thermo Fisher Scientific) to generate *pENTR207*-RPAP3 and then transferred into *pGADT7-GW* and *pGBKT7-GW* as previously described. *pGADT7 and* pGBKT7 of PFD2 and PFD6 were already described in Blanco-Touriñán *et al.,* 2021. The expression vectors derived from pGADT7 and pGBK7 were introduced into Y187 and Y2HGold yeast strains, respectively. The transformants were selected with Synthetic Defined (SD) medium, which lacked leucine (-Leu) or tryptophan (-Trp), respectively, where haploid yeasts were mated to obtain diploid cells by selection in SD-Leu-Trp medium. Protein interactions were tested by the nutrient requirement of histidine (His), where SD-Leu-Trp was used as a growth control, and SD-Leu-Trp-His was used to test for protein-protein interactions. Interaction assays were performed using serial dilution of diploid cultures (1:1, 1:10, 1:100 and 1:1000) dripping. The same-fold dilutions were photographed two days after plating.

Confocal microscopy

Leaves of three-week-old Nicotiana plants grown at LD were agroinfiltrated with *pEG104-URI1, URI1-PFDD, URI1-ΔPFDD, URI1-ΔUri1Box* and the p19 silencing suppressor. Leaf confocal fluorescence was recorded on the third day after agroinfiltration using a Zeiss Axio-Observer 780 Pascal with a water immersion objective (C-Apochromat 40X/1.2; Zeiss) lens. The YFP signal was

excited with an argon laser at the wavelength of 488 nm, and its emission was detected at 505-530 nm.

The seedlings of *pURI1::URI1-GFP* were grown vertically for five days under continuous light conditions. Roots were stained with 10 µg/ml of propidium iodide (PI) for 3 mins and washed with water twice before imaging with the Axio-Observer 780 Pascal Zeiss microscope, with a water immersion objective (C-Apochromat 40X/1.2; Zeiss). The GFP signal was excited with an argon laser at 488 nm and, its fluorescence was detected at 505-530 nm. The images were taken from the quiescent centre of the root tip.

To image the inflorescence apices of *Arabidopsis* WT and *uri1_sarl1* the apices were prepared and imaged as described (Serrano-Mislata *et al*. 2015). The dissected apices were imbibed in 10 µg/ml PI staining for 5 mins and imaged with an Axio-Observer 780 Pascal Zeiss microscope with a water-immersion objective lens (Apochromat 40X/1.0; Zeiss).

Protein co-immunoprecipitation assays

Leaves of three-week-old *Nicotiana* plants grown under LD conditions were infiltrated with different mixtures of *Agrobacterium* C58 cells carrying the expression vectors *p35S:YFP-URI1* and *p35S::HA-UXT* and the p19 silencing suppressor.

Three days after infiltration, the leaves were collected and frozen in liquid nitrogen. Approximately 1 ml of the frozen tissue was carefully minced before homogenisation in 0.5 ml of extraction buffer containing 25 mM Tris-HCl pH 7.5, 10% glycerol, 1 mM EDTA pH 8.0, 150 mM NaCl and 1X protease inhibitor cocktail (cOmplete, EDTA-free; Roche). The resulting extracts were kept on ice for 15 mins, followed by 2 rounds of centrifugation at maximum speed in a benchtop centrifuge at 4ºC to remove cell debris. Quantification of total protein content was performed using the Bradford assay, and 150 µg of total proteins were subjected to denaturation in 1 volume of 2X Laemmli buffer and stored for later use as input samples. In addition, 850 µg of total protein was incubated in 1 ml of extraction buffer containing 25 µl of anti-GFP-coated paramagnetic beads (Miltenyi) at 4ºC for 2 hrs, facilitated by a rotating wheel.

The extracts were added to µColumns (Miltenyi) at room temperature. The columns were then washed once with 800 µl of cold extraction buffer and then subjected to two further washes with 200 µl Wash Buffer Number 2, as provided in the Miltenyi kit. Next, the proteins were eluted under denaturing conditions, using 70 µl of elution buffer according to the manufacturer's instructions. For analysis, 63 µl of the immunoprecipitated samples (representing 90% of the total) were loaded onto a 10% SDS-PAGE gel together with 20 µg of the starting material. After electrophoresis, the proteins were transferred to a PVDF membrane and subjected to immunodetection with an anti HA-HRP antibody (HA-HRP 3F10, 1:5000, Roche). The remaining 10% of the immunoprecipitated samples were subjected to the same procedure together with 20 µg of the starting material, but probed with an anti GFP antibody (JL-8, 1:5000, Living Colours). The chemiluminescence signal was recorded with SuperSignalTM West Femto (Thermo-Fisher Scientific) and visualised with the ImageQuant 800 (Amersham).

Subcellular fractionation assay

Subcellular fractionation was performed as described previously in Zhang *et al*. 2014 with minor modifications. 2 g of seven-old-seedlings were ground in liquid nitrogen and homogenised in 4 ml of cold Honda buffer (0.44M sucrose, 20 mM HEPES KOH pH 7.4, 2.5% Percoll, 5% Dextran T40, 10 mM MgCl2, 0.5% Triton X100, 5 mM DTT, 1 mM PMSF and 1X protease inhibitor cocktail (cOmplete, EDTA-free; Roche)). The homogenate was filtered through a layer of Miracloth and

centrifuged at 2000g at 4ºC for 5 mins. 1 ml of the supernatant was centrifuged at 10000g at 4ºC for 10 mins and collected as a cytoplasmic fraction.

The pellet was resuspended in 1 ml Honda buffer and centrifuged at 1800g for 5 mins at 4ºC to pellet the nuclei. The nuclear pellet was washed 5 times with Honda buffer (137 mM NaCl, 2.7 mM KCl, 10 mM Na2HPO4, 2 mM KH2PO4, 1 mM EDTA), rinsed with 1X PBS and then resuspended with 150 µl cold glycerol buffer (20 mM Tris-HCl pH 7.9, 50% glycerol, 75 mM NaCl, 0.5 mM EDTA, 0.85 mM DTT, 0.125 mM PMSF and 1X protease inhibitor cocktail (cOmplete, EDTA-free; Roche)), then 150 µl cold nucleus lysis buffer (10 mM HEPES KOH pH 7.4, 7.5 mM MgCl2, 0.2 mM EDTA, 0.3 M NaCl, 1M urea, 1% NP -40, 1 mM DTT, 0.5 mM PMSF, 10 mM β-mercaptoethanol and 1X protease inhibitor cocktail (cOmplete, EDTA-free; Roche)) was added. The mixture was vortexed twice for 5 secs and incubated on ice for 2 mins. It was then centrifuged at 14000 rpm at 4ºC for 2 mins. The supernatant was collected as a nucleoplasmic fraction.

The chromatin pellet was rinsed with 1X PBS+1mM EDTA and resuspended in 150 ul of cold glycerol buffer and 150 ul of cold nuclei lysis buffer. The protein concentrations were determined using the Pierce 660 nm Protein Assay (22662, Thermo Fisher Scientific) according to the manufacturer's instructions, and the fractions were analysed by western blot.

Analysis of protein levels by Western Blot

Approximately 1 ml of ground frozen tissue was homogenised in 0.5 ml of extraction buffer (25 mM Tris-HCl p 7.5, 10% glycerol, 1 mM EDTA pH 8.0, 150 mM NaCl and 1X protease inhibitor cocktail (cOmplete, EDTA-free; Roche)). Extracts were kept on ice for 15 mins and cell debris was removed by centrifugation twice at maximum speed in a bench top centrifuge at 4ºC, and the total proteins were quantified using the Bradford assay. The protein samples were mixed with 1 volume of 2X Laemmli buffer and denatured at 95ºC for 5 mins. 25 µg of proteins were separated in a 10% SDS-PAGE, transferred to a 0.45 µm PVDF membrane (Amersham) and immunodetected with specific antibodies: anti FLAG-HRP (A8592, 1:5000, Sigma-Aldrich), anti GFP (JL-8, 1:5000, Living Colours), anti HA-HRP (3F10, 1:5000, Roche), anti RPS6 (AS194292, 1:1000, Agrisera), anti RPS6 P240 (AS194302, 1:1000, Agrisera), anti RPL13 (1:10000, provided by Dr. Cecile Bousquet-Antonelli, LGDP – CNRS, Université de Perpignan Via Domitia), HRP anti-HRP (P1291, 1:5000, Sigma), anti MBP (PA1-989, 1:5000, Invitrogen), anti H3 (AB1791, 1:5000, Abcam), horseradish peroxidase (HRP)–conjugated anti-rabbit (AS09-602, 1:20000, Agrisera) and anti-mouse HRP (NA931V, 1:10000, Amersham) were used as secondary antibodies. The PVDF membranes were stained with Ponceau S to check for protein loading consistency.

Chemiluminescence was detected using Supersignal west FEMTO substrate with maximum sensitivity (Thermo Fisher Scientific) and imaged using ImageQuant 8000 (Amersham). The protein bands were quantified using the NIH ImageJ software.

Gene expression analysis

Three different RNA-sequencing (RNA-seq) were performed with three independent biological replicates for each condition. The specific growth and extraction conditions for each of these analyses are described below.

For the first RNA-seq, Arabidopsis seedlings of *uri1-1* and WT were grown for 7 days under continuous white fluorescent light (80 µmol $m^{-2}s^{-1}$) at 20ºC. Total RNA was isolated using the NucleoSpin™ RNA Plant Kit (Macherey-Nagel) according to the manufacturer's instructions, and the RNA concentration and integrity (RNA Integrity Number – RIN) were measured with a RNA Nano Chip (Bioanalyzer, Agilent Technologies 2100).

For the second RNAseq, the calli obtained from hypocotyls of WT and *uri1-1* plants (the protocol for callus generation is described in detail later) were exposed to shoot induction media for three weeks. The calli were harvested and rapidly frozen with liquid nitrogen. Total RNA was extracted from the frozen samples using RNAzol reagent (RNAzol® RT, R4533, Sigma) using a method described in Chomczynski *et al*. 2010. Subsequently, the RNA concentration and its RIN, were determined with an RNA nano-chip on a bioanalyzer (Agilent Technologies 2100).

For the third RNA-seq, the WT and *uri1-1* seedlings were maintained for 5 days in minimal MS media (3 mM CaCl2, 1.5 mM MgSO4, 5 mM KCl, 1.25 mM KH2PO4, 0.5% D-mannitol, 3 mM MES and 1X Murashige and Skoog basalt salts micronutrient solution Ref. M0529 RNBL1484, Sigma) and transferred to a new plate containing minimal MS media as control, or to a new minimal MS media supplemented with 8 µM DCMU (#45463, Sigma) under white fluorescent light (80 µmol $m^{-2}s^{-1}$) at 20ºC for 2 days. Total RNA was isolated using the NucleoSpin™ RNA Plant Kit (Macherey-Nagel) according to the manufacturer's instructions. RNA concentration and integrity (RNA Integrity Number – RIN) were measured in an RNA Nano Chip (Bioanalyzer, Agilent Technologies 2100).

cDNA library construction, mRNA fragmentation, sequencing and analysis for each RNA-seq was performed by the Beijing Genomics Institute (BGI, Shenzhen, China). The data were analyzed on the Dr. Tom system from BGI.

Identification of the *Arabidopsis* URI1 and UXT proteome

To generate the Protein_G-URI1 (GS-URI1) and GS-UXT fusion proteins, the URI1 and UXT CDS were transferred into the *pKNGs::Rhino-GS* vector using the Gateway LR Clonase II enzyme mix (Thermo Fisher Scientific). This vector expresses the fusion protein under the 35S promoter. *pKGNs::Rhino-GS* fused to a nonsense sequence was used as a control. *Agrobacterium* C58 cells carrying *pKNGs::Rhino-GS-URI1*, *pKNGs::Rhino-GS-UXT* and the control construct were used to transform PSB-D cell cultures following the protocol previously described with minor modifications (Van Leene *et al*. 2015). Cultures of *Arabidopsis* cell lines were increased to obtain 50 g per cell culture. 10 g of cells were used per replicate, and three replicates were performed per line. The cells from each line and replicate were harvested, frozen in liquid nitrogen and ground into fine powder using a protocol adapted from Antosz *et al*. 2017, with minor modifications. After the single immunoprecipitation affinity purification and elution, the proteins were precipitated overnight with cold acetone at -20ºC. The pellet was washed three times with cold acetone and then dried at room temperature. The dried white protein pellet was dissolved with 1X PBS. Finally, the samples were mixed with 1 volume of 2X Laemmli buffer and boiled for 5 mins before sending to the Servicio de Proteómica of the Universidad de Córdoba to identify the proteins in the immunoprecipitate with Liquid Chromatography-Mass Spectrometry (LC-MS/MS).

The proteins identified in the purification of the control proteins were referred to as the control list and include all proteins that bind non-specifically to the GS tag. The proteins from the control list were excluded from the proteins identified in the immune-precipitated-URI1 (IP-URI1) and IP-UXT protein precipitation.

Callus formation and regeneration assays

Surface-sterilised seeds of WT and *uri1-1* were sown on half-strength MS (Duchefa) plates containing 1% (w/v) sucrose, 8 g/L agar (pH 5.7), stratified at 4ºC for 3 days and then germinated under continuous light for 48 hrs. The plates were then covered with aluminium foil to promote hypocotyl elongation. After five days in the dark, the cotyledons and roots were removed with a sterile scalpel, and the trimmed hypocotyls of similar length were transferred to a callus-inducing

medium (CIM: 3 g/L Gamborg B5 medium, 0.5 g/L MES, 0.8% agar, 20 g/L sucrose, 2.2 µM 2,4-diclorophenoxyacetic acid (2,4-D) and 0.46 µM kinetin). The plates were stored in the dark at 23ºC for 30 days. The 30-day-old calli were weighed with a laboratory balance and images were taken with a brightfield filter using a Leica DMS 1000 macroscope.

To test the ability of the 30-day-old hypocotyl calli to form shoots, they were transferred to shoot-inducing media (SIM: 3 g/L Gamborg B5 medium, 0.5 g/L MES, 0.8% agar, 20 g/L sucrose, 4.4 µM 6-(γ,γ-dimethylallymino) purine (2iP) and 0.5 1-naphthylacetic acid). The plates were set up for 30 days at LD photoperiod and imaged in brightfield with a Leica DMS 1000 macroscope.

Cell free protein degradation assays

Assays for cell-free protein degradation were performed in vitro with extracts of *Nicotiana*, various Arabidopsis lines, Arabidopsis lines that had the recombinant MBP-URI1 protein, (as described below).

The leaves of three-week-old *N.benthamiana* plants were infiltrated with mixtures of *Agrobacterium* C58 cells carrying the vector *p35S::HA-URI1*, *p35SS::GFP* and the p19 silencing suppressor. The leaves were harvested after three days and frozen in liquid nitrogen. Approximately 1 ml of the grinded frozen tissue was homogenised in 0.5 ml extraction buffer (25 mM Tris-HCl pH 7.5, 10% glycerol, 1mM EDTA pH 8.0, 150 mM NaCl). The extracts were kept on ice for 15 mins and cell debris was removed by centrifugation twice at maximum speed in a benchtop centrifuge at 4ºC. The total protein concentration in the extracts was adjusted to be equal to the extraction buffer. To the final supernatant, 0.5 mM cycloheximide (CHX) (C7698, Merck) was added, and the mixtures were then divided into two parts. One part was mixed with 100 µM MG132 (Insolution™, 474791, Merck) or 50 µM PYR41 (N2915, Sigma), and the other with 2% DMSO, as control. The mixtures were then incubated at 30 ºC for 0, 5, 10, and 20 mins prior to western blot.

For the degradation assays with recombinant MBP-URI1, the *pTH1::MBP-URI1* construct was generated by transferring the URI1 CDS from *pENTR223-URI1* to the *pTH1:: MBP-GW* (Hammarström, Martin *et al*. 2002) by LR reaction. For MBP-URI1 protein production, *pTH1::MBP-URI1* was transformed into *Escherichia coli* (*E. coli*) BL21 Rosetta strain and a single colony was collected to inoculate a 50 ml Terrific-Broth (TB) medium containing 34 µg/ml chloramphenicol and 100 µg/ml carbenicillin, and incubated at 37ºC overnight. Then, 200 ml of Rich-Broth medium containing 0.2% glucose, 34 µg/ml chloramphenicol and 100 µg/ml carbenicillin was inoculated with 400 µl of the overnight cultured cells. The cells were grown at 37ºC in a shaking incubator set at 250 rpm. To induce protein expression, 0.5 mM of IPTG at an Optical Density of 600 (OD600) of 0.53 was added to the culture.

The cells were incubated at 16ºC for 16 hrs, and harvested by centrifugation at 4500 rpm for 15 mins and the medium was discarded. The pellet was stored at -80ºC until ready for use. To purify MBP-URI1, the pelleted cells were resuspended in 5 ml of column buffer (20 mM Tris-HCl pH 7.4, 200 mM NaCl, 1 mM EDTA), and sonicated with a cell disruptor (Fisherbrand™ Model 120 Sonic Dismembrator) until the cells were completely homogenised. The sonicated sample was centrifuged at 14000 rpm for 20 mins at 4ºC, then the supernatant was collected and diluted with column buffer to a final volume of 35 ml, which was filtered through a 0.45 µmpore membrane for further purification. Amylose resin (E8021S, New England Biolabs) was used to purify MBP-URI1, where 1 ml of amylose resin was added into a 1.5 x 10 cm column at 4ºC. The column was washed with column buffer using 5 column volumes (CVs). The diluted crude extract was loaded, and the

non-specifically bound proteins were washed from the column using 10 CVs of column buffer. MBP-URI1 protein was eluted with 5 CVs of column buffer supplemented with 10 mM maltose. Up to 20% glycerol was added to the eluted fractions. The MBP-URI1 protein was stored at -80ºC for further use. Seven-day-old seedlings of WT and *uri1-1* were harvested and ground in liquid nitrogen, and the total proteins were then extracted with the same extraction buffer. The total protein extracts of WT and *uri1-1* were adjusted to equal concentration in the extraction buffer for each assay. 100 ng of recombinant MBP-URI1 protein was incubated in 250 µg of total protein for each assay. The same amount of solvent was used for each drug in all the controls. For the WT, 100 µM of MG132 and 150 µM of PYR41 were added and incubated at 30 ºC. The samples were collected at the following time points (0, 5, 10, 20, 30 and 60 mins) before Western blot analysis was performed. The quantification of all the results obtained was performed on the NIH ImageJ software after Western blot.RNA extraction and real-time qPCR

The *Arabidopsis* URI1 overexpressor lines 4.9, 5.3, 6.7, 16.11, 29.6 and WT were grown under continuous white fluorescent light (80 µmol $m^{-2}s^{-1}$) at 20ºC for 7 days. Total RNA was isolated using the NucleoSpinTM RNA Plant Kit (Macherey-Nagel) according to the manufacturer's instructions. The cDNA was prepared from 1 µg of total RNA using the NZY-First Strand cDNA Synthesis Kit (NZYTech) according to the manufacturer's instructions. The resulting cDNA was used for real-time quantitative Polymerase Chain Reaction (RT-qPCR). The primers used for the amplification during the different assays are listed on Supplemental Table 1.

Stress tolerance assays.

NaCl, H_2O_2 and mannitol tolerance was analysed by transferring 5-day-old seedlings grown on vertical under continuous light to new half strength MS plates supplemented with or without 100 mM NaCl, 300 mM mannitol and 1 mM H_2O_2. Time points sampling were done after 8 hours and 24 hours on NaCl treatment; 6 hours and 12 hours after mannitol treatment and; 30 minutes, 60 minutes and 180 minutes for H_2O_2 treatment. Samples were taken and used for, protein extraction and western blot analysis, confocal imaging and qRT-PCR (protocol and primers used described at RNA extraction and RT-qPCR section).

Heat shock treatments were done by transferring 5-day-ols seedlings grown on vertical under continuous light to darkness and 37ºC in darkness during 3 hours (control samples were also under darkness but at 22ºC). After the heat shock treatment, plants were recovered at 22ºC during 4 hours and under continuous light. Time points sampling were done before the treatment, just after 3 hours of heat shock and after 2 hours and 4 hours of recovery at 22ºC. Samples taken were used for protein extraction, western blot analysis and confocal imaging.

For confocal imaging, in order to preserve the integrity of the granules observed, the samples were placed in 1.5 mL of 2% paraformaldehyde in 1X PBS buffer. Afterwards, vacuum was applied for 1 minute (twice). Seedlings were washed twice for 5 minutes each in NH4Cl, and transferred to 1X PBS until the confocal images were obtained.

Carbon starving assays and hypocotyl length measurement

Arabidopsis PSB-D cells expressing *pKNGs::Rhino-GS-URI1* were grown in MSMO (4,43 g/L MS [MS minimal organics Sigma #M6899], 30g/L sucrose, 0.5 µg/ml of alpha-naphthaleneacetic acid [NAA], 0,05 µg/ml of kinetin, pH 5.7) fresh media supplemented during three days, the fourth day cells were transferred to MSMO media with or without sucrose, and let them grown at 22ºC during 24 hours under darkness. Samples were taken and frozen in liquid nitrogen. Total protein extracts were analysed using western blot.

Seeds of *pURI1:URI1-3xFLAG* were surface-sterilised as previously described, and incubated at 4ºC for 3 days, then they were germinated in continuous light at 22ºC for 3 days. The seedlings were transferred into half strength MS supplemented with 1% sucrose or to half strength MS without sugar and let them grow under darkness during 48 hours. Samples were taken at 24 hours and 48 hours. Total protein extracts were analysed using western blot.

Seeds were surface-sterilised as previously described, and incubated at 4ºC for 3 days, then they were germinated in continuous light at 22ºC for 2 days. The seedlings were transferred into minimal MS media (3 mM CaCl2, 1.5 mM MgSO4, 5 mM KCl, 1.25 mM KH2PO4, 0.5% D-mannitol, 3 mM MES and 1X Murashige and Skoog basalt salts micronutrient solution Ref. M0529 RNBL1484, Sigma) and were grown in the light for 4 days. The seedlings were then transferred to different sugar conditions [MS minimum, MS 90 mM sucrose, MS 5 mM 2DG (D8375, Sigma), and MS 8 uM DCMU (#45463, Sigma)], and grown in continuous light for another 3 days. Hypocotyl length was measured using NIH ImageJ software. Total protein extracts were analysed using western blot.

Analysis of primary metabolism

Arabidopsis seedlings of WT and *uri1_sarl1* were grown under the same conditions as for RNA-seq analysis in both control and 8 µM DCMU treatments (described in the gene expression analysis section). Primary metabolite analysis was performed at the IBMCP Metabolomics Platform as described previously (Minebois *et al*. 2020). 100 mg of lyophilised tissue samples were homogenised with liquid nitrogen and extracted in 1400 µl of 100% methanol and 60 µl of internal standard (0.2 mg ribitol in 1 ml water). The mixture was extracted at 70°C for 15 mins and centrifuged at 14, 000 rpm for 10 mins. The supernatant was transferred to a glass vial and 750 µl of CHCl3 and 1500 µl of water were added. The mixture was shaken for 15 secs and centrifuged at 14,000 rpm for 15 mins. 150 µl aliquots of the methanol/water supernatant were dried rapidly for 3 hrs.

For derivatisation, the dry residues were dissolved in 40 µl of 20 mg/mL methoxyamine hydrochloride in pyridine and incubated at 37 ºC for 90 mins. Then, 70 µl of MSTFA (N-methyl-N-[trimethylsilyl]trifluoroacetamide) and 6 µl of a retention time standard mixture (3.7% [w/v] mixture of fatty acid methyl esters ranging from 8 to 24C) were added and the samples were incubated at 37ºC for 30 mins. Sample volumes of 2 µl were injected in split and splitless modes into a 6890 N gas chromatograph (Agilent Technologies Inc. Santa Clara, CA) coupled to a Pegasus4D TOF mass spectrometer (LECO, St Joseph, MI). Gas chromatography was performed on a BPX35 (30 m × 0.32 mm × 0.25 µm) column (SGE Analytical Science Pty Ltd, Australia) with helium as carrier gas, and a constant flow of 2 ml/min. The liner was set at 250°C. The oven programme was 85°C for 2 min, 8°C/min ramp to 360°C. Mass spectra were collected at 6.25 spectra s^{-1} in the m/z range of 35–900 and an ionisation energy of 70 eV. Chromatograms and mass spectra were analysed using the CHROMATOF programme (LECO, St. Joseph, MI), and the metabolites were identified by comparison with a custom library prepared using commercial standards.

REFERENCES

Antosz, W., Pfab, A., Ehrnsberger, H. F., Holzinger, P., Köllen, K., Mortensen, S. A., Bruckmann, A., Schubert, T., Längst, G., Griesenbeck, J., Schubert, V., Grasser, M., & Grasser, K. D. (2017). The Composition of the *Arabidopsis* RNA Polymerase II Transcript Elongation Complex Reveals the Interplay between Elongation and mRNA Processing Factors. *The Plant cell*, *29*(4), 854–870.

Barik A, Katuwawala A, Hanson J, Paliwal K, Zhou Y & Kurgan L. (2020). DEPICTER: Intrinsic Disorder and Disorder Function Prediction Server. *J Mol Biol* **432**, 3379–3387.

Blanco-Touriñán N, Esteve-Bruna D, Serrano-Mislata A, Esquinas-Ariza RM, Resentini F, Forment J, Carrasco-López C, Novella-Rausell C, Palacios-Abella A, Carrasco P, Salinas J, Blázquez M & Alabadí D. (2021). A genetic approach reveals different modes of action of prefoldins. *Plant Physiol* 187, 1534–1550.

Chen, H., Zou, Y., Shang, Y., Lin, H., Wang, Y., Cai, R., Tang, X., & Zhou, J. M. (2008). Firefly luciferase complementation imaging assay for protein-protein interactions in plants. *Plant physiology*, *146*(2), 368–376.

Chomczynski, P., Wilfinger, W., Kennedy, A., Rymaszewski, M., & Mackey, K. (2010). RNAzol® RT: a new single-step method for isolation of RNA. Nat Methods **7**, 4–5□□

Clough, S. J., & Bent, A. F. (1998). Floral dip: a simplified method for Agrobacterium-mediated transformation of Arabidopsis thaliana. *The Plant journal: for cell and molecular biology*, *16*(6), 735–743.

Earley, K. W., Haag, J. R., Pontes, O., Opper, K., Juehne, T., Song, K., & Pikaard, C. S. (2006). Gateway-compatible vectors for plant functional genomics and proteomics. *The Plant journal: for cell and molecular biology*, *45*(4), 616–629.

Fujii, H., Verslues, P. E., & Zhu, J. K. (2011). Arabidopsis decuple mutant reveals the importance of SnRK2 kinases in osmotic stress responses in vivo. *Proceedings of the National Academy of Sciences of the United States of America*, *108*(4), 1717–1722.

Gestaut D, Roh SH, Ma B, Pintilie G, Joachimiak LA, Leitner A, Walzthoeni T, Aebersold R, Chiu W & Frydman J. (2019). The Chaperonin TRiC/CCT Associates with Prefoldin through a Conserved Electrostatic Interface Essential for Cellular Proteostasis. *Cell* 177, 751-765 e15.

Goodstein, D. M., Shu, S., Howson, R., Neupane, R., Hayes, R. D., Fazo, J., Mitros, T., Dirks, W., Hellsten, U., Putnam, N., & Rokhsar, D. S. (2012). Phytozome: A comparative platform for green plant genomics. Nucleic Acids Research, 40(D1).

Hammarström, M., Hellgren, N., van Den Berg, S., Berglund, H., & Härd, T. (2002). Rapid screening for improved solubility of small human proteins produced as fusion proteins in Escherichia coli. *Protein science: a publication of the Protein Society*, *11*(2), 313–321.

Ishizaki, K., Nishihama, R., Ueda, M., Inoue, K., Ishida, S., Nishimura, Y., Shikanai, T., & Kohchi, T. (2015). Development of Gateway Binary Vector Series with Four Different Selection Markers for the Liverwort Marchantia polymorpha. *PloS one*, *10*(9), e0138876.

Katoh, K., & Standley, D. M. (2013). MAFFT multiple sequence alignment software version 7: Improvements in performance and usability. Molecular Biology and Evolution, 30(4).

Kumar, S., Stecher, G., Li, M., Knyaz, C., & Tamura, K. (2018). MEGA X: Molecular evolutionary genetics analysis across computing platforms. Molecular Biology and Evolution, 35(6).

Lemoine, F., Correia, D., Lefort, V., Doppelt-Azeroual, O., Mareuil, F., Cohen-Boulakia, S., & Gascuel, O. (2019). NGPhylogeny.fr: New generation phylogenetic services for non-specialists. Nucleic Acids Research, 47(W1).

Minebois, R., Pérez-Torrado, R., & Querol, A. (2020). A time course metabolism comparison among Saccharomyces cerevisiae, S. uvarum and S. kudriavzevii species in wine fermentation. *Food Microbiology*, *90*, 103484.

Piovesan D, Del Conte A, Clementel D, Monzon AM, Bevilacqua M, Aspromonte MC, Iserte JA, Orti FE, Marino-Buslje C & Tosatto SCE. (2023). MobiDB: 10 years of intrinsically disordered proteins. *Nucleic Acids Res* 51, D438–D444.

Prilusky J, Felder CE, Zeev-Ben-Mordehai T, Rydberg EH, Man O, Beckmann JS, Silman I & Sussman JL. (2005). FoldIndex©: A simple tool to predict whether a given protein sequence is intrinsically unfolded. Bioinformatics 21, 3435–3438.

Rueden, C. T., Schindelin, J., Hiner, M. C., DeZonia, B. E., Walter, A. E., Arena, E. T., & Eliceiri, K. W. (2017). ImageJ2: ImageJ for the next generation of scientific image data. BMC Bioinformatics, 18(1).

Serrano-Mislata, A., Schiessl, K., & Sablowski, R. (2015). Active Control of Cell Size Generates Spatial Detail during Plant Organogenesis. *Current biology : CB*, *25*(22), 2991–2996.

Van Leene, J., Eeckhout, D., Cannoot, B., De Winne, N., Persiau, G., Van De Slijke, E., Vercruysse, L., Dedecker, M., Verkest, A., Vandepoele, K., Martens, L., Witters, E., Gevaert, K., & De Jaeger, G. (2015). An improved toolbox to unravel the plant cellular machinery by tandem affinity purification of *Arabidopsis* protein complexes. *Nature protocols*, *10*(1), 169–187.

Wang, L., Yu, G., Macho, A. P., & Lozano-Durán, R. (2021). Split-luciferase Complementation Imaging Assay to Study Protein-protein Interactions in *Nicotiana benthamiana*. *Bio-protocol*, *11*(23), e4237.

Webb B & Sali A. (2016). Comparative protein structure modeling using MODELLER. Curr Protoc Bioinforma 2016, 5.6.1-5.6.37.

Zhang, H., Tang, K., Qian, W., Duan, C. G., Wang, B., Zhang, H., Wang, P., Zhu, X., Lang, Z.,

Yang, Y., & Zhu, J. K. (2014). An Rrp6-like Protein Positively Regulates Noncoding RNA Levels and DNA Methylation in Arabidopsis. Molecular Cell, 54(3), 418–430.